Physiological roles of the DNA demethylation-associated proteins Gadd45a and Ing1

Dissertation

Zur Erlangung des Grades

Doktor der Naturwissenschaften

Am Fachbereich Biologie

Der Johannes Gutenberg-Universität Mainz

Bernadette Mekker

geb. am 14.03.1986 in Sathmar (Rumänien)

Mainz, 2015

Dekan:

1. Berichterstatter:

2. Berichterstatter:

Tag der mündlichen Prüfung: 10.11.2015

Angabe D77

TABLE OF CONTENTS

1. SUMMARY

Methylation of the 5' position of cytosine in the DNA (5mC) is an important epigenetic mark that regulates gene transcription. Removal of 5mC can occur either genome-wide by passive dilution during DNA replication or site-specifically via an active, enzymatic pathway. The Growth arrest- and DNA damage-inducible protein 45 alpha (Gadd45a) is involved in site-specific DNA demethylation and is targeted to chromatin by the H3K4me3 reader Inhibitor of growth protein 1 (Ing1). While the roles of Gadd45a and Ing1 in local DNA demethylation are well-established *in vitro*, the physiological roles of Gadd45a- and Ing1 mediated DNA demethylation are largely unknown. Using knockout mice, I demonstrate that loss of Gadd45a and Ing1 synergistically leads to premature aging. Mice deficient for Gadd45a and Ing1 suffer from shortened lifespan, failure to thrive, kyphosis, weight reduction, ovarian atrophy, female infertility, skin senescence and depletion of bone marrow cells. Hypotrophy of adipose tissue in Gadd45a- and Ing1-deficient mice is correlated to browning of white adipose tissue, which is reflected both in histological changes and altered global gene expression signatures in white adipose tissue. Adipose tissue hypotrophy is recapitulated *in vitro* by a failure of Gadd45a- and Ing1 deficient cells to differentiate along the adipogenic lineage – a phenotype that is correlated with the downregulation of the adipocyte master regulator PPARγ in Gadd45a- and Ing1 deficient cells. Analysis of several known aging-related pathways narrowed down the list of potential contributors to the Gadd45a$^{-/-}$ Ing1$^{-/-}$ segmental progeria and revealed a dampened Igf-1 signaling cascade, increased cellular senescence and a potential stem cell exhaustion. Gadd45a- and Ing1 deficient mouse embryonic fibroblasts show local DNA hypermethylation specifically at enhancer regions, which is correlated to reduced expression of differentiation-associated genes. These results uncover a role for Gadd45a and Ing1 in aging and highlight DNA demethylation as a potential determinant of lifespan regulation.

2. ZUSAMMENFASSUNG

Methylierung der 5‘- Position von Cytosin in der DNA (5mC) ist eine wichtige epigenetische Modifikation, die die Genexpression reguliert. 5mC kann entweder genomweit durch passive Dilution während der DNA-Replikation oder lokal durch einen aktiven, enzymatischen Mechanismus entfernt werden. Growth arrest- and DNA damage-inducible protein 45 alpha (Gadd45a) ist beteiligt an lokaler DNA-Demethylierung und wird von dem H3K4me3-erkennenden Protein Inhibitor of Growth 1 (Ing1) zum Chromatin geführt. Während die Rollen von Gadd45a und Ing1 bei der lokalen DNA-Demethylierung *in vitro* ausführlich untersucht sind, ist die physiologische Rolle von Gadd45a- und Ing1-vermittelter DNA-Demethylierung weitestgehend unbekannt. Mit Hilfe von Knockout-Mäusen demonstriere ich, dass ein Fehlen von Gadd45a und Ing1 synergistisch zu vorzeitiger Alterung führt. Gadd45a- und Ing1-defiziente Mäuse haben eine verkürzte Lebenserwartung, Wachstumsstörungen, Kyphose, verringertes Körpergewicht, atrophierte Ovarien, weibliche Infertilität, seneszente Haut und atrophiertes Knochenmark. Eine Hypotrophie des Fettgewebes in Gadd45a-und Ing1-defizienten Mäusen korreliert mit einer partiellen Umwandlung von weißem zu braunen Fettgewebe, was sich sowohl in histologischen Veränderungen als auch Unterschieden in der globalen Genexpression des Fettgewebes widerspiegelt. Diese Fettgewebshypotrophie wird *in vitro* rekapituliert durch eine verringerte Differenzierung von Gadd45a- und Ing1-defizienten Zellen zu Adipozyten – einem Phänotyp, der mit einer reduzierten Expression von PPARγ, einem Schlüsselfaktor der Adipozytendifferenzierung, einhergeht. Eine Analyse bekannter alterungsrelevanter Signalwege identifizierte eine verringerte Aktivierung des Igf-1 Signalwegs, eine erhöhte Seneszenz und eine potentiell verringerte Stammzellanzahl als Faktoren, die zur segmentalen Progerie der Gadd45a- und Ing1-defizienten Mäuse beitragen könnten. Gadd45a- und Ing1-defiziente embryonale Fibroblasten weisen eine lokale DNA-Hypermethylierung spezifisch in Enhancer-Regionen auf, die mit einer reduzierten Expression Differenzierungs-assoziierter Genen korreliert. Diese Ergebnisse enthüllen eine Funktion von Gadd45a und Ing1 im Alterungsprozess und stellen DNA-Demethylierung als einen potentiellen Faktor in der Regulation der Lebenserwartung heraus.

3. INTRODUCTION

3.1 AGING

3.1.1 DEFINITION OF AGING

Since the beginning of the 19th century, life expectancy in Europe has been steadily increasing from on average 35 years to over 80 years. World-wide, life expectancy has more than doubled in the last 200 years to a global average of around 70 years [1]. However, as lifespan of human populations is progressively increasing, so are the numbers of elderly people, the prevalence of aging-related diseases and consequently also their associated health care costs. These social challenges have fueled both the interest and the need to research the causes and molecular mechanisms responsible for aging.

Aging can be defined as a process of physiological deterioration, leading to a progressive decline in organismal fitness [2] that affects virtually [3] all eukaryotes. The aging process has a genetic component, and pathways influencing aging are evolutionary conserved from yeast over *C. elegans* and Drosophila to mammals [4]. In many cases, these various organisms employ highly related genes to counteract physiological deterioration, making them useful models for the molecular analysis of aging. The search for aging-associated molecular pathways has concentrated on three strategies: (1) Correlative studies between young and old, (2) treatments prolonging normal lifespan, and (3) studies of premature aging models [5].

Both in humans and in mice, a number of premature aging disorders have been identified. In order for mouse models to be considered *bona fide* models of accelerated aging, three criteria have been proposed [6]: First, their phenotype should manifest itself after maturation to discriminate aging from developmental defects; second, control mice should show similar phenotypes at older age; and third, mice should present several phenotypes that affect multiple organs. Mouse models meeting these three criteria include mice lacking the DNA repair proteins Ku80 [7], Xpd [8, 9], Xpa/Csb [10], Xpa/Xpb [11], Xpf [12], and Brca1 [13], the telomerase component Terc [14, 15], the nuclear lamina component Lmna [16], the Lmna processing factor Zmpste24 [17, 18] and mice with certain p53 mutations [19].

All of these mouse models exhibit similar symptoms of aging at comparatively young ages, including reduced life span, loss of body weight, osteoporosis, kyphosis, muscle atrophy, hair greying, hair loss, reduced dermal thickness, depletion of subcutaneous fat and total body fat, declined reproductive fitness, and reduced cellular proliferation. Despite overlapping symptoms in models of premature and

physiological aging, no unanimously agreed upon biomarkers of mouse aging have been determined so far [5].

3.1.2 MOLECULAR PATHWAYS ASSOCIATED WITH AGING AND LONGEVITY

Using comparative studies, lifespan extending treatment and premature aging models, many molecular causes and contributors of aging have been identified [20-26]. These include genomic instability, cellular senescence, telomere attrition, epigenetic alternations, loss of protein homeostasis, mitochondrial dysfunction, altered cell-cell communications, stem cell exhaustion, and deregulated nutrient sensing (Figure 3.1) [20], all of which will be discussed in detail below. These causes and contributors of aging and longevity are highly interconnected, with defects in one pathway usually affecting several others.

FIGURE 3.1 THE HALLMARKS OF AGING

This scheme enumerates nine causes and contributors of aging: Genomic instability, telomere attrition, epigenetic alterations, loss of protein homeostasis, deregulated nutrient sensing, mitochondrial dysfunction, cellular senescence, stem cell exhaustion, and altered intracellular communications. Figure from [20].

3.1.2.1 GENOMIC INSTABILITY

The integrity of both chromosomal and mitochondrial DNA is constantly endangered by a range of endogenous and exogenous stressors. Genomic integrity is threatened by reactive oxygen species generated as a byproduct of mitochondrial activity, the spontaneous hydrolytic deamination and depurination of nucleotides, polymerase errors during DNA replication and mutagenic chemicals as well as irradiation encountered in an organism's environment [27]. Approximately 10^4 to 10^5 DNA lesions of various natures are estimated to occur per cell and day in mammals, the majority being UV-induced pyrimidine dimers and abasic sites derived from spontaneous depurination [28-30]. If unrepaired, these DNA lesions are detrimental to cellular function: They can mutate and inactivate genes, impair DNA polymerase progression and thus cell proliferation, and cause DNA double strand breaks leading to chromosomal aberrations and rearrangements [20].

In contrast to any other cellular macromolecule, the DNA of a cell cannot be replaced and thus relies solely on an intricate array of DNA repair pathways to restore its integrity. Depending on the type of DNA damage, different pathways are employed for this purpose. Mispaired DNA bases are replaced using DNA mismatch repair, single damaged nucleotides are replaced by base excision repair, DNA interstrand crosslinks are repaired by interstrand crosslink repair, and bulky lesions that distort the DNA double helix are treated by nucleotide excision repair. DNA double strand breaks are repaired by an error-prone non-homologous end joining pathway, and in G2 phase of the cell cycle additionally by an error-free homologous recombination pathway that uses the sister chromatid as a template for DNA repair [29, 31].

Accumulation of DNA damage above a certain threshold induces cell cycle arrest. This allows time for prolonged DNA repair before lesions have an opportunity to compromise DNA replication or mitosis. If DNA damage is too severe to be repaired, cells will undergo either senescence (see chapter 3.1.2.6) or apoptosis to prevent malignant transformation [32, 33].

During aging, the repair capacities of many DNA repair pathways decline, resulting in an accumulation of various sorts of DNA lesions [32, 34]. Diminished DNA repair is not only correlated with but can also be causative for aging, as demonstrated by the occurrence of premature aging in the absence of functional repair pathways. Mutations in proteins involved in nucleotide excision repair, base excision repair or double strand break repair have been linked to segmental premature aging disorders including Werner syndrome, Bloom syndrome, Seckel syndrome, Xeroderma pigmentosum, Tichothiodystrophy, and Cockayne syndrome [20, 35]. A caveat in interpreting these segmental premature aging syndromes is that many DNA repair proteins are additionally constitutive components of basal transcriptional complexes [36].

In addition to chromosomal DNA lesions, mitochondrial lesions also contribute to premature aging, as evidenced by the accelerated aging of mice harboring an error-prone version of mitochondrial polymerase γ [37]. Mitochondrial DNA mutations are thought to give rise to suboptimally functioning mitochondrial respiratory chain proteins, thereby increasing production of reactive oxygen species that further damage cellular macromolecules [38, 39] (see chapter 3.1.2.4), even though this was not observed for polymerase γ mutant mice [40].

Unrepaired DNA damage is especially detrimental to adult stem cells, as this will impair not only short-term cellular function, but also cell renewal and tissue regeneration. In this manner DNA damage contributes to the exhaustion of the stem cell pool, a further hallmark of aging (see chapter 3.1.2.7).

3.1.2.2 TELOMERE ATTRITION

Telomeres are several kb long stretches of TTAGGG repeats that protect the ends of chromosomes from being recognized and "repaired" as DNA double strand breaks [41]. However, due to intrinsic properties of DNA polymerases, telomeres cannot be fully replicated up to their last nucleotide. Every cell division, telomeres shorten at a theoretical rate of 20 bp and an *in situ* observed rate of 50-100 bp [42], until they are fully eroded after 40 to 60 rounds of cell divisions [43]. Thereafter, to protect against further loss of DNA information and chromosomal instability, cells undergo senescence or apoptosis. They have reached their so-called Hayflick limit [44]. In contrast to most somatic cells, embryonic and adult stem cells are required to divide potentially indefinitely to fulfill their functions in establishing, maintaining and repairing tissues in an organism. To circumvent the Hayflick limit, stem cells have the unique property to express the enzyme telomerase, which is able to elongate telomeres.

The crucial role of telomeres in aging is demonstrated by mice deficient for telomerase developing a premature aging syndrome [15, 45], and telomerase mutations in humans causing the accelerated aging syndrome dyskeratosis congenita [46-48]. In elderly people, short telomeres are associated with increased mortality, showing that telomeres contribute to aging and aging-associated diseases also outside the context of individuals with telomerase loss-of-function [46, 49]. Conversely, telomerase overexpression in elderly mice is sufficient to reverse many aging-associated phenotypes and to extend longevity [50].

3.1.2.3 LOSS OF PROTEIN HOMEOSTASIS

Proteins can be damaged during the lifetime of a cell. To counteract accumulation of damaged proteins and to maintain protein homeostasis, three major quality control mechanisms have evolved. First, chaperones reinforce correct folding of newly synthesized or misfolded proteins. Second, the ubiquitin-proteasome system degrades irreparably damaged proteins. Third, the autophagy/lysosomal system degrades damaged larger intra-and extracellular structures up to the size of whole organelles [51, 52]. Inefficient protein quality control will lead to accumulation of misfolded and damaged proteins, to formation of protein aggregates and consequently to age-associated pathologies including neurodegenerative diseases, myopathies and liver diseases [51].

Protein homeostasis declines during aging due to a combination of increased protein damage and decreased protein clearance [51, 53]. Protein damage increases during aging as a consequence of accumulating DNA mutations and oxidative protein damage [54]. These damaged proteins then cannot be efficiently cleared, as chaperone synthesis [55], proteasomal degradation and autophagy are all impaired with age [174, 268]. Conversely, overexpression of chaperones prolongs lifespan in flies [56], worms [57], and mice [58]. Pharmacological induction of specific chaperones delays disease progression in a mouse model of muscular dystrophy [59]. Furthermore, indirectly increasing autophagy via Rapamycin [60, 61] or Spermidine treatment [62] prolongs lifespan in several model organisms, underlining the importance of protein homeostasis pathways in delaying aging.

3.1.2.4 MITOCHONDRIAL DYSFUNCTION AND REACTIVE OXYGEN SPECIES

During aging, mitochondrial function declines as a consequence of a combination of factors. Absolute mitochondrial numbers are reduced with age, since mitochondrial biogenesis is decreased [63]. The remaining mitochondria are increasingly dysfunctional due to accumulating damage to the DNA coding for mitochondrial proteins (chapter 3.1.2.1). These damaged mitochondria furthermore fail to be efficiently removed, since clearance of mitochondria via autophagy (chapter 3.1.2.3) is impaired with age [20, 64]. As a consequence, damaged mitochondrial respiratory chain proteins generate reactive oxygen species via electron leakage. Increased levels of reactive oxygen species in turn damage cellular macromolecules, including mitochondrial proteins and mitochondrial DNA, leading to a vicious cycle of mitochondrial dysfunction [21, 23, 38].

A direct role of mitochondrial defects in aging has been demonstrated by the generation of mitochondrial mutator mice, which harbor a mutated mitochondrial polymerase γ. These mice show an

accelerated aging syndrome, however unexpectedly no increased reactive oxygen species levels [65, 66].

In contrast to that, a mild mitochondrial dysfunction may even prolong lifespan by the upregulation of compensatory mechanisms that surpass initial detrimental effects of mitochondrial impairment [20, 64]. As an example, diminished mitochondrial function leads to a mild energy depletion that activates life-extending nutrient sensing pathways [20, 67, 68] (chapter 3.1.2.5). In *C. elegans*, slight mitochondrial dysfunction triggers a life-extending defensive response not only in directly affected but also in distant tissues [69]. Similarly, slightly increased levels of reactive oxygen species can increase lifespan by upregulating compensatory antioxidative mechanisms, with only high reactive oxygen species levels negatively affecting cellular functions [64]. This is reflected in a lack of a clear correlation between deletion or overexpression of antioxidant defense genes and lifespan in many model organisms [64, 70].

3.1.2.5 DEREGULATED NUTRIENT SENSING

A cell has multiple pathways to sense nutrient availability and energy levels [71]. Low energy levels are recognized in a cell through activation of AMPK by high AMP levels and activation of Sirtuins through high NAD^+ levels. Availability of glucose is communicated body-wide through the Insulin/Insulin-like growth factor (IGF-1) signaling pathway whereas amino acid levels are sensed through the mTOR (mammalian target of Rapamycin) pathway. Of note, mTOR is a central integrator of energy and nutrient status, as both AMPK and Insulin/IGF-1 signaling cascades feed into the mTOR pathway [71, 72]. All of the above described nutrient sensing pathways influence aging and longevity. Low energy status as communicated by either inactive IGF-1 signaling, inactive mTOR signaling, AMPK activation or Sirtuin activation will prolong lifespan in a number of model organisms [20, 73].

Especially the role of the Insulin/IGF-1 and mTOR signaling pathways in aging has been well analyzed [73, 74]. Insulin and IGF-1 are body-wide circulating hormones that activate the membrane-bound IGF-1 receptor in target tissues. Ensuing phosphorylation events lead to the activation of the kinases PI3K and subsequently AKT. AKT on the one hand activates mTOR and inhibits the FOXO family of transcription factors on the other hand [75]. Both the mTOR and FOXO signaling branches mediate aging- and longevity-related outcomes [20, 73, 74]: By a reduced IGF-1 signaling, FOXOs are upregulated and induce their target stress resistance genes including Glutathione-S-transferase, Catalase and Superoxide Dismutase, reducing the load of oxidative stress in the cell. mTOR inhibition on the other side promotes longevity by activating autophagy as well as reducing protein synthesis,

both of which ease the burden of damaged proteins and organelles in the cell to improve protein homeostasis (see chapter 3.1.2.3). Moreover, mTOR inhibition reduces cellular glucose uptake and thus the substrate for mitochondrial energy generation. Since electron leakage in mitochondria is the main source of intrinsic reactive oxygen species, attenuated Insulin-IGF-1 signaling also ameliorates damage-inducing oxidative stress (see chapter 3.1.2.4).

Attenuation of Insulin/IGF-1 signaling through caloric restriction is currently the strongest known means of lifespan extension [76, 77] and delays aging-related pathologies in model organisms ranging from yeast [78] over *C.elegans* [79] to mammals [80]. Similarly, mice deficient for various components of the IGF-1 signaling axis enjoy a significantly extended lifespan in comparison to wildtype mice [81-84]. Surprisingly, not only long-lived, but also short-lived mouse models show reduced IGF-1 signaling [10, 85, 86]. This is thought to be a compensatory mechanism trying to prolong lifespan in the presence of other hallmarks of aging.

3.1.2.6 CELLULAR SENESCENCE

Senescence, a specific state of permanent cell cycle arrest, is primarily an anti-cancer mechanism preventing mutated cells to proliferate uncontrollably. It is initiated in the presence of excessive DNA damage caused by DNA mutations (chapter 3.1.2.1), telomere erosion (chapter 3.1.2.2) or reactive oxygen species (chapter 3.1.2.4), and is mediated mainly by two pathways, $p16^{INK4A}$/Rb and $p19^{ARF}$/p53 signaling [87, 88]. While senescent cells can still fulfill their functions, they are in the long term intended to be cleared from the tissue and replaced by new, undamaged cells. If cell clearance or cell replacement are impaired, e.g. due to stem cell exhaustion (chapter 3.1.2.7), senescent cells will accumulate in the tissue. During aging, senescent cells accumulate especially in highly renewable tissues [89] and are particularly common in liver, skin, spleen and lung [20].

Although senescence is a compensatory reaction of cells which promotes longevity, the continued presence of senescent cells can have detrimental consequences for the lifespan of an organism. Senescent cells express high levels of specific set of pro-inflammatory cytokines, which has been termed senescence-associated secretory phenotype (SASP) [90, 91]. SASP proteins like TNFα, IL-6 or matrix metalloproteases increase with chronological aging in multiple tissues [89] and promote low-grade chronic inflammation by attracting macrophages and lymphocytes [89]. Continued inflammation then accelerates aging processes by leading to immune cell exhaustion, tissue degradation trough matrix metalloproteases and destruction of bystander cells by the innate immune system [89]. The contribution of SASP to physiological aging has been elegantly demonstrated in a mouse model in

which selective removal of senescent cells via a p16-driven inducible toxin is sufficient to increase lifespan and to delay aging-associated symptoms [92].

3.1.2.7 STEM CELL EXHAUSTION

If differentiated somatic cells are irreparably damaged, they will be replaced by new cells generated by the tissue's stem cell pool to ensure tissue homeostasis. If however adult stem cells themselves are damaged, the resulting impairment of both stem cell self-renewal as well as tissue regeneration has a more severe impact on organismic aging. Stem cell aging is caused by the same mechanisms that also promote aging in any other cell type. These include all the factors discussed above, such as DNA damage, telomere shortening, oxidative damage, mitochondrial dysfunction, epigenetic alterations and cellular senescence [20, 21, 23, 25] (Figure 3.2).

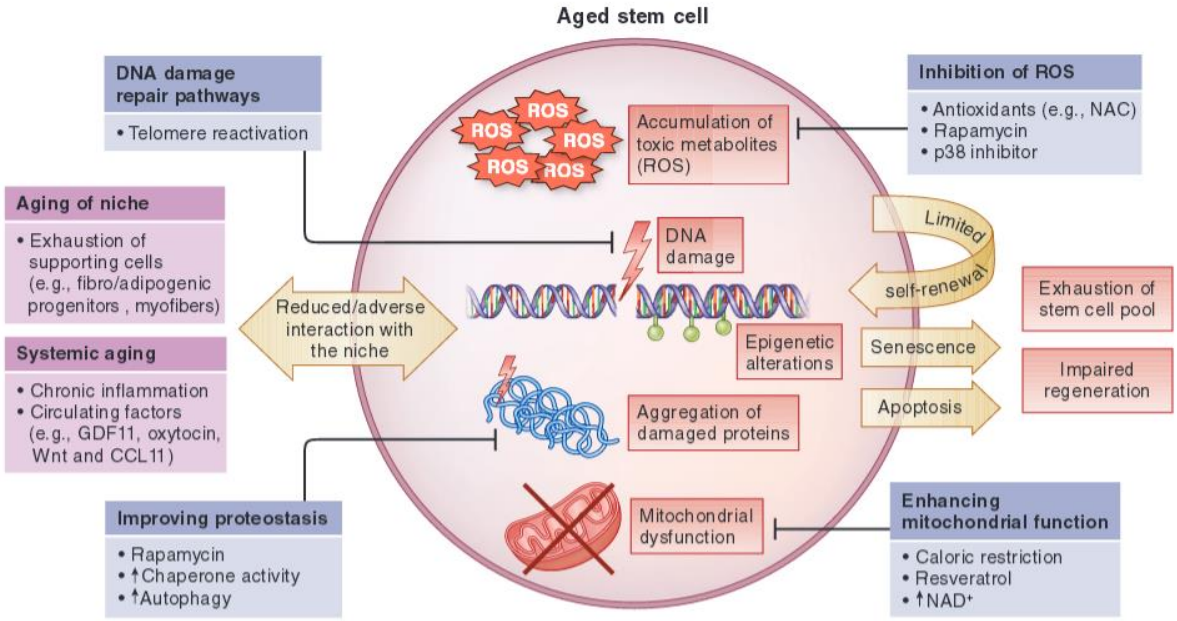

FIGURE 3.2 MOLECULAR PATHWAYS CONTRIBUTING TO CELLULAR AGING
Common cell-intrinsic aging pathways are depicted in pink, interactions of a stem cell with its niche that contribute to aging are shown in purple, and potential strategies to counteract aging are displayed in blue. Further details concerning molecular mechanisms of aging can be found in the main text. Figure from [21].

The importance of adult stem cells in the aging process depends on a tissue's proliferation rate, with fast-proliferating tissues being more susceptible to stem cell attrition [25]. Consequently, blood, intestine and skin show the strongest phenotypes in case of stem cell depletion, but also low-proliferating tissues like e.g. muscle are dependent on functional stem cells for regeneration after injury [25]. All examined adult stem cells undergo exhaustion during aging, with hematopoietic stem cells

being the best analyzed example. In this system stem cell exhaustion is characterized by anemia, impaired adaptive immunity, and a lineage skew towards myeloid cell types [93]. In other tissues, stem cell aging frequently results in lineage skews as well: Aged neural stem cells favor differentiation into astrocytes over neuronal lineages, and aged muscle stem cells will develop in fibroblasts rather than myoblasts, increasing the rate of fibrosis after muscle injury [25].

Stem cells require a delicate equilibrium between quiescence and proliferation, with an excess of either accelerating tissue aging. On the one side, the tumor suppressors p16, p19, p21 and p53 expedite aging through the promotion of cell cycle exit, senescence and apoptosis [23]. On the other side, increased tissue proliferation due to e.g. augmented Wnt signaling leads to accelerated aging through premature exhaustion of the stem cell pool [94, 95]. Different Wnt signaling branches seem to have either pro- or anti-aging effects in this regard [96, 97].

3.1.2.8 ALTERED INTERCELLULAR COMMUNICATION

Most of the described molecular mechanisms of aging are cell-intrinsic and affect each of a body's cells independently. Additionally to that, there are also systemically acting factors that contribute to aging. Several lines of evidence point to the fact that life-expanding interventions restricted to one organ can have beneficial effects organism-wide [15, 42, 44]. Parabiosis experiments furthermore demonstrate that blood from young mice is able to rejuvenate old mice whereas blood from old mice in turn accelerates aging in young mice [45, 95]. This points to the existence of both anti- and pro-aging factors circulating through the bloodstream.

Systemic factors that promote aging are predominantly proinflammatory cytokines. For example, hyperactive NF-κB signaling is correlated with physiological aging [46] and is sufficient to induce aging-associated phenotypes by dampening the gonadotropic axis [47] and promoting inflammation [48]. Conversely, inhibition of NF-κB signaling attenuates aging symptoms both in chronologically aged [46] and prematurely aged mice [49, 50]. Additionally, the pro-inflammatory factor Interleukin 6 is sufficient to cause premature aging [98, 99].

Systemic factors delaying aging include the hormone oxytocin [100] and growth differentiation factor 11 (GDF11), which is potentially [101] able to ameliorate age-related dysfunction in several murine organs [65, 102, 103]. However, little is known about their molecular mode of action in this respect.

3.1.2.9 EPIGENETIC ALTERATIONS

Several epigenetic regulators, including the Sirtuin family of deacetylases, histone modifications, and DNA methylation have been correlated to aging and longevity.

Sirtuins are a class of protein deacetylases with multiple chromatin- and non-chromatin targets [104]. Overexpression of the Sirtuin family members Sirt1 [105], Sirt3 [106] and Sirt6 [66] can delay the onset of aging-associated phenotypes and extend life span in mouse models by deacetylating a number of key metabolic and stress-related proteins [7, 18]. Conversely, knockout of Sirt1 or Sirt6 leads to the development of segmental progeroid syndromes [107, 108]. As Sirtuins sense cellular energy levels through NAD^+, they form a link between metabolism and aging and partly mediate the lifespan extending effects of caloric restriction [13] (see chapter 3.1.2.5).

Global levels of the histone marks H4K16ac (chromatin decondensation), H4K20me3 (transcriptional repression), and H3K4me3 (transcriptional activation) increase, while global amounts of H3K9me (transcriptional repression) and H3K27me3 (transcriptional repression) decrease during aging [14, 20]. Similarly, the expression of several histone modifying enzyme complexes changes with age [22, 24]. For the histone modifier Suv39h1, also a causal role in regulating longevity could be demonstrated [109]. Partially due to deregulation of histone marks, aging is associated with increased transcriptional noise and aberrant expression especially of inflammatory, mitochondrial and lysosomal genes [110]. Additionally, a reduction of constitutive heterochromatin during aging [111, 112] contributes to aberrant gene expression and chromosomal instability.

Similar to patterns of histone modifications, DNA methylation patterns during aging change due to epigenetic drift. Accumulating epigenetic changes in response to a combination of environmental stimuli and stochastic changes contribute to the phenotypic variability observed in aging organisms [113]. Globally, aging is correlated to reduced DNA methylation levels [114] especially in CpG island shores [115]. This global DNA hypomethylation can be attributed to a decreased function of the Dnmt1 maintenance methyltransferase during aging [116] and leads to a reactivation of transposable elements. The causal contribution of global DNA hypomethylation to aging has been demonstrated in mice hypomorphic for the chromatin remodeler PASG/Lsh. PASG deficiency causes DNA hypomethylation of both repetitive elements and single-copy genes [117], with PASG mutant mice developing a premature aging phenotype [118].

On top of global DNA hypomethylation, local DNA hypermethylation is occurring during aging. Examples of hypermethylated genes from different tissues include *ER, Igf2, p14ARF, p16INK4A, E-Cadherin, Collagen 1a1, Brca1, Lmna, Wrn, Rb, Ercc1, Rad50, APC, c-FOS*, and the *rDNA* locus,

many of which are prominent tumor suppressor genes [22, 24, 34]. Indeed, both cancer and aging share patterns of global DNA hypomethylation and local DNA hypermethylation, with a high overlap of individual hypermethylated genes [20]. The causes of local DNA hypermethylation during aging however have not been determined yet. Also, despite the correlation of DNA methylation changes and aging, it is not clear to what degree DNA methylation is causally contributing to this process. To gain further insight in the role of DNA methylation in aging and longevity, a detailed knowledge of pathways mediating DNA methylation and DNA demethylation is required.

3.2 DNA METHYLATION AND DEMETHYLATION

3.2.1 MECHANISMS OF DNA METHYLATION AND DNA DEMETHYLATION

DNA methylation occurs in the context of cytidine-guanosine dinucleotides (CpGs) at the 5' position of cytosines (5mC). Due to the palindromic nature of CpGs, DNA methylation occurs symmetrically on both strands of the DNA [119, 120]. 5mC is set by the *de novo* DNA methyltransferases Dnmt3a and Dnmt3b. During replication, the incorporation of unmodified cytidines in the newly synthesized DNA strand results in hemimethylation. These hemimethylated sites are recognized by the maintenance methyltransferase Dnmt1 and its constitutive binding partner Uhrf1 and are re-methylated to propagate DNA methylation over successive rounds of cell divisions [119-121]. DNA methylation was long considered a stable epigenetic mark with no enzymatic means of removal due to the chemical inertness of C-C bond that would have to be cleaved to remove a methyl moiety from DNA. Correspondingly, the only known way to eliminate 5mC was passive dilution during cell replication in the absence of Dnmt1/Uhrf1. Only in the last years has an enzymatic pathway of DNA demethylation been identified that is unanimously agreed upon.

The Ten-eleven-translocation (TET) family of enzymes is able to iteratively oxidize 5mC to 5-hydroxymethylcytosine (5hmC), 5-formylcytosine (5fC), and 5-carboxylcytosine (5caC) [122, 123] [52, 124, 125]. Dnmt1 has a strongly reduced affinity for any of these oxidized cytosine derivates [119, 126]. Thus, oxidized cytosine modification can be passively diluted out during DNA replication even in the presence of active maintenance methylation. Moreover, 5fC and 5caC are substrates for Thymine DNA glycosylase (TDG) and can be excised from the DNA by base excision repair proteins [52, 127, 128]. Consequently, three main pathways DNA demethylation seem to exist [119, 129]: (1) Replication-dependent passive DNA demethylation by dilution of 5mC during DNA replication in the absence of maintenance methylation, (2) Replication-dependent active demethylation, in which TET-mediated oxidation of 5mC is followed by dilution of cytosine modifications during DNA replication,

and (3) Replication-independent DNA demethylation, in which TET-mediated oxidation of 5mC is followed by active removal via TDG and base excision repair (Figure 3.3).

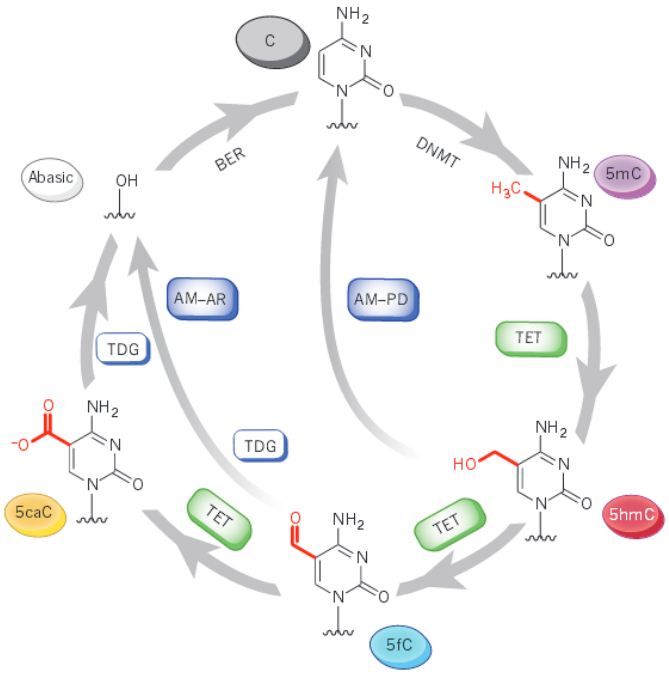

FIGURE 3.3 DNA METHYLATION AND DNA DEMETHYLATION PATHWAYS

Cytosine is methylated at its 5' position by DNA methyltransferases (DNMT) to yield 5-methylcytosine (5mC). 5mC is iteratively oxidized by ten-eleven-translocation (TET) enzymes to 5-hydroxymethylcytosine (5hmC), 5-formylcytosine (5fC) and 5-carboxylcytosine (5caC). These active modifications (AM) can be removed from DNA either by passive dilution (PD) of 5hmC, 5fC and 5caC during DNA replication or by active restoration (AR) of 5fC and 5caC to C using thymine DNA glycosylase (TDG) and the base excision repair (BER) pathway. Figure from [129].

In addition to TET-mediated DNA demethylation, other pathways of active DNA demethylation have been put forward, but are not unanimously agreed upon. The involvement of Activation-induced cytidine deaminase (AID) in DNA demethylation has been proposed via either deamination of 5mC to T or deamination of 5hmC to 5hmU and subsequent restoration of unmodified cytosines by DNA repair pathways [130-134]. However, a role for AID in DNA demethylation has been questioned, since this would generate many C to T transitions, thereby increasing mutation risk. Furthermore, deamination of 5mC or 5hmC by AID is sterically unlikely, as they do not fit in the binding pocket of AID [135] and AID's affinity for 5mC and 5hmC is orders of magnitude below that for its canonical substrate cytosine [136]. Another proposed player in DNA demethylation is the Growth arrest and DNA damage 45 (Gadd45) family of proteins. Several pathways have been suggested through which Gadd45 proteins could contribute to DNA demethylation [131, 137-140]. In chapter 3.4, a detailed discussion of these pathways and further Gadd45 properties will follow.

3.2.2 BIOLOGICAL ROLES OF DNA DEMETHYLATION

DNA demethylation on a global or on a gene-specific scale plays a role in a number of biological processes, including restoration of pluripotency in early zygotes, resetting of imprinted gene loci in primordial germ cells and several differentiation processes.

After the fusion of sperm and oocyte, DNA methylation is globally erased to re-establish pluripotency in developing zygotes [119, 120, 129, 141]. Of the three Tet family proteins, only Tet3 is expressed at this stage at detectable levels [142]. Tet3 oxidizes 5mC to 5hmC specifically in the male pronucleus [143-145]. The female pronucleus contains H3K9me2 marks that recruit Stella/Dppa3, a protein that repels Tet3 and thus prevents Tet3-mediated oxidation of maternal CpGs [146]. After the subsequent fusion of male and female pronucleus, both 5mC and 5hmC are diluted out passively during DNA replication via exclusion of Dnmt1 and Uhrf1 from the nucleus [142, 144, 147]. Active DNA oxidation of only the male pronucleus may be necessary since sperm contains significantly higher DNA methylation levels than oocytes. Promoting DNA demethylation in the male pronucleus is thus required to equilibrate methylation levels before passive DNA demethylation takes place. A failure to oxidize 5mC in the male pronucleus in Tet3-deficient mice leads to embryonic lethality, emphasizing the biological significance of this event [143].

A second wave of global DNA demethylation is occurring during the maturation of primordial germ cells in the developing embryo [120, 129, 141]. During the migration of early primordial germ cells into the genital ridges, DNA demethylation first occurs passively via downregulation of Dnmts and the resultant absence of maintenance methylation [148]. In a second phase of demethylation, specific loci are oxidized by the activity of Tet1 and Tet2 [149]. 5hmC is set specifically at imprinted genes and certain promoters and gene bodies [149]. Later on, 5hmC is passively removed in subsequent cell divisions [148, 150]. Failure of Tet1/2-mediated demethylation in primordial germ cells leads to meiotic errors and imprinting defects , causing lethality of the progeny [151-153].

Further examples of DNA demethylation during development are gene-specific active demethylation events during cellular differentiation. During e.g. epidermal, muscular or neuronal differentiation, expression of Dnmts is downregulated, indicating a role for DNA demethylation during cellular differentiation [154]. Genomic regions that are demethylated during differentiation have been characterized in spermatogenesis [155], hematopoiesis [156, 157], hair follicle differentiation [157], dendritic cell differentiation [158], and monocyte-to-osteoclast differentiation [159]. Additionally, stimulus-triggered local DNA demethylation is occurring in postmitotic neurons in the hippocampus [126, 130, 160-162]. In many cases during differentiation and neuronal stimulation, an active, Tet-mediated demethylation mechanism has been demonstrated [130, 155, 159, 160].

In summary, both global and gene-specific DNA demethylation events occur at different stages of development. DNA demethylation via replication-dependent dilution is a comparatively slow process, but does not pose the risk of DNA breaks that is inherent in using base excision repair. Thus, it seems to be preferentially used for global DNA demethylation processes. During differentiation, when few loci require quick demethylation, TET-mediated 5mC oxidation followed by TDG-mediated removal of 5fC and 5caC seems to be preferred [129, 163].

3.2.3 GENOMIC LOCATIONS OF ACTIVE DNA DEMETHYLATION

Not all CpGs in the genome have equal propensity to undergo methylation changes, and the majority of all CpGs indeed has unvarying methylation levels [120, 164, 165] (Figure 3.4). 60% to 80% of all CpGs are constitutively methylated across all tissues and developmental stages [166]. These CpGs are predominantly located in pericentromeric regions and repetitive elements to ensure silencing and compaction of those regions. CpGs located in gene bodies are usually methylated as well, most likely to prevent usage of aberrant alternative start sites or to regulate alternative splicing [167]. Approximately 10% of all CpG dinucleotides lie in particularly CpG-dense regions, so-called CpG islands. They are predominantly located at transcription start sites of housekeeping genes and developmental regulators. Throughout tissues and developmental stages, most CpG islands remain unmethylated to facilitate expression of nearby genes. CpG islands are kept unmethylated by repelling Dnmts through a combination of transcription factor binding and the presence of active histone marks. Sporadic, undesirable DNA methylation is removed from these sites by active DNA demethylation involving TET and TDG [120].

Genomic regions in which DNA methylation levels differ across cell types are located chiefly at enhancers and lineage-specific transcription start sites [164, 166] (Figure 3.4). On average, these regions have a low CpG density and intermediate DNA methylation levels [168]. Differentially methylated enhancers and promoters are frequently sites of active DNA demethylation, as demonstrated by their preferential occupancy by TET1 and TDG and the enrichment of 5fC and 5caC at these sites [169-171].

Similarly, also 5hmC occurs preferentially at promoters with low CpG density, gene bodies, enhancers, and lowly methylated regions [119, 141, 172-175]. Furthermore, deletion of Tet1-3 in mouse embryonic stem cells causes hypermethylation primarily of enhancers and poised promoters [176], strongly suggesting that those are the sites at which active DNA demethylation is taking place.

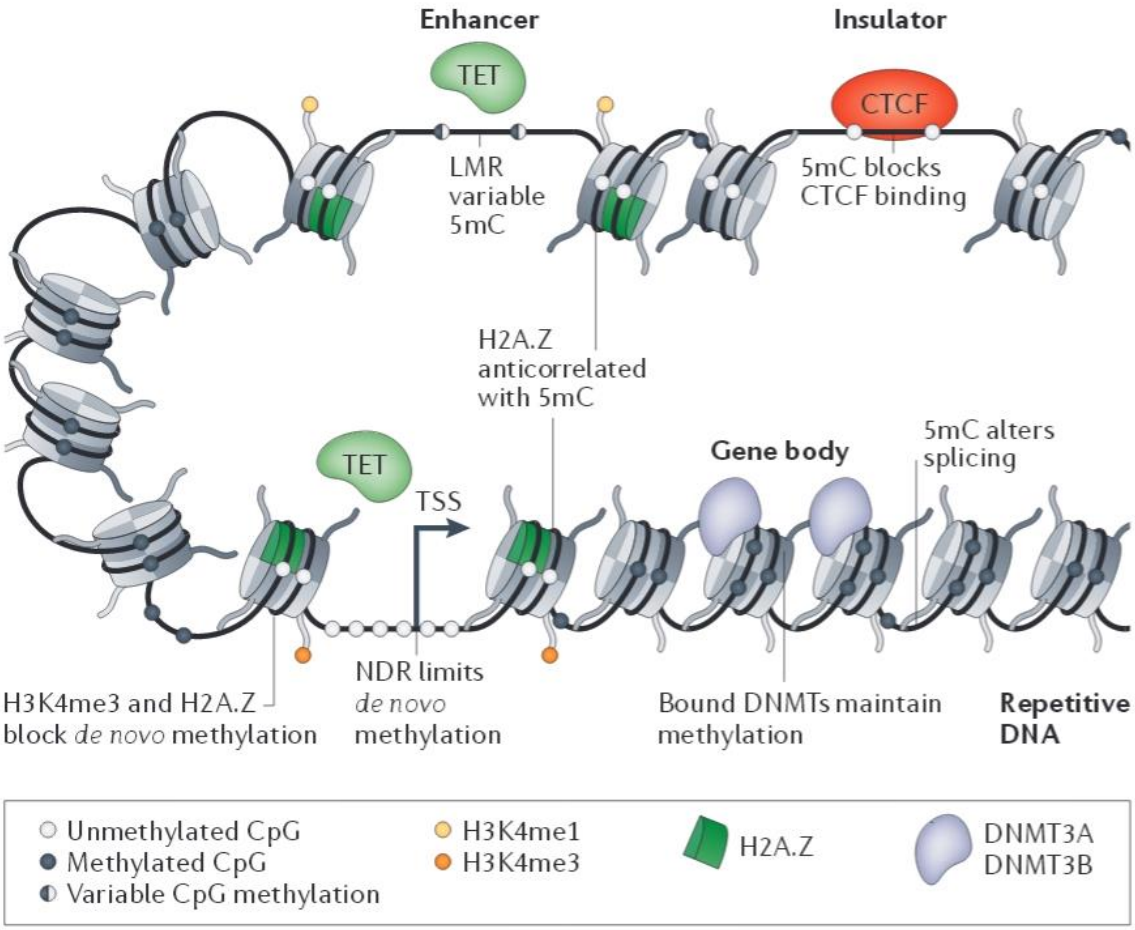

FIGURE 3.4 DISTRIBUTION OF DNA METHYLATION ACROSS GENOMIC REGIONS

The DNA of most intergenic regions, repetitive elements and heterochromatic regions is constitutively methylated in all cells of a body. Gene bodies as well contain predominantly methylated DNA that might be involved in suppressing the use of alternative transcription start sites or in controlling alternative splicing. Around 60% of human genes have CpG islands at their promoters that remain unmethylated independently of the cell type. Transcription start sites (TSS) of the corresponding genes lie in nucleosome depleted regions (NDRs), with surrounding nucleosomes marked by trimethylation of histone 3 at lysine 4 (H3K4me3) and the histone variant H2A.Z. Insulator regions are further regions with nucleosome depletion and unmethylated DNA, as the presence of 5mC can block binding of the insulator proteins CTCF to these sites. Regions that are regulated by variable DNA methylation lie predominantly at enhancers. They are characterized by relative nucleosome depletion, the presence of histone 3 monomethylated at lysine 4 (H3K4me1), H2A.Z, and contain lowly methylated regions (LMRs). Figure from [51].

During differentiation, DNA methylation changes occur very locally and often at early stages of cell type determination [157, 177, 178]. Local DNA demethylation patterns have been mapped to cell type-specific enhancers and promoters during differentiation of hematopoietic stem cells [156, 179], cardiomyocytes [180], mouse embryonic stem cells [174] and human embryonic stem cells [181].

During aging, despite an increasing variability of methylation patterns due to stochastic drift [182], consistently hypermethylated regions could be identified in different cell types. Again, they are preferentially located at enhancers and promoters [183, 184], but have also been linked to CpG islands [182, 185].

It seems likely that local DNA hypermethylation during aging is attributable to failing DNA demethylation processes. However, the precise causes of local hypermethylation during aging remain unknown. Furthermore, it is unclear how the exquisite local specificity of active DNA demethylation during differentiation is achieved. A potential hint might come from the involvement of Gadd45a in TET/TDG-mediated DNA demethylation [139]. Previous work in our laboratory has identified the chromatin reader Ing1 as a factor that recruits Gadd45a to sites of demethylation, linking DNA demethylation to the presence of active histone marks [186]. However, further work is needed to elucidate the role of Gadd45a and Ing1 in DNA demethylation during differentiation and aging.

3.3 INHIBITOR OF GROWTH 1 (ING1)

3.3.1 MOLECULAR FUNCTIONS OF ING1

Inhibitor of growth protein 1 (Ing1) has been first discovered in a screen to identify tumor suppressors [187] and has since been recognized to be a potent inducer of senescence and apoptosis (reviewed in [188-195]). The Ing1 protein comprises several distinct protein domains: Ing1 contains a nuclear localization signal, a nucleolar targeting sequence, and a Lamin interacting domain [196], all of them important for localizing Ing1 predominantly to the nucleus. Moreover, Ing1 contains a plant homeodomain, which mediates binding to H3K4me3 and to a lesser extent also H3K4me2 [197]. A last important domain is the PCNA interacting domain, crucial for PCNA interaction and for mediating many cellular functions of Ing1.

Importantly, Ing1 is a direct interactor of the key tumor suppressor p53. Ing1 and p53 are functionally interdependent and none of the two proteins can exert its functions in cell growth control in the absence of the other [198]. Accordingly, Ing1 and p53 have highly overlapping functions: In response to DNA damage, both induce cell cycle arrest and promote DNA repair, cellular senescence or apoptosis, depending on the severity of the DNA damage [188, 189, 191, 193]. The Ing1/p53 complex directly promotes p21 expression, thereby initiating G1 cell cycle arrest [198]. Furthermore, Ing1 promotes p53 activity and stability through several protein interactions. Ing1 recruits the acetyltransferase p300, which acetylates and activates p53. Furthermore, Ing1 interacts with the deacetylase Sirt1 to inhibit Sirt1-mediated p53 deacetylation and inactivation [199]. Finally, Ing1 prolongs p53 half-life by

competing with the E3 ligase Mdm2 for the same binding site on p53, thus impeding proteasomal degradation of p53 [200].

All characterized Ing1 functions are fully dependent its Ing1's plant homeodomain domain [197, 198, 201], which is required for binding H3K4me3 [197, 202]. Recognizing this histone modification, Ing1 is able to recruit both the histone acetyltransferase complex p300/CBP and the histone demethylase complex Sin3a/HDAC1/HDAC2, thus potentially having activating as well as repressive roles in gene expression regulation [188, 190, 192] (Figure 3.5).

Ing1-mediated histone acetylation is additionally important for DNA repair. Specifically after UV damage, Ing1 associates with the DNA clamp PCNA. Subsequently, Ing1 recruits the p300 to PCNA, initiating histone H4K14 acetylation. This serves as a recruiting signal for Rad18, which mono-ubiquitinates PCNA and initiates translesion DNA synthesis [194, 203-205]. Ing1-mediated histone acetylation relaxes the chromatin structure and is required upstream of several DNA repair pathways, including nucleotide excision repair, base excision repair, homologous recombination and non-homologous end joining [201, 203, 206]. Ing1 recruits the DNA repair protein Gadd45a to its target sites both by promoting histone acetylation [207] and by direct interaction with Gadd45a [203]. After recruitment by Ing1 to the DNA, Gadd45a promotes DNA repair [208-210], and additionally has been shown to promote DNA demethylation [186].

Similar to Gadd45a, Ing1 has been described to directly interact with the MAPK signaling components MAP3K4 and p38. However, the relevance of these interactions has not been further characterized so far [211]. Ing1 can, similar to p53 [212], also translocate to mitochondria after UV or γ-irradiation stress and directly induce apoptosis by stabilizing the apoptosis-promoting protein Bax in a p53-independent fashion [213]. Furthermore, Ing1 might contribute to microRNA regulation by promoting expression of the microRNA processor DGCR8 [214].

The above described functions of Ing1 as a p53 interaction partner mediating cell cycle arrest, DNA repair, senescence and apoptosis make Ing1, similar to p53, a type II tumor suppressor. While rarely mutated, Ing1 is frequently mislocalized or downregulated in tumors [195, 215-217]. A causative role of Ing1 in tumor development has been demonstrated by the analysis of Ing1 knockout mice, which develop normally besides having a slightly smaller body size and frequently develop B cell lymphomas [218].

3.3.2 REGULATION OF ING1

Ing1 expression is induced by various cellular stresses, including UVC irradiation, ionizing radiation, and H_2O_2. Upon DNA damage occurring as a consequence of those stresses, ATM/ATR signaling leads to phosphorylation of Ing1 by the Chk1 protein kinase. This phosphorylation of Ing1 at its Ser126 stabilizes Ing1 protein levels [219].

Cellular localization of Ing1 is crucial for its activity: active Ing1 is localized to the nucleus, while cytoplasmic Ing1 cannot exert its functions. Lamin A, an integral component of the nuclear lamina, tethers Ing1 to the nucleus [196]. Ser199 phosphorylation of Ing1 leads to its displacement to the cytoplasm and consequently to its functional inactivation. Ser199 phosphorylation of Ing1 is catalyzed by Src [220], and acts as a recognition signal for 14-3-3, which shuttles Ing1 from the nucleus to the cytoplasm [221]. There, Ing1 can be ubiquitinated and degraded in the proteasome [222]. Additionally, Ing1 can be sumoylated by PIAS4, with not yet fully elucidated consequences [223]. Stress-inducible phospholipids are able to bind and activate Ing1, adding a further layer of stress-inducible regulation to the Ing1 protein [195] (see also Figure 3.5).

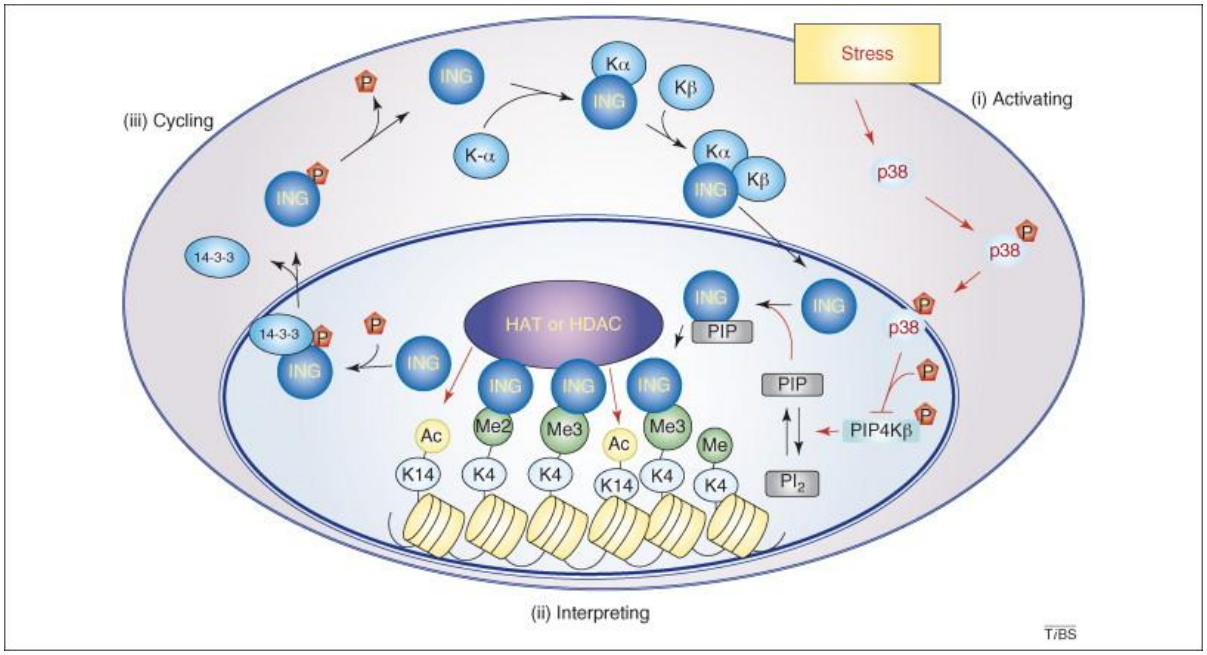

FIGURE 3.5 REGULATION AND MOLECULAR FUNCTIONS OF ING1
Ing1 is activated by several cellular stresses causing DNA damage, which promote Ing1 localization to chromatin. Binding histone 3 trimethylated at lysine 4 (H3K4me3), Ing1 is able to recruit histone acetyltransferases (HAT) or histone deacetylates (HDAC) to chromatin, which leads to altered histone acetylation levels and different biological outcomes such as cell cycle regulation, DNA repair, senescence or apoptosis. Ing1 activity can be regulated by controlling its cellular localization through protein phosphorylation. ING: Inhibitor of growth protein 1; PIP: Phosphatidylinositol monophosphate; K14: Histone H4 Lysine 14; K4: Histone H3 Lysine 4; Me: methyl group; Ac: Acetyl group. Figure from [193].

3.4 GROWTH ARREST AND DNA DAMAGE 45 ALPHA (GADD45A)

3.4.1 MOLECULAR FUNCTIONS OF GADD45A

3.4.1.1 GADD45A IN CELL CYCLE REGULATION AND APOPTOSIS

Growth arrest and DNA damage 45 alpha (Gadd45a) is a small histone fold protein that is located both in the nucleus and cytoplasm. It is a multifunctional protein that is induced by DNA-damaging agents and several cellular stresses. As a direct downstream target of p53 [32] and as an interaction partner of Ing1 [203], Gadd45a functions are highly overlapping with those two proteins and include DNA-damage dependent cell cycle inhibition, DNA repair, and induction of apoptosis. Lacking enzymatic activity, Gadd45a is relying on several interaction partners to exert its various functions.

For inducing cell cycle arrest at the G2 phase, Gadd45a interacts with Cdc2, thereby releasing Cyclin B1 from the Cdc2/Cyclin B1 complex and inhibiting further progression trough the cell cycle [71, 99] [224]. While Gadd45a can also arrest cell cycle at the G1 phase, molecular mechanisms leading to this outcome are less well elucidated. Potentially, Gadd45a interaction with the cell cycle inhibitor p21 and the DNA polymerase processivity factor PCNA inhibits PCNA function, thereby blocking DNA synthesis [108].

Regulation of apoptosis by Gadd45a is mediated through Gadd45a interaction with the MAPK signaling components MAP3K4 and p38 [225-227] (Figure 3.6). All three members of the Gadd45 family, including Gadd45a, are able to bind to MAP3K4, leading to conformational changes in the MAP3K4 protein that allow its dimerization, autophosphorylation and activation [225-227]. Activated MAP3K4 in turn triggers both the p38 and JNK branches of MAPK signaling, with both p38 and JNK being able to initiate apoptosis [41]. Additionally, Gadd45a can directly bind and activate p38 [87, 228]. Depending on the cellular context, Gadd45a has been described to act either anti-apoptotic at low DNA damage levels or pro-apoptotic at high DNA damage levels [42]. Besides apoptosis, Gadd45a-mediated p38 and JNK activation can regulate cell-type specific gene expression and in this manner influence further pathways, including Bmp-, NF-κB- and Wnt-signaling [72, 75, 229].

3.4.1.2 GADD45A IN DNA REPAIR AND DNA DEMETHYLATION

Gadd45a acts in nucleotide excision repair and base excision repair, leading to increased genomic instability and tumorigenesis in Gadd45a knockout mice [210, 230-232]. The exact role of Gadd45a in DNA repair is not well understood, but Gadd45a interacts with several DNA repair associated proteins,

including p53, Ing1 [203], PCNA [108, 233], TDG [138-140] and XPG[137], possibly functioning as an adaptor protein.

Gadd45a is recruited to UV-damaged and hyperacetylated histones [207], with the Gadd45a interaction partner Ing1 promoting the histone acetylation required for Gadd45a recruitment [234]. At these sites, Gadd45a stimulates DNA repair by facilitating chromatin decondensation and thereby increasing accessibility of DNA repair factors to the damaged sites [206, 207]. Gadd45a furthermore facilitates base excision repair by acting as a bridging factor for the base excision repair enzyme Ape1 to PCNA[235].

Its role in nucleotide and base excision repair puts Gadd45a in a position to be potentially involved in DNA repair-mediated DNA demethylation (see chapter 3.2). Recruitment of Gadd45a to specific sites of DNA demethylation can involve transcription initiation complexes [236], the H3K4me3-binding protein Ing1 [186], nuclear hormone receptors [78] or the long non-coding RNA TARID [140]. Subsequent to Gadd45a recruitment, three main molecular mechanisms have been proposed by which Gadd45a might contribute to site-specific DNA demethylation: (1) Gadd45a-dependent recruitment of nucleotide excision repair proteins to excise 20-30 nucleotides around methylated CpGs [36, 137, 236], (2) Deamination of 5mC by AID, followed by Gadd45a-assisted base excision repair [131, 138], and (3) promotion of TET-dependent cytosine oxidation followed by base excision repair [139, 140]. The precise mechanism or mechanisms of how Gadd45a contributes to DNA demethylation are a matter of ongoing investigations.

While Gadd45a is not required for global DNA demethylation [237, 238], several site-specific and cell type-specific targets of Gadd45a-mediated DNA demethylation have been identified. These include the *rDNA* locus, *MAGEB2, DHRS2, TCEAL7* and *TAF7L* in HEK293T cells [186, 236], *Mageb2, Cxcl1* and *Hoxd8* in mouse embryonic fibroblasts [186], and the *TCF21* tumor suppressor in cancer cell lines [140]. Frequently, Gadd45a-depedent DNA demethylation occurs after cell stimulation, e.g. by retinoic acid of HeLa cells [239] or by T cell activating signals [79]. Importantly, differentiation signals lead to Gadd45a-mediated DNA demethylation of crucial cell-type specific genes e.g. during epidermal [240], muscular [80, 121, 240], and osteogenic differentiation [241].

Another protein of the highly homologous Gadd45 protein family, Gadd45b, has been strongly implicated in brain-specific DNA demethylation. Neuronal stimulation elicits DNA demethylation of *Bdnf IX*, *Reelin* and *Fgf1* in mouse hippocampi [126, 242], and Gadd45b-deficient mice show selective deficits in hippocampal long-term potentiation and learning [243]. *Bdnf IX* is also demethylated in human psychosis in a Gadd45b-dependent manner [162], further corroborating the functional relevance of Gadd45b-mediated DNA demethylation in the brain.

3.4.1.3 GADD45A IN DIFFERENTIATION PROCESSES AND AGING

Gadd45a is expressed during mouse development predominantly in cells undergoing differentiation [244]. Indeed, several of Gadd45a's functions, including promoting G1 arrest, MAPK signaling and DNA demethylation could have functional relevance in cellular differentiation processes. While the exact contribution of the various Gadd45a functions has not always been elucidated, many differentiation processes have been shown to be affected by Gadd45a. For example, Gadd45a promotes myeloid differentiation by so far uncharacterized mechanisms [245, 246]. In Xenopus, combined loss of Gadd45a and Gadd45g impairs neuronal differentiation [247], while Gadd45a knockdown in zebrafish causes neuronal loss [131]. *Gadd45a* knockout mice develop partially penetrant exencephaly and neural tube defects [230]. Gadd45a's role in DNA demethylation has been shown to be crucial for differentiation in keratinocytes [240], striated muscle [80, 121, 240] and for osteogenesis [241]. Similarly, especially Gadd45b has likewise been implicated in several differentiation processes, often overlapping with Gadd45a function [75, 232, 240, 248]. Mutants with a combined deficiency for two or all three of the Gadd45 family members have been generated, but not conclusively analyzed yet with regard to their phenotype [249, 250].

Gadd45a expression is regulated by at least two known longevity pathways, namely Sirtuin 1 and Insulin/Igf-1 signaling [31] (chapter 3.4.2). A first indication that Gadd45a might be directly involved in regulating lifespan came from a study that showed that neuron-specific Gadd45 overexpression prolongs lifespan [179] and delays neurodegeneration [88] in *Drosophila*, although ubiquitous Gadd45 overexpression in *Drosophila* caused lethality [251]. However, a potential contribution of Gadd45a to aging and longevity needs to be further corroborated.

3.4.2 REGULATION OF GADD45A

Like Ing1, its interaction partner (Gadd45a) is regulated by a plethora of cellular stresses, including UV irradiation, y-irradiation, hypoxia or hyperosmotic stress [31] and is often induced as a consequence of DNA damage. Upon DNA damage, p53 is activated and promotes Gadd45a expression by directly binding to the third intron of the *Gadd45a* gene [32]. Likely, p53 acts together with its binding partner WT1, which also contains a binding site within the *Gadd45a* locus [33]. Additionally to p53 stimulation, DNA damage activates the ATM and ATR kinases and their downstream target Brca1. Brca1 in turn promotes Gadd45a transcription via interaction with the transcription factors Oct1 and NF-YA, both of which have binding motifs in the Gadd45a promoter [35, 39, 70].

In addition to reacting to DNA damage, Gadd45a levels are also sensitive to the presence of growth factors, e.g. Insulin/IGF-1. Phosphorylation cascades initiated by growth factors ultimately inhibit

FOXO3a, a direct positive regulator of Gadd45a expression. Furthermore, FOXO3a integrates signals from the aging-associated protein acetylase Sirtuin 1 and stress-activated p38 signaling [252, 253]. Activated FOXO3a is able to bind to the three FOXO binding sites in the Gadd45a promoter and promote Gadd45a expression [209] (Figure 3.6).

Gadd45a levels are not only regulated on the transcriptional level, but also controlled via mRNA and protein stability. The ribonuclear proteins AUF-1 and TIAR are negative regulators of Gadd45a levels by destabilizing Gadd45a mRNA or preventing Gadd45a mRNA association with the translation machinery, respectively [254]. Gadd45a protein is ubiquitinated by the E3 ligase Mdm2 and thus targeted for proteasomal degradation. Stress signals may stabilize Gadd45a protein levels by utilizing the ribosomal protein S7 to prevent Mdm2-mediated proteasomal degradation of Gadd45a [255] (Figure 3.6). Gadd45a forms homo- and heterodimers with other proteins of the Gadd45 family, namely Gadd45 beta and Gadd45 gamma [256]. Hence, Gadd45a can potentially act redundantly with other members of the Gadd45 family. While all three Gadd45 family members are stress-induced, they are expressed differentially across tissues and developmental stages, thus likely fulfilling at least partially distinct biological roles.

3.5 AIM OF THE THESIS

Gadd45a and Ing1 are interacting proteins [203] that cooperate in DNA demethylation in HEK293T cells and mouse embryonic fibroblasts [186]. However, it is unclear what biological relevance this interaction has and in which physiological processes Gadd45a- and Ing1-mediated DNA demethylation plays a role. Furthermore, *in vivo* targets of Gadd45a- and Ing1-mediated DNA demethylation that could mediate the affected physiological processes are not known.

In order to phenotypically and molecularly characterize the biological relevance of Gadd45a-Ing1 interaction, I analyzed mutant mice lacking Gadd45a and Ing1. I examined embryonic phenotypes as well as adult phenotypes of these knockout mouse strains by characterizing macroscopic and histological defects, studying whole genome gene expression changes in different affected tissues and elucidating molecular pathways that are affected by single or combined loss of Gadd45a and Ing1. Moreover, I established a differentiation model to recapitulate phenotypes caused by loss of Gadd45a and Ing1 in a cell culture model and used it to gain further insights in affected molecular pathways. Together with Medhavi Mallick, regions that were differentially methylated in cells deficient for Gadd45a and Ing1 were identified.

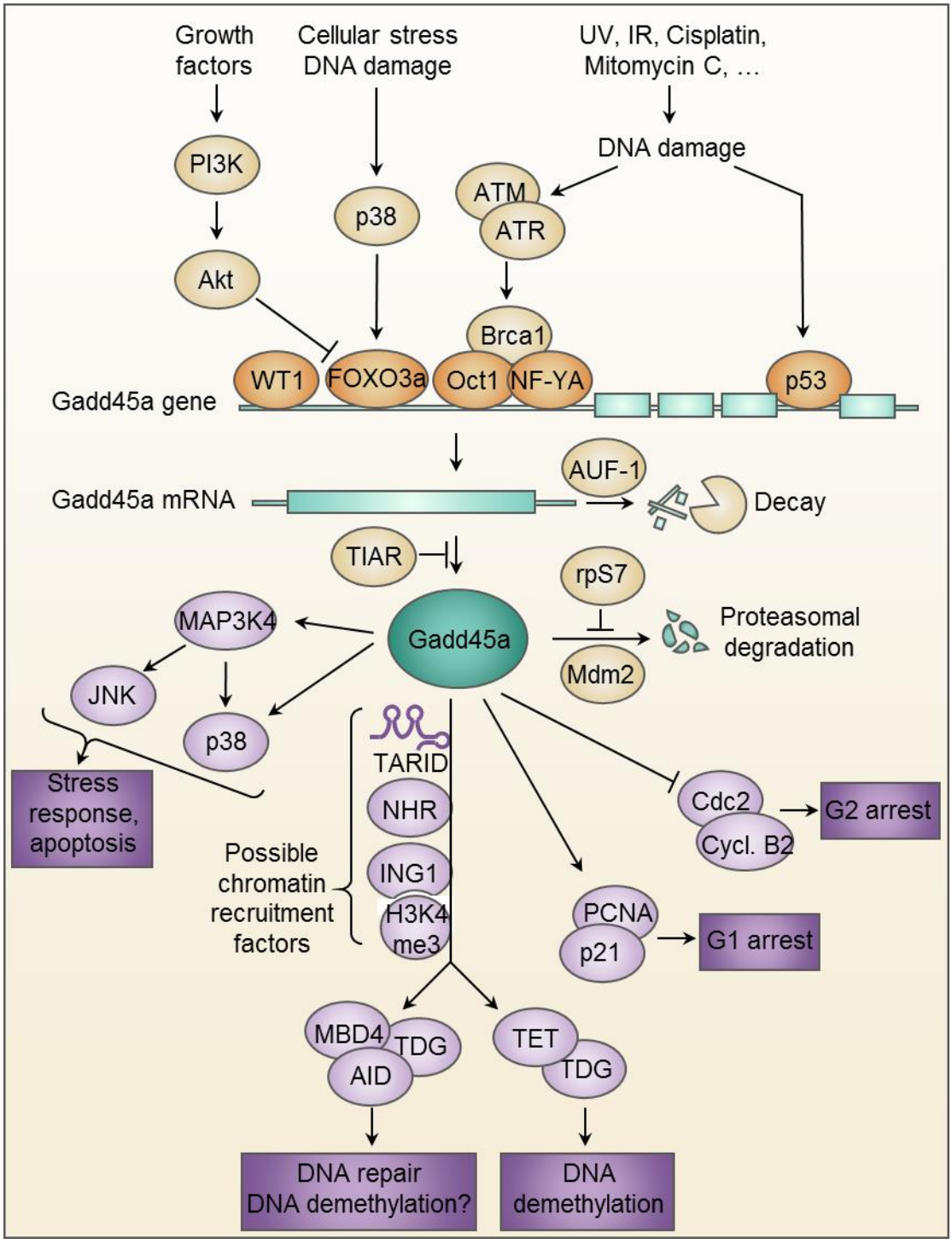

FIGURE 3.6 REGULATION AND MOLECULAR FUNCTIONS OF GADD45A

Gadd45a expression is induced by several cellular stresses, many of which lead to DNA damage. Gadd45a has a high turnover and is regulated on gene expression, mRNA stability and protein stability levels. Having no enzymatic function, Gadd45a exerts its function by interactions with several proteins. Various protein-protein interactions mediate its functions in cell cycle arrest at the G1 or G2 phase, DNA repair, senescence, apoptosis and DNA-repair mediated DNA demethylation. Brown: Proteins regulating Gadd45a. Green: Gadd45a. Light purple: Gadd45a interacting proteins. Dark purple: Biological processes regulated by Gadd45a. See main text for further information and abbreviations.

4. Results

4.1 G45A$^{-/-}$ ING1$^{-/-}$ MICE SHOW PARTIALLY PENETRANT NEURAL TUBE AND SKELETAL PHENOTYPES

Gadd45a and Ing1 have been shown to synergize in promoting active DNA demethylation on a reporter plasmid and on endogenous loci in human HEK293T and mouse embryonic fibroblast (MEF) cells [186]. However, it was unknown what consequences Gadd45a and Ing1's role in DNA demethylation has *in vivo* on e.g. development and disease. Knockout mice for Gadd45a (from hereon called G45a) as well as for Ing1 have been described, however loss of either G45a or Ing1 is compatible with normal development and leads to only mild phenotypes [218, 230]. Thus, to more thoroughly investigate a biological role of G45a and Ing1 interaction, compound homozygous G45a$^{-/-}$ Ing1$^{-/-}$ knockout mice were bred and analyzed.

As a first step, embryonic phenotypes in G45a and Ing1 single and double knockout mice were examined. Matings of double heterozygous animals (G45a$^{+/-}$ Ing1$^{+/-}$) were set up and embryos were analyzed at embryonic day 15 (E15.5). In 459 embryos obtained from 64 individual matings, all expected genotypes were present at approximately Mendelian ratios (Figure 4.1A). No bias towards males or female animals was observed.

Embryos deficient for G45a displayed partially penetrant exencephaly, as already reported by Hollander et al. [230]. Due to missing cranial vaults, brains of affected embryos protruded and were abnormally large. In addition, loss of G45a lead to partially penetrant spina bifida, besides exencephaly a related neural tube closure defect. These neural tube closure defects were compatible with embryonic survival, but lead to perinatal death of affected pups. Additionally, loss of G45a caused curly tails in 16% of the animals. Having one of the above G45a$^{-/-}$ defects did not predispose to others, as each of the three described phenotypes could occur either by itself or in combination with any of the other phenotypes. Phenotypes present in Ing1 deficient embryos included a small body size in 2% of embryos and generalized edema in 11% of embryos. All of the phenotypes detected in G45a$^{-/-}$ or Ing1$^{-/-}$

FIGURE 5

embryos were also apparent in embryos lacking both G45a and Ing1. However, no further developmental abnormalities appeared that were not already observed in the single mutants (Figure 4.1B and Figure 4.1C).

A subset of G45a$^{+/-}$ Ing1$^{-/-}$ embryos displayed exencephaly and spina bifida, which otherwise only occurred in embryos fully deficient of G45a. Conversely, a fraction of G45a$^{-/-}$ Ing1$^{+/-}$ embryos developed generalized edemas, otherwise a sign of homozygous Ing1 deletion (Figure 4.1B). This appearance of phenotypes in G45a/Ing1 heterozygous backgrounds might be a first hint at a genetic interaction and potential synergism between G45a and Ing1 *in vivo*.

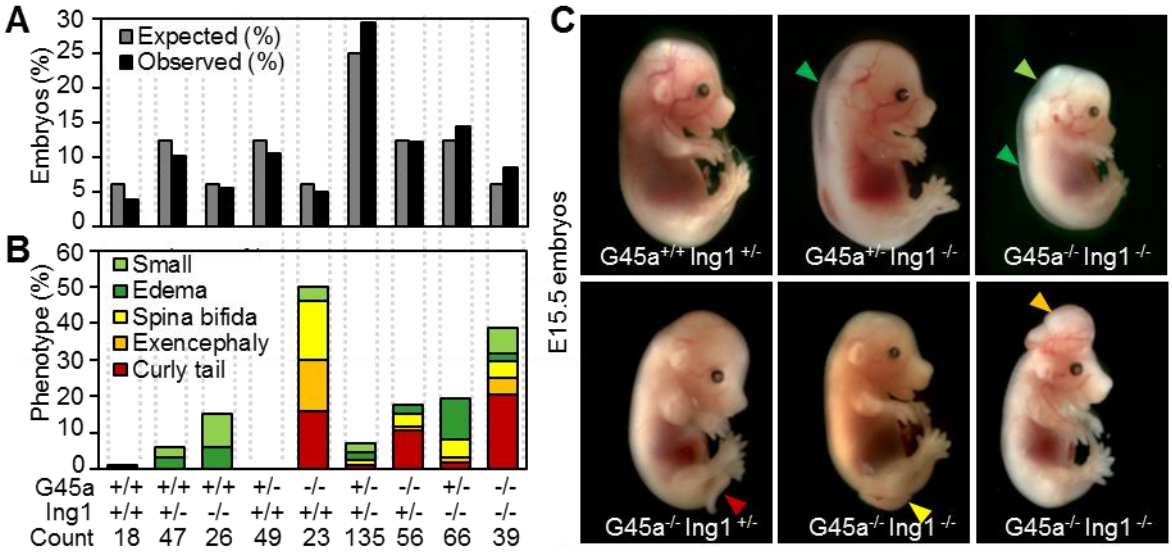

FIGURE 4.1 LOSS OF G45A OR ING1 CAUSES DISTINCT PARTIALLY PENETRANT EMBRYONIC PHENOTYPES
A Expected and observed occurrence of genotypes in progenies from G45a/Ing1 double heterozygous matings. **B** Occurrence of embryonic phenotypes in progenies of G45a/Ing1 double heterozygous matings. **C** Phenotypes appearing in E15.5 mouse embryos. Arrows point to developmental defects. Color code of arrows identical to color code of Figure 4.1B.

Clear synergism between G45a and Ing1 was observed when analyzing young adult knockout animals at 8 weeks of age. About 40% of examined G45a$^{-/-}$ Ing1$^{-/-}$ mice displayed dysmorphic facial features with a shortened snout and a domed head, a phenotype never observed in WT or single knockout animals. This was apparent both upon exterior observation of mice as well as on skulls stained with Alizarin Red and Alcian Blue to visualize bone and cartilage (Figure 4.2A). Morphometric analysis of skulls confirmed a shortening specifically of the mandibular region in G45a$^{-/-}$ Ing1$^{-/-}$ animals, while other cranial measurements were normally proportioned (Figure 4.2B). Since G45a$^{-/-}$ Ing1$^{-/-}$ mice were often smaller than wildtypes (see Figure 4.4), quantifications were carried out as ratios of different cranial measurements to identify only disproportionate skull features rather than systematic size differences.

Alizarin Red and Alcian Blue staining of skulls further revealed open sagittal and posterior frontal sutures in 4 out of 5 analyzed G45a$^{-/-}$Ing1$^{-/-}$ mice, but none of the wildtype or single knockout mice. In contrast to G45a$^{-/-}$ Ing1$^{-/-}$ mice, these structures fuse in healthy animals at the latest at 6 weeks of age [257, 258].

In 2 out of 5 analyzed G45a$^{-/-}$ Ing1$^{-/-}$ skulls, an asymmetric hypoplasia of maxillae and nasal bones caused a curvature of the snout to either the left or right side, which resulted in a misalignment of upper and lower incisors (Figure 4.2A). Since rodent teeth grow throughout the animals' lifetime and need to be ground against each other to keep their lengths constant, malocclusion will result in unrestrained incisor growth. This will, if left uncontrolled, impede food uptake of the affected animal. Thus, incisors of mice suffering from malocclusion were regularly trimmed. Nonetheless, one cannot exclude secondary effects of incisor overgrowth on animal health that are not directly caused by the loss of G45a or Ing1. Thus, to minimize confounding factors, any mice showing incisor overgrowth were excluded from further analyses.

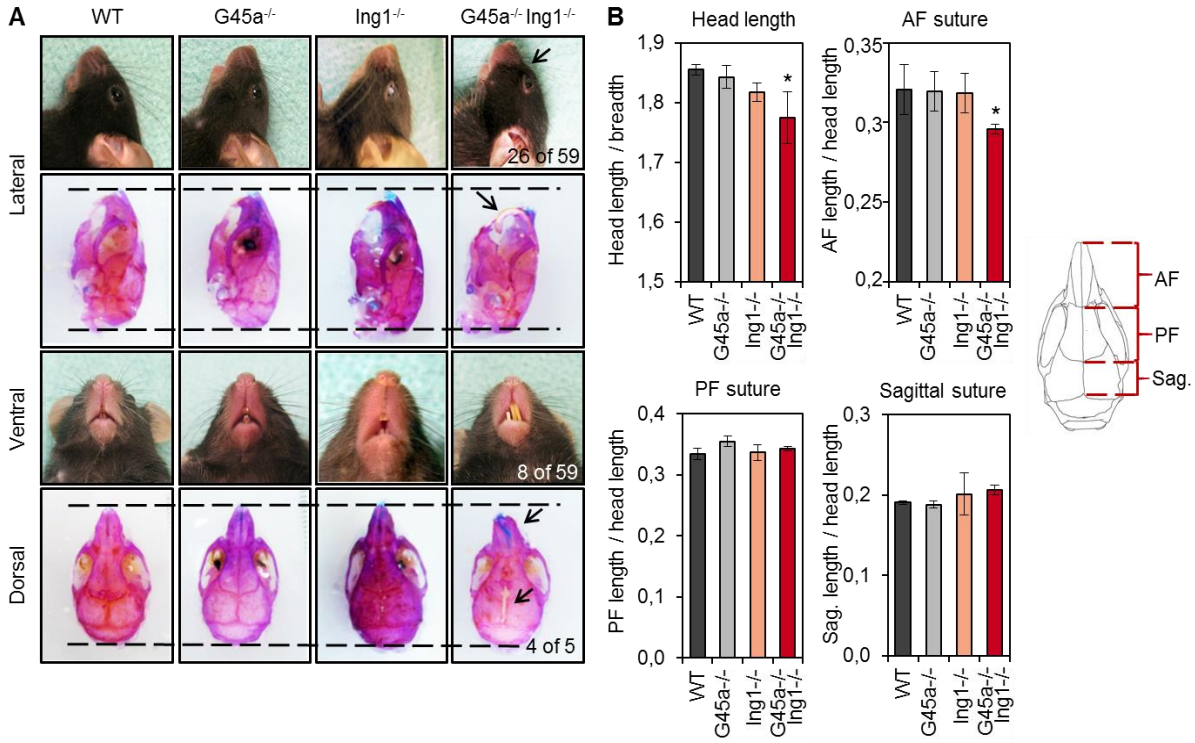

FIGURE 4.2 G45A$^{-/-}$ ING1$^{-/-}$ ADULT MICE DISPLAY INCISOR MISALIGNMENT AND OPEN SAGITTAL SUTURES

A Macroscopic views of heads and Alcian/Alizarin stainings of skulls. Arrows point to G45a$^{-/-}$ Ing1$^{-/-}$ phenotypes (from top to bottom): Domed head, incisor overgrowth, curved nose, and open sagittal and posterior frontal sutures. Numbers indicate the penetrance of displayed phenotypes in G45a/Ing1-deficient mice. **B** Quantification of skull measurements and scheme of analyzed regions. AF: Anterior frontal suture. PF: Posterior frontal suture. Sag.: Sagittal suture. n=4-5/genotype. Data presented as mean ± STDEV, * $p<0.05$ (Student's t test).

4.2 G45A$^{-/-}$ ING1$^{-/-}$ MICE DEVELOP PREMATURE AGING

While embryos at E15.5 were present at the expected Mendelian ratios (Figure 4.1A), only about 80% of expected numbers of 3-week-old G45a$^{-/-}$ and Ing1$^{-/-}$ mice, respectively, were present as detected after genotyping. For mice deficient for both G45a and Ing1, this ratio fell to approximately 60%. This means that during the first weeks of life, a fraction of single and double knockout animals have died. This can be explained at least partially by perinatal death of pups with exencephaly and spina bifida. However, any potentially additional reasons of death cannot be excluded.

After weaning, G45a$^{-/-}$ Ing1$^{-/-}$ mice were successively dying at young ages and reached a median lifespan of only 3 months. At 6 months of age, at a time where over 80% of G45a$^{-/-}$ and 95% of Ing1$^{-/-}$ animals were alive, only 10% of G45a$^{-/-}$ Ing1$^{-/-}$ mice had survived (Figure 4.3). Thus, the observed high lethality was specific to a combined loss of G45a and Ing1. Survival curves of WT animals could not be determined since WT mice were rarely bred until their natural death.

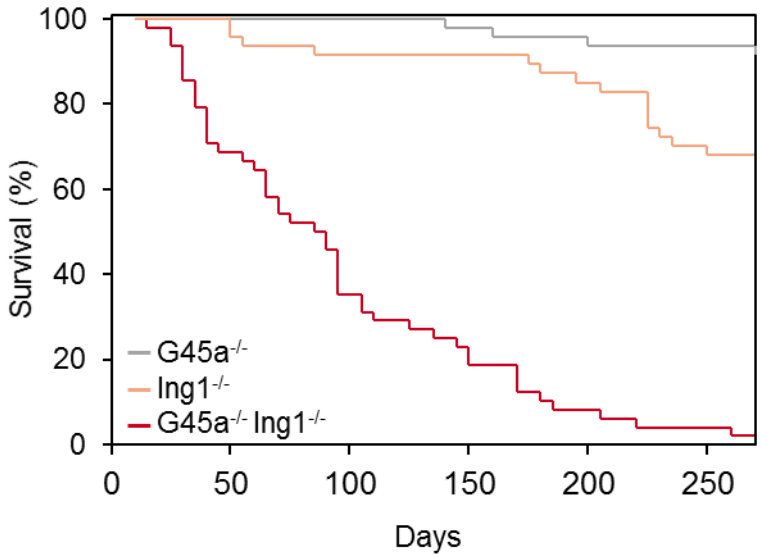

FIGURE 4.3 G45A$^{-/-}$ ING1$^{-/-}$ MICE HAVE A MEDIAN LIFESPAN OF 2 MONTHS
Kaplan-Meier survival curves of G45a$^{-/-}$, Ing1$^{-/-}$, and G45a$^{-/-}$ Ing1$^{-/-}$ mice. Evaluation performed by Dr. Andrea Schäfer.

Post-mortem analysis of euthanized moribund G45a$^{-/-}$ Ing1$^{-/-}$ animals revealed heterogeneous pathologies including intestinal hemorrhages, enlarged gall bladders, renal cysts and one ovarian tumor. In most cases however, the cause of death of G45a- and Ing1-deficient mice could not be conclusively determined. Due to the early lethality of G45a$^{-/-}$ Ing1$^{-/-}$ mice, all following phenotypic and molecular examinations were carried out in mice of approximately 60 days of age, corresponding to the

median life span of G45a$^{-/-}$ Ing1$^{-/-}$ animals. Several highly variable and partially penetrant phenotypes were observed that are consistent with a premature aging syndrome.

8-week old G45a$^{-/-}$ Ing1$^{-/-}$ mice, but not single mutant mice, frequently had a smaller body size than age- and sex-matched WT animals (Figure 4.4A). This was accompanied by a body weight reduction in 71% of G45a$^{-/-}$ Ing1$^{-/-}$ mice, with both male and female mice being equally affected (Figure 4.4B). G45a$^{-/-}$ Ing1$^{-/-}$ animals suffering from incisor overgrowth were excluded from these analyses in order to remove potential confounding factors. Reduced body weight, however without a reduction of body size, was also observed in 69% of analyzed Ing1$^{-/-}$ mice (Figure 4.4A,B). Thus, loss of Ing1 seems to be the driver of the body weight reduction, while decreased body size is a compound phenotype of a combined loss of G45a and Ing1. Similarly decreased body sizes, due to growth retardations and failure to thrive, are a frequently observed symptoms of segmental premature aging [9-11, 259].

Reduced body size and weight could potentially also be secondary to decreased food uptake. However, the food and water consumption of G45$^{-/-}$ Ing1$^{-/-}$ mice was comparable to WT (data not shown). Another potential reason for decreased body size and weight is a decreased resorption of nutrients in the gastrointestinal tract. While this cannot be fully excluded, histological analysis of stomach, small intestine and colon did not reveal any obvious defects in the analyzed animals (data not shown). Thus, reduced body weight in Ing1$^{-/-}$ and G45a$^{-/-}$ Ing1$^{-/-}$ mice is likely not caused by undernourishment.

14 % of examined G45a$^{-/-}$ Ing1$^{-/-}$ animals developed a clearly visible kyphosis (convex curvature of the spine, or hunchback), and scoliosis (lateral curvature of the spine) was detectable in a subset of G45a$^{-/-}$ Ing1$^{-/-}$ animals at closer examination. None of the WT or single knockout mice showed comparable phenotypes at the analyzed age of 60 days (Figure 4.4A). Kyphosis and scoliosis were not caused by congenital skeletal defects, as skeletons analyzed by Alizarin and Alcian staining showed no abnormalities apart from the skull (see chapter 4.1). Both kyphosis and scoliosis are frequently observed in old wildtype mice as well as several mouse models of premature aging [9, 37, 260] and are indicative of an underlying osteoporosis. Osteoporosis affects predominantly females [261], which is reflected in the occurrence of kyphosis in 26% of female but only 8% of male G45a$^{-/-}$ Ing1$^{-/-}$ mice. However, further analyses are needed to corroborate a *bona fide* osteoporotic phenotype in G45a$^{-/-}$ Ing1$^{-/-}$ mice.

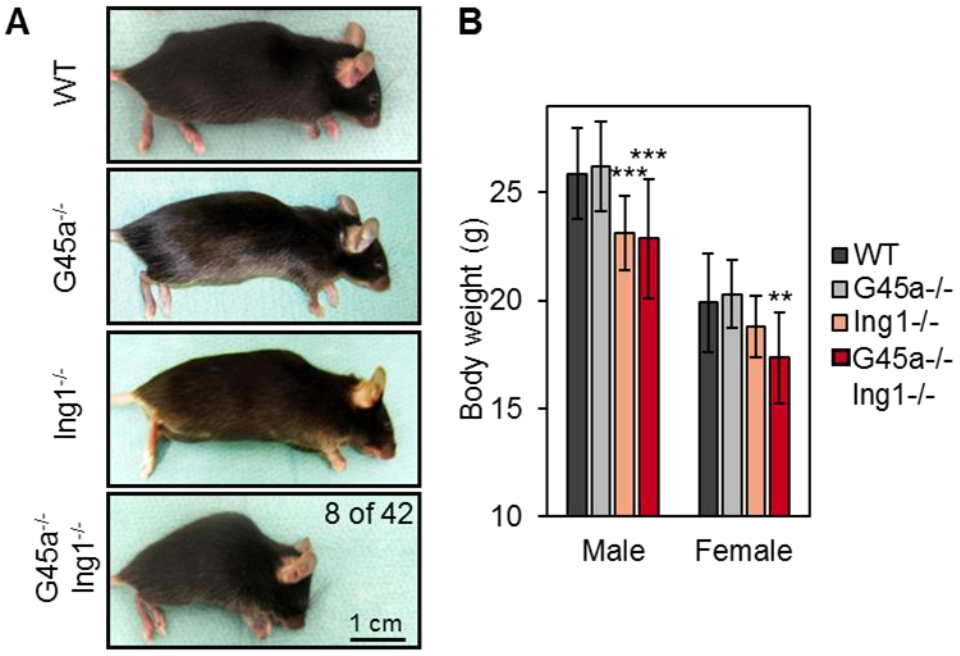

FIGURE 4.4 MICE WITH COMBINED LOSS OF G45A AND ING1 FREQUENTLY DEVELOP KYPHOSIS, A REDUCED BODY SIZE AND A REDUCED BODY WEIGHT

A Lateral view of 8-week old female mice from indicated genotypes. Numbers indicate phenotypic penetrance in G45a$^{-/-}$ Ing1$^{-/-}$ mice. **B** Body weight of male and female 8-week old mice from indicated genotypes. Data presented as mean ± s.d. of 10-33 animals per sex and genotype. ** $p<0.01$, *** $p<0.001$ (Student's t test).

To gain a more detailed insight into possible phenotypes of G45a and Ing1 knockout mice, a histological analysis of all major organs via H&E stainings was conducted in three 6-week old female mice per genotype. Many of the examined organs, including brain, pituitary gland, thymus, heart, lung, spleen, stomach, small intestine, colon, pancreas, kidneys, or adrenal glands did not show any defects visible by histological examination (data not shown). On the other hand, reproductive organs of both sexes, skin, femoral bone, and adipose tissue attached to the ovaries and kidneys showed reproducible phenotypes that will be elaborated in the following sections.

Female mice deficient for G45a and Ing1 were infertile and did not produce offspring when mated to WT males. While loss of G45a alone had no discernible effect on reproductive performance, females deficient of Ing1 alone were subfertile, produced smaller litter sizes and frequently cannibalized their offspring. These phenotypes were accompanied by morphological changes of the ovaries: Severe ovarian atrophy was observed in 68% of G45a$^{-/-}$ Ing1$^{-/-}$ females both macroscopically and on H&E-stained ovary sections, whereas a slight atrophy was already apparent in 11% of Ing1$^{-/-}$ ovaries (Figure 4.5A).

While G45a$^{-/-}$ Ing1$^{-/-}$ ovaries contained some (albeit few) follicles of all developmental stages, corpora lutea were absent in their ovaries (Figure 4.5A,B). Since corpora lutea are formed after successful ovulation, it is likely that oocytes in G45a$^{-/-}$ Ing1$^{-/-}$ ovaries developed but never ovulated. Indeed, mature tertiary follicles of G45a$^{-/-}$ Ing1$^{-/-}$ mice contained high amounts of apoptotic cells indicating that follicles were instead resorbed (data not shown). An absent ovulation was also confirmed by microscopical analysis of vaginal smears, which allows the determination of estrus cycle phases according to the presence of characteristic cell types at each phase [262]. Using this analysis, normal estrus cycles with an average duration of 4-6 days were observed in WT and G45a$^{-/-}$ animals. Ing1$^{-/-}$ females however had in 1 out of 3 analyzed cases disturbed ovulatory cycles with irregular and infrequent estrus phases. In G45a$^{-/-}$ Ing1$^{-/-}$ females, no estrus was observed during the whole observation period of 16 days, confirming that no ovulation was taking place (Figure 4.5A).

Quantification of absolute follicle numbers on H&E stained ovary sections showed that G45a$^{-/-}$ Ing1$^{-/-}$ ovaries already contained less primary follicles than WT controls (Figure 4.5B). Potential reasons include an impaired development of follicles, early exhaustion of follicles or hormonal imbalance.

To test for hormonal dysregulation, pituitary glands from WT, single and double knockout females were isolated and pituitary hormone gene expression was measured by qPCR. Since hormonal gene expression follows a circadian rhythm and times of tissue isolations were not synchronized, observed gene expression patterns showed considerable variation. With this caveat in mind, no significant difference in hormone levels were detected between the analyzed genotypes, except for an elevation in follicle stimulating hormone levels in G45a$^{-/-}$ Ing1$^{-/-}$ females (data not shown). Increased levels of follicle stimulating hormone are indicative of premature ovarian aging and likewise occur during menopause [263, 264].

Another potential cause of reduced primary follicle numbers in G45a/Ing1-deficient mice is a developmental defect. Early steps in follicle generation include the development of primordial germ cells in the embryo and the start of meiosis in embryonic ovaries. To analyze whether meiotic defects might contribute to the paucity of follicles in G45a$^{-/-}$ Ing1$^{-/-}$ ovaries, expression of genes crucial for meiosis was analyzed in E15.5 embryonic ovaries. Expression of genes necessary for the formation of meiotic complexes including *Mael*, *Sycp1* and *Sycp3* were at least 30% reduced in ovaries lacking both G45a and Ing1, and interestingly already in ovaries deficient for G45a alone (Figure 4.5C). Taken together, these results show that loss of G45a and Ing1 leads to female infertility due to a combination of meiotic defects during oocyte generation and impaired ovulation resulting from a menopause-like phenotype.

Male reproductive phenotypes were milder than those observed in female G45a/Ing1 knockout mice. A histological examination showed a reduction of spermatid numbers but a normal count of spermatogonia, again hinting at a mild meiotic defect also in males (data not shown). An attempted corroboration of this observation by flow cytometric analysis of different testis cell populations failed to show any defects in an independent set of G45a$^{-/-}$ Ing1$^{-/-}$ males (data not shown). A failure to confirm the histological results in independent animals could however also be explained by a low penetrance of male reproductive phenotypes.

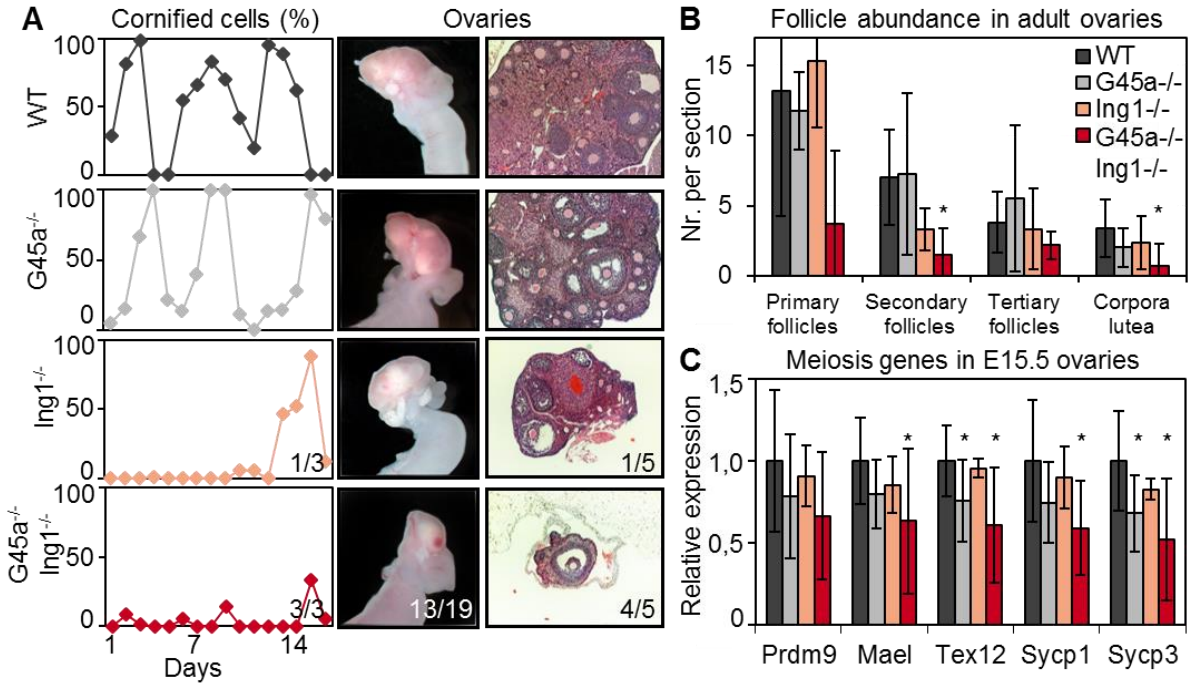

FIGURE 4.5 COMBINED LOSS OF G45A AND ING1 CAUSES FEMALE INFERTILITY THROUGH ATROPHIED OVARIES, FOLLICLE DEPLETION AND ABSENT OVULATION

A Left: Percentage of cornified epithelial cells in vaginal smears, indicating estrus. Middle: Macroscopic view of ovaries. Right: H&E stainings of ovaries at 250x magnification. Embedding, sectioning and staining performed by Gabriele Schmidt, Gröhne lab, DKFZ. **B** Quantification of oocytes in different stages from ovary H&E sections. **C** qPCR analysis of gene expression of meiosis-related genes in E15.5 embryonic ovaries. n=9-11/genotype except for Ing1$^{-/-}$ (n=3). Data presented as mean ± s.d., * $p<0.05$ (Student's t test).

Another frequently observed phenotype during physiological and premature aging is a decreased skin thickness and loss of subcutaneous adipose tissue [261, 265]. Dorsal skin of 6-week old WT, single and double knockout animals was analyzed with H&E stainings, and indeed, a reduction specifically in dermal thickness was detected (Figure 4.6A,B). This was accompanied by a strong increase in the amount of senescent cells in the dermis, as analyzed by senescence-associated β-Galactosidase staining on skin sections (Figure 4.6A,C).

Hair follicles and glands appeared normal in histological analyses. However, mild alopecia and partial hair greying were observed in over 200 day old male G45a$^{-/-}$ Ing1$^{-/-}$ animals (data not shown), indicating that G45a-and Ing1-deficient mice might be prone to premature hair greying or hair loss. This was rarely observed (n=2), likely since most G45a$^{-/-}$ Ing1$^{-/-}$ animals die before this phenotype can manifest.

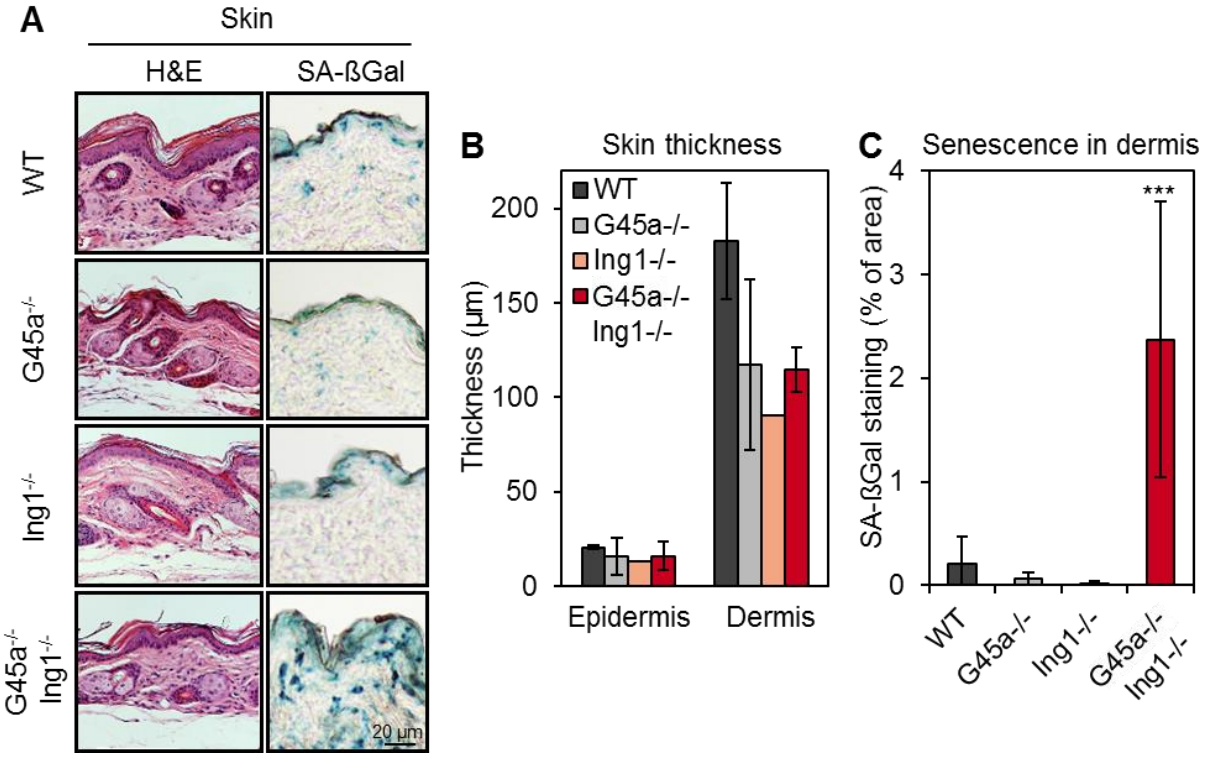

FIGURE 4.6 LOSS OF G45A AND ING1 LEADS TO ATROPHIED AND SENESCENT SKIN

A Left: H&E stainings of paraffin-embedded hindlimb skin at 100x magnification. Embedding, sectioning and staining performed by Gabriele Schmidt, Gröhne lab, DKFZ. Right: Senescence-associated β-Galactosidase (SA-βGal) staining at pH 6.0 of cryosectioned dorsal skin. **B** Quantification of epidermal and dermal thickness of skin H&E stainings shown in (A). Values represent mean ± s.d., n=1-4 animals/genotype. **C** Quantification of SA-βGal staining in (A) as percent of stained area using thresholded signal intensities. Data presented as mean ± s.d, n=5 animals per genotype, *** $p<0.001$ (t test).

An additional affected tissue in G45a$^{-/-}$ Ing1$^{-/-}$ mice was the bone marrow. Histological analysis at two different sites (femur and coxa) revealed a partial loss of hematopoietic bone marrow cells and their replacement by lipid-filled vacuoles (Figure 4.7A). This phenotype, like most other observed phenotypes, was partially penetrant in G45a$^{-/-}$ Ing1$^{-/-}$ animals (Figure 4.7B). Like the ovary phenotypes described above, mild defects were already apparent in animals lacking Ing1 alone, showing that loss of Ing1 was the driver of the phenotype. Again, the more severe defect caused by combined loss of G45a and Ing1 points to a synergism between the two proteins.

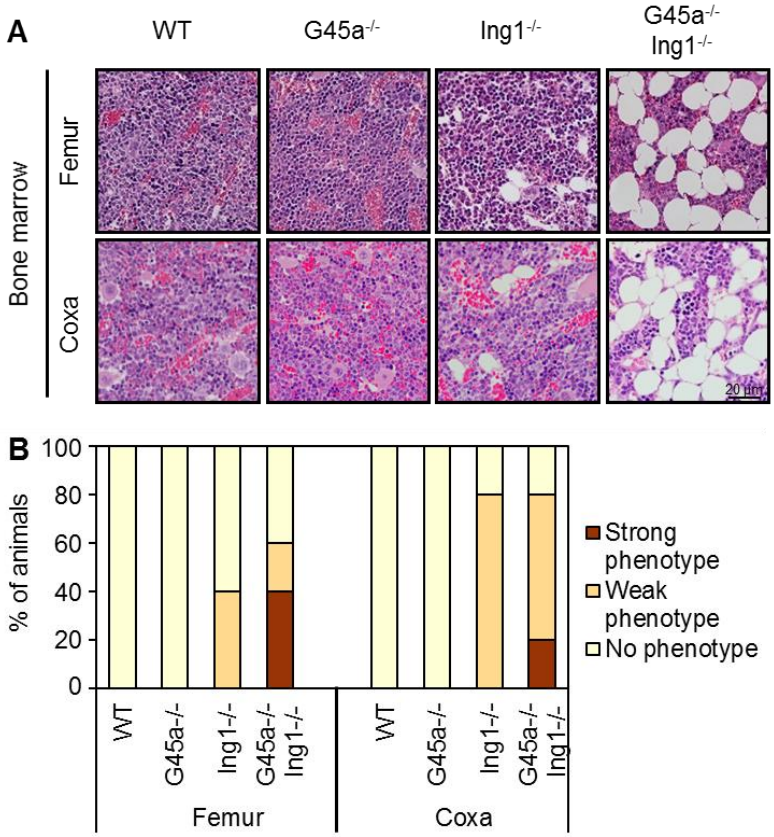

FIGURE 4.7 COMBINED LOSS OF G45A AND ING1 PROMOTES REPLACEMENT OF BONE MARROW CELLS BY ADIPOCYTES

A H&E stainings of bone marrow within decalcified, paraffin-embedded bones of indicated regions. n=3-5 animals/genotype. Embedding, sectioning and staining performed by Gabriele Schmidt, Gröhne lab, DKFZ. **B** Quantification of (A).

Since G45a has been previously implicated in the development of systemic lupus erythematosus [79, 266], an autoimmune disease manifesting itself predominantly in kidneys, kidneys of 8-week old G45a- and Ing1- deficient mice (3 pools of 3 sex-and age-matched mice each) were analyzed by gene expression microarrays. In G45a$^{-/-}$ Ing1$^{-/-}$ kidneys, 257 genes were downregulated and 319 genes were upregulated at a cutoff of 1.2-fold differential expression. Comparable numbers of genes were also deregulated in G45a$^{-/-}$ and Ing1$^{-/-}$ kidneys, with a modest overlap of deregulated genes between the

different genotypes (Figures 4.8A, C). Downregulated genes in G45a$^{-/-}$ Ing1$^{-/-}$ kidneys were slightly enriched for ion transporters (Figure 4.8B), pointing to a mild functional impairment of G45a$^{-/-}$ Ing1$^{-/-}$ kidneys. Upregulated genes in G45a$^{-/-}$ Ing1$^{-/-}$ kidneys were preferentially involved in immune response, wound healing, and extracellular matrix functions (Figure 4.8D). This hints at an early autoimmune glomerulonephritis in G45a$^{-/-}$ Ing1$^{-/-}$ mice, consistent with reports of a similar phenotype at older ages in G45a$^{-/-}$ mice [266].

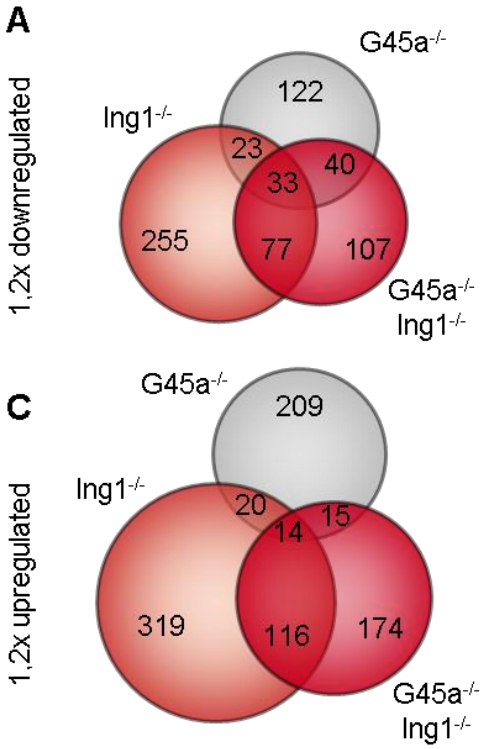

B

GO term	Gene count	P value
Transmembrane transport	13	3,2E-3
Lipid biosynthesis	9	1,0E-2
Steroid hormone biosynthesis	4	1,5E-2
Ion transport	13	1,2E-2
ATPase activity	5	2,2E-2

D

GO term	Gene count	P value
Extracellular matrix	21	1,7E-8
Response to wounding	22	9,6E-9
Immune response	23	4,1E-7
B cell mediated immunity	6	1,8E-3

FIGURE 4.8 TRANSCRIPTOMIC ANALYSIS OF G45A$^{-/-}$ ING1$^{-/-}$ KIDNEYS SUGGESTS FUNCTIONAL IMPAIRMENT AND INCREASED IMMUNE RESPONSE

Microarray gene expression analysis of kidneys from 3 pools à 3 animals per genotype. Initial bioinformatic analysis by Dr. Emil Karaulanov. **A** Venn diagram showing the overlap of ≥ 1.2x downregulated genes in kidneys of indicated genotypes. **B** Gene ontology (GO) classification of ≥ 1.2-fold downregulated genes in G45a$^{-/-}$ Ing1$^{-/-}$ kidneys compared to WT. **C** Venn diagram showing the overlap of ≥ 1.2x upregulated genes in kidneys of indicated genotypes. **D** Gene ontology (GO) classification of ≥ 1.2-fold upregulated genes in G45a$^{-/-}$ Ing1$^{-/-}$ kidneys compared to WT.

To characterize metabolic changes, microarray expression analysis of WT, G45a$^{-/-}$, Ing1$^{-/-}$ and G45a$^{-/-}$ Ing1$^{-/-}$ livers (3 pools of 3 sex-and aged matched mice each) was conducted, since liver is one of the most important metabolic organs. At a cut-off of 1,2x differential expression, 485 genes were upregulated and 532 genes were downregulated in G45a$^{-/-}$ Ing1$^{-/-}$ livers (Figure 4.9A). Already loss of Ing1 caused a subset of G45a$^{-/-}$ Ing1$^{-/-}$ deregulated genes to be misexpressed, while knockout of G45a alone had a smaller effect (Figure 4.9A). Upregulated pathways in G45a$^{-/-}$ Ing1$^{-/-}$ livers included fatty acid catabolism, peroxisomes, glucose catabolism, glycolysis, and stress responses. This highlights a

globally increased catabolism of G45a$^{-/-}$ Ing1$^{-/-}$ mice. Downregulated genes in G45a$^{-/-}$Ing1$^{-/-}$ liver were enriched for genes involved in steroid hormone biosynthesis, cholesterol biosynthesis, complement system and immune response (Figure 4.9B). Examples of deregulated genes from all analyzed gene ontology categories could be validated in independent liver samples by qPCR (Figure 4.9C).

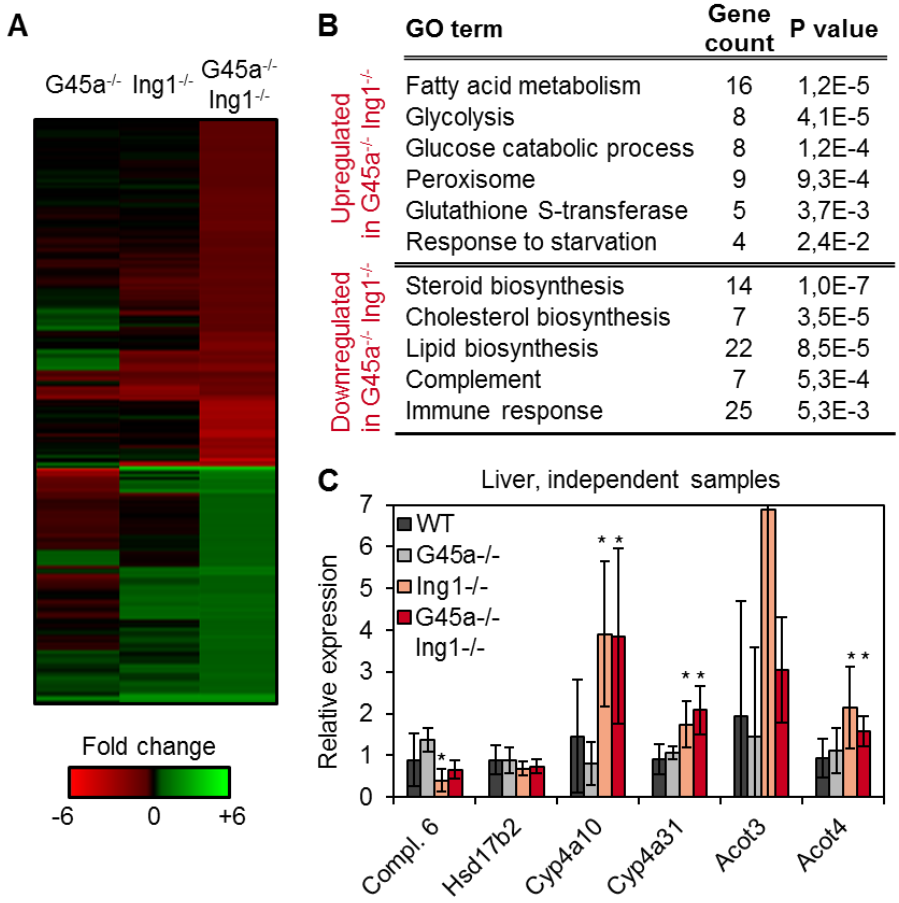

FIGURE 4.9 LOSS OF G45A AND ING1 LEADS TO INCREASED CATABOLIC ACTIVITY AND A PARTIALLY AGING-ASSOCIATED GENE EXPRESSION SIGNATURE IN THE LIVER
Microarray gene expression analysis of liver from 3 pools à 3 animals per genotype. Initial bioinformatic analysis by Dr. Emil Karaulanov. **A** Heatmap of upregulated genes (green) and downregulated genes (red) in G45a$^{-/-}$ Ing1$^{-/-}$ liver. Color intensities are proportional to strength of expression deregulation. **B** Gene ontology (GO) classification of genes upregulated or downregulated ≥ 1.2-fold in G45a$^{-/-}$ Ing1$^{-/-}$ liver compared to WT. **C** Validation of liver microarray results by qPCR of deregulated genes from different GO categories in independent samples (n=6-10 per genotype). Data presented as mean ± s.d., * $p<0.05$ (t test).

Following up on the elevated expression of catabolic genes in G45a$^{-/-}$ Ing1$^{-/-}$ livers, I analyzed whether increased catabolism occurred organism-wide in mice lacking G45a and Ing1. One of the central signaling pathways to coordinate metabolic activity throughout the organism is the growth hormone – Insulin/Igf1 axis. The pituitary gland secretes growth hormone (GH), which binds to growth hormone receptor (GhR) and leads to Igf1 secretion predominantly in the liver. Secreted Igf1 binds to Insulin

receptor (InsR) in a multitude of target tissues and regulates cell-specific anabolic functions, e.g. triglyceride synthesis in adipose tissue [267] (Figure 4.10A).

While growth hormone expression in the pituitary gland and GhR expression in the liver of G45a/Ing1 knockout mice was indistinguishable from WT, Igf1 expression was significantly reduced in Ing1$^{-/-}$ and G45a$^{-/-}$ Ing1$^{-/-}$ livers (Figure 4.10B). This diminished Igf1 production had systemic effects in the periphery, as adipose tissue of Ing1$^{-/-}$ and G45a$^{-/-}$ Ing1$^{-/-}$ mice showed a compensatory upregulation of Insulin receptor (Figure 4.10B) as well as many additional components of the Igf1/Insulin signaling cascade (data not shown).

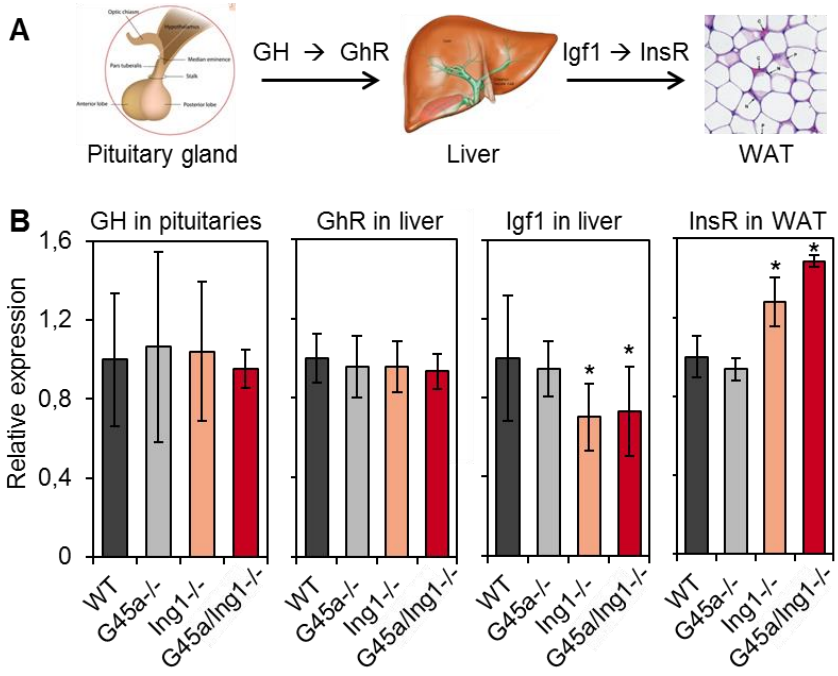

FIGURE 4.10 THE GROWTH HORMONE – IGF1 AXIS IS ATTENUATED BY LOSS OF G45A AND ING1
A Schematic depiction of the core growth hormone-Igf1 axis. Growth hormone is secreted by the pituitary gland and activates the growth hormone receptor (GhR) in (most importantly) the liver. This stimulates Insulin-like growth factor 1 (Igf1) secretion from the liver, which binds to both insulin receptor (InsR) and insulin-like growth factor receptor (Igf1r) in peripheral organs, e.g. white adipose tissue (WAT). **B** Expression analysis of growth hormone – Igf1 axis genes by qPCR. n=3-9 per genotype, data presented as mean ± s.d., * $p<0.05$ (t test).

Taken together, G45a$^{-/-}$ Ing1$^{-/-}$ mice displayed defects in several organs. The high mortality of G45a$^{-/-}$ Ing1$^{-/-}$ mice over time without a clustering at certain time periods, together with kyphosis, small body size and body weight, atrophied reproductive organs, senescent and atrophied dermis, adipocyte replacement of bone marrow cells, as well as a dampened Igf1 signaling show a striking correlation to phenotypes observed in several premature aging mouse models [9, 19, 107, 268, 269]. Thus, the phenotype caused by a combined loss of G45a and Ing1 is consistent with an accelerated aging syndrome or segmental progeria.

4.3 SELECTIVE REDUCTION OF ADIPOSE TISSUE DEPOTS IN G45A$^{-/-}$ ING1$^{-/-}$ MICE

A further phenotype frequently appearing in prematurely aging mice is a hypoplasia of adipose tissue [270, 271]. A first indication for adipose tissue hypoplasia in the analyzed animals was the reduced body weight caused by combined loss of G45a and Ing1, and partially also of Ing1 alone. Analysis of abdomens of 8-week old mice confirmed a reduced amount of adipose tissue both in male and female G45a$^{-/-}$ Ing1$^{-/-}$ mice (Figure 4.11A). Quantification of the weight of five easily accessible adipose tissue depots and five control organs revealed a selective weight reduction in all analyzed adipose tissue depots, but no significant differences in the weight of control organs (Figure 4.11B). This reduction of G45a$^{-/-}$ Ing1$^{-/-}$ adipose tissue weight still held true when normalized to the reduced body weight of G45a$^{-/-}$ Ing1$^{-/-}$ mice. Unexpectedly, a reduction in adipose tissue weight was also observed in G45a$^{-/-}$ males and females, despite a normal total body weight and no further abnormalities in adipose tissue histology or gene expression, as shown later.

A decreased adipose tissue weight could derive from hypoplasia (reduced number) or hypotrophy (reduced size) of adipocytes or from a combination of both. Since the total number of adipocytes in a fat pad cannot be easily determined experimentally, I focused on assessing a potential hypotrophy of adipocytes in the knockout mice. For this purpose, H&E stainings of paraffin-embedded gonadal white adipose tissue depots (gWAT) were carried out.

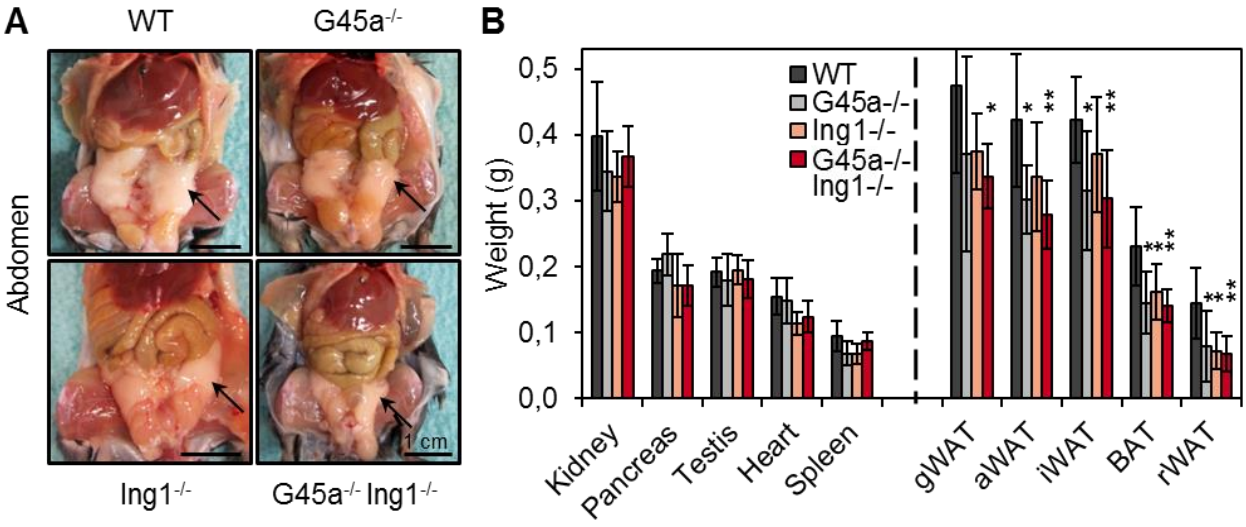

FIGURE 4.11 COMBINED LOSS OF G45A AND ING1 PROMOTES SELECTIVE LOSS OF ADIPOSE TISSUE
A *In situ* overview of mouse abdominal cavities of 8-week old male mice. Arrows point to gonadal white adipose tissue. **B** Weights of excised adipose tissue depots and control organs in male 8-week old mice from indicated genotypes. Data presented as mean ± s.d, n=5-8 animals/genotype. * $p < 0.05$, ** $p<0.01$ (t test). gWAT: gonadal white adipose tissue. aWAT: axillary white adipose tissue. iWAT: inguinal white adipose tissue. BAT: interscapular brown adipose tissue. rWAT: retroperitoneal white adipose tissue.

Histological analysis of gWAT showed a decreased adipocyte size specifically in mice deficient for both G45a and Ing1, while single knockout gWAT was histologically indistinguishable from wildtype (Figure 4.12A). A quantification of adipose tissue H&E stainings indicated an average reduction of adipocyte diameter by 29.0% and of adipocyte area by 50.2% in G45a$^{-/-}$ Ing1$^{-/-}$ gWAT (Figure 4.12B). Additionally to white adipose tissue, lipid content was also reduced in G45a$^{-/-}$ Ing1$^{-/-}$ brown adipose tissue (BAT), as observed in H&E stainings (Figure 4.12A). This confirmed a generalized reduction in triglyceride storage throughout the body, as indicated by a hypotrophy of both white and brown adipocytes. In G45a$^{-/-}$ Ing1$^{-/-}$ mice, but not in single knockout or WT animals, white adipose tissue additionally contained islands of cells with brown adipose tissue-like morphology, which were excluded from the quantification of white adipocyte size. Instead of unilocular adipocytes, these islands contained cells with multiple small lipid droplets and increased cytoplasmic content (Figure 4.12A). This presence of cells with classical hallmarks of brown or beige/brite adipocytes [272] demonstrates a browning of white adipose tissue specifically in G45a$^{-/-}$ Ing1$^{-/-}$ mice.

From all the described phenotypes of G45a$^{-/-}$ Ing1$^{-/-}$ mice, hypotrophy of adipose tissue depots was the most penetrant phenotype encountered. 71% of analyzed G45a$^{-/-}$ Ing1$^{-/-}$ animals (42 of 59) showed a decreased body weight, 6 out of 9 G45a$^{-/-}$ Ing1$^{-/-}$ showed reduced adipose tissue weights, and all 5 G45a$^{-/-}$ Ing1$^{-/-}$ animals analyzed by histology had a reduced white adipocyte size as well as islands of beige/brite adipocytes.

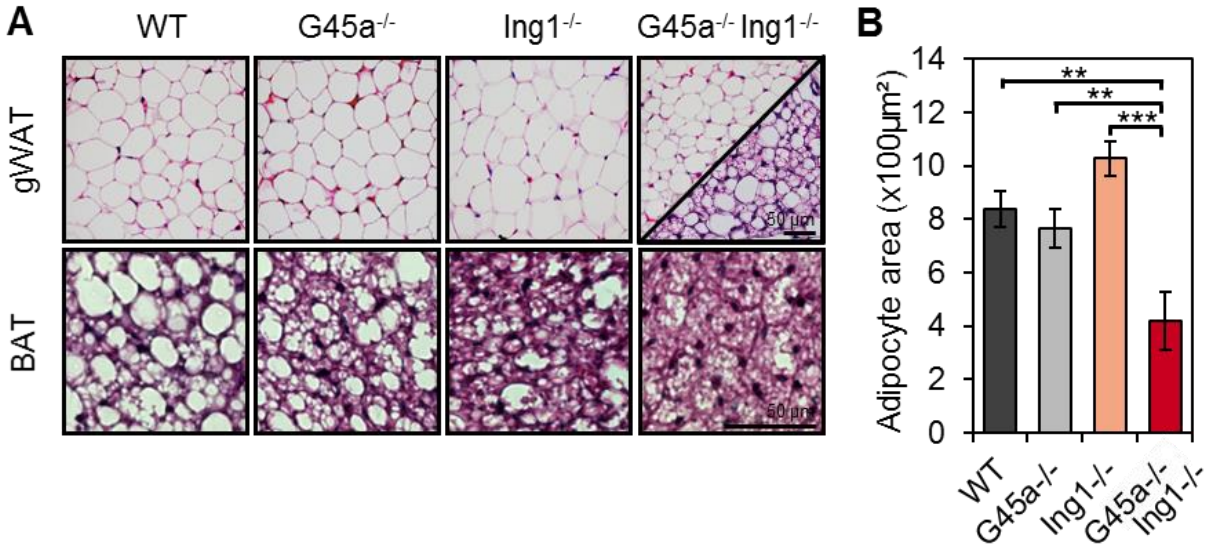

FIGURE 4.12 BOTH WHITE AND BROWN ADIPOSE TISSUE OF G45A$^{-/-}$ ING1$^{-/-}$ MICE STORE LESS TRIGLYCERIDES

A H&E stainings of gonadal white adipose tissue sections (gWAT) and interscapular brown adipose tissue sections (BAT). The gWAT panel of G45a$^{-/-}$ Ing1$^{-/-}$ mice is divided to display two areas with distinct morphological appearances. Classical WAT-like morphology is depicted in the upper half, and beige/brite adipocyte islands are depicted in the bottom half. **B** Individual adipocyte size in gWAT from (A) quantified by measurement of >200 adipocytes each on sections from 4-5 animals/genotype. Data presented as mean ± s.d, ** $p<0.01$, *** $p<0.001$ (t test).

4.4 BROWNING OF WHITE ADIPOSE TISSUE IN G45A$^{-/-}$ ING1$^{-/-}$ MICE

Next, I concentrated on molecular characterizations to gain insight in potential pathways and targets regulated by G45a and Ing1. For this purpose, white adipose tissue was chosen as a model, since it displayed the most penetrant and least variable phenotype in G45a$^{-/-}$ Ing1$^{-/-}$ mice. To elucidate deregulated pathways in adipose tissue, expression microarrays were conducted of gWAT of age- and sex-matched WT, G45a$^{-/-}$, Ing1$^{-/-}$, and G45a$^{-/-}$ Ing1$^{-/-}$ mice using 3 pooled samples à 3 animals per genotype.

Whereas in G45a$^{-/-}$ WAT, gene expression was nearly unaffected compared to WT, 136 genes were upregulated and 142 genes were downregulated at least 1.5-fold in Ing1$^{-/-}$ WAT. Combined loss of G45a and Ing1 exacerbated gene expression changes in WAT and caused upregulation of 620 genes and downregulation of 621 genes. There was a strong overlap between the genes deregulated in Ing1$^{-/-}$ and G45a$^{-/-}$ Ing1$^{-/-}$ WAT (Figure 4.13B). Moreover, the vast majority of genes deregulated in G45a$^{-/-}$ Ing1$^{-/-}$ WAT showed a similar trend already in Ing1$^{-/-}$ WAT, even if not being detected as significantly changed according to the selected cutoff criteria (Figure 4.13A). The overlap of misexpressed genes in Ing1$^{-/-}$ and G45a$^{-/-}$ Ing1$^{-/-}$ WAT together with the larger number and stronger deregulation of affected genes in G45a$^{-/-}$Ing1$^{-/-}$ mice indicate that Ing1 is the driver of the adipose tissue gene expression changes, but that loss of G45a exacerbates the phenotype. Thus, G45a and Ing1 act synergistically in WAT gene expression regulation, similar to their synergistic actions in many above described premature aging phenotypes (Figure 4.3-4.12).

Next, gene ontology of the genes up- and downregulated in G45a$^{-/-}$ Ing1$^{-/-}$ WAT was determined using the DAVID gene ontology tool. Downregulated genes in G45a- and Ing1-deficient WAT were strongly enriched for immune functions, mainly due to strong overrepresentation of adaptive immunity-linked genes in the downregulated fraction (Figure 4.13C). A diminished expression of immune system-related genes was already detected in liver expression analysis (Figure 4.9). Observing a similar phenotype in yet another organ hints at a systemic deregulation of immune functions. Alternatively, the recruitment of B and T cells to adipose tissue has been linked to low-grade inflammation in obesity [273, 274]. Thus a reduced adipocyte tissue content might be conversely correlated with a paucity of lymphocytes.

Genes overexpressed in G45a$^{-/-}$ Ing1$^{-/-}$ WAT were strongly enriched for gene ontology terms including mitochondrial function, aerobic respiration, glycose catabolism, fatty acid catabolism and citrate cycle (Figure 4.13D). This points to an increased abundance of mitochondria and elevated catabolic activity. Molecularly, this signature is well corresponding to the WAT browning discovered in the histological analysis of G45a$^{-/-}$ Ing1$^{-/-}$ adipose tissue (Figure 4.12). Predictably, brown adipocyte differentiation

genes were also upregulated by loss of G45a and Ing1 (Figure 4.13D). Thus, gene expression changes in G45a$^{-/-}$ Ing1$^{-/-}$ WAT reflect the increased energy expenditure and elevated catabolism that derive from brown adipocyte activity.

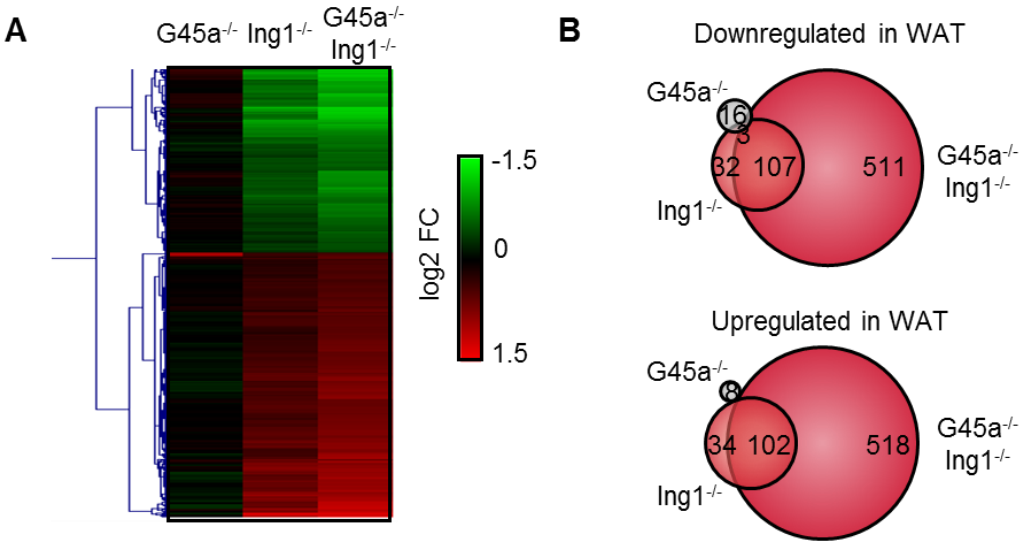

C **Downregulated in Ing1$^{-/-}$ G45a$^{-/-}$ WAT**

GO term	Gene count	P value
Immune response	61	1,0E-23
Leukocyte activation	41	8,9E-22
T cell activation	26	1,4E-16
T cell differentation	20	1,6E-13
B cell activation	15	2,0E-10
Cytokine production	19	5,7E-8

D **Upregulated in Ing1$^{-/-}$ G45a$^{-/-}$ WAT**

GO term	Gene count	P value
Mitochondria	143	8,20E-41
Oxidation/reduction	76	1,70E-31
Fatty acid catabolic process	41	6,60E-24
Aerobic respiration	15	3,90E-15
Citrate cycle (TCA cycle)	14	8,50E-15
Brown fat cell differentiation	10	8,60E-08
Peroxisome	15	7,00E-06
Glucose metabolism	16	1,50E-06

FIGURE 4.13 GENE EXPRESSION ANALYSIS OF GONADAL WHITE ADIPOSE TISSUE CONFIRMS BROWNING OF G45A$^{-/-}$ ING1$^{-/-}$ WAT

Microarray expression analysis of gonadal white adipose tissue (gWAT) from 3 pools à 3 animals per genotype. Analysis of microarrays excluding panels B-D performed by Dr. Emil Karaulanov. **A** Heatmap of upregulated genes (red) and downregulated genes (green) in G45a$^{-/-}$ Ing1$^{-/-}$ gWAT. Color intensities are proportional to strength of expression deregulation. **B** Venn Diagrams showing overlap of up- and downregulated genes in gWAT using a cutoff of 1.5-fold deregulation. Numbers within circles denote number of deregulated genes in the respective genotype. **C** Gene ontology (GO) classification of genes downregulated ≥ 1.5-fold in G45a$^{-/-}$ Ing1$^{-/-}$ gWAT compared to WT. **D** GO classification of genes upregulated ≥ 1.5-fold in G45a$^{-/-}$ Ing1$^{-/-}$ gWAT compared to WT.

To verify results obtained by WAT microarrays, gene expression of selected candidate genes was analyzed by qPCR in independent WAT samples. Indeed, genes representing different functional

categories like mitochondria, peroxisomes, lipid catabolism and brown adipose tissue were confirmed to be upregulated in G45a$^{-/-}$ Ing1$^{-/-}$ WAT. Again, loss of Ing1 already caused a slight but not significant overexpression of analyzed genes from all categories (Figure 4.14A,B).

As H&E stainings pointed to decreased storage of triglycerides not only in WAT, but also in interscapular BAT, molecular patterns of BAT activity might also be increased there. Thus, as signs for increased BAT activity, expression of the mitochondria-coded genes Cox4i1 and Cox5b as well as the expression of BAT-specific genes Cidea and Elovl3 was analyzed in BAT from WT, G45a$^{-/-}$, Ing1$^{-/-}$ and G45a$^{-/-}$ Ing1$^{-/-}$ mice. Consistent with histological findings, all examined genes were upregulated in G45a-and Ing1-deficient BAT (Figure 4.14C). This shows that increased catabolism and energy expenditure is not restricted to browned areas in G45a$^{-/-}$ Ing1$^{-/-}$ WAT, but is also apparent in *bona fide* brown adipose tissue. Thus, G45a and Ing1 might exert cell-intrinsic functions in both WAT and BAT, or else lead to systemic changes causing a secondary elevation of adipose metabolism.

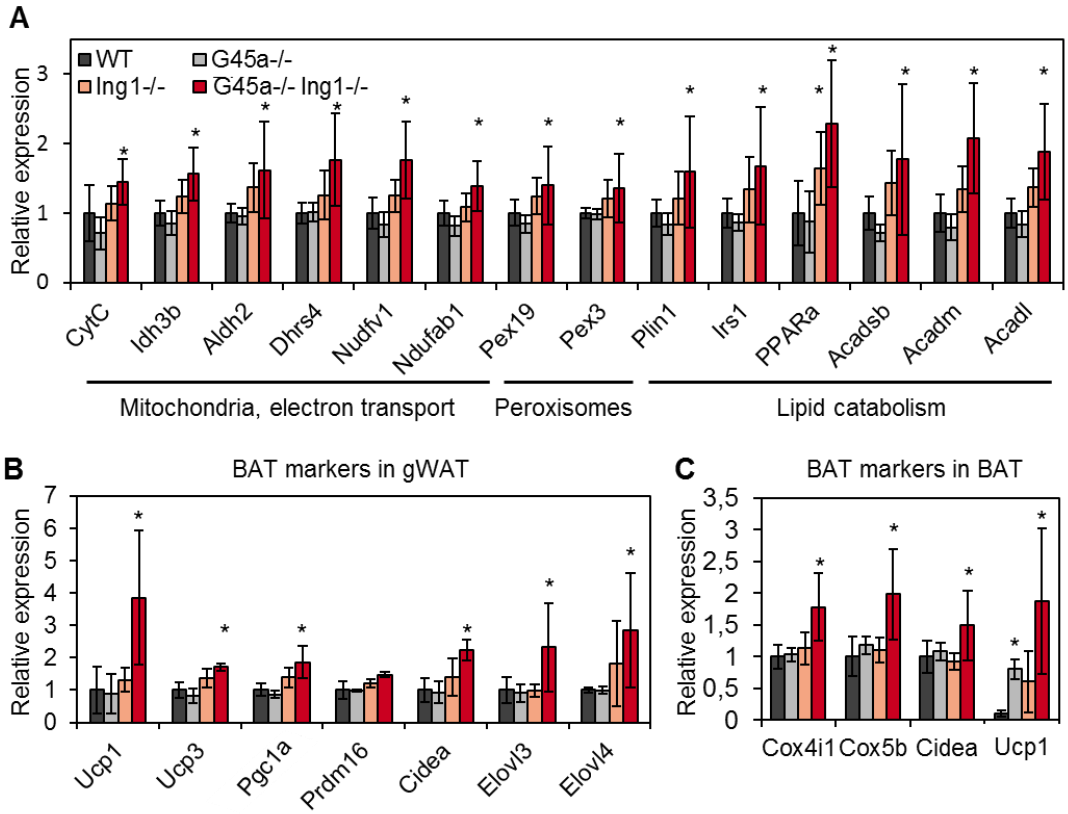

FIGURE 4.14 COMBINED LOSS OF G45A AND ING1 CAUSES SYSTEMIC UPREGULATION OF LIPID CATABOLISM AND BROWN-ADIPOSE-TISSUE-RELATED GENES IN FAT DEPOTS

A qPCR validation of gene expression changes detected in WAT microarray analysis in adipose tissue from independent animals (n=5-9/genotype). **B** Expression analysis of genes regulating brown adipocyte differentiation, performed on gonadal white adipocyte tissue (gWAT). **C** Expression analysis of brown adipocyte activity related genes in brown adipose tissue (BAT) (n=3-5 animals per genotype). Gene expression was normalized to mean Gapdh and Tbp expression. Color-coding in panels B and C identical to panel A. All data is presented as mean ± s.d. * $p<0.05$ (Student's t test).

4.5 LOSS OF G45A AND ING1 IMPAIRS ADIPOCYTE DEVELOPMENT IN A CELL CULTURE MODEL

To determine whether G45a and Ing1 act cell-autonomously in adipocytes and to facilitate the search for molecular mechanisms of G45a and Ing1 function, further investigations were transferred from the *in vivo* situation to an easier manipulable cell culture model of adipocytes. For this purpose, I used a mouse embryonic fibroblast (MEF)-to-adipocyte-differentiation model, in which adipocyte differentiation is stimulated by a cocktail of insulin, isobutylmethylxanthine and dexamethasone [275-277].

To get a first indication whether G45a and Ing1 might directly play a role in adipocyte differentiation, WT MEFs were differentiated into adipocytes and samples were harvested at various time points to analyze gene expression. Both G45a and Ing1 expression was transiently induced upon stimulation of adipocyte differentiation and fell back to basal levels for the rest of the differentiation process after approximately 2h (Figure 4.15). This suggests a role for G45a and Ing1 at the onset of adipocyte differentiation, as this pattern of gene expression coincides with expression patterns of other early response genes in adipocyte differentiation like C/EBPβ or C/EBPδ [278] (see also Figure 4.18).

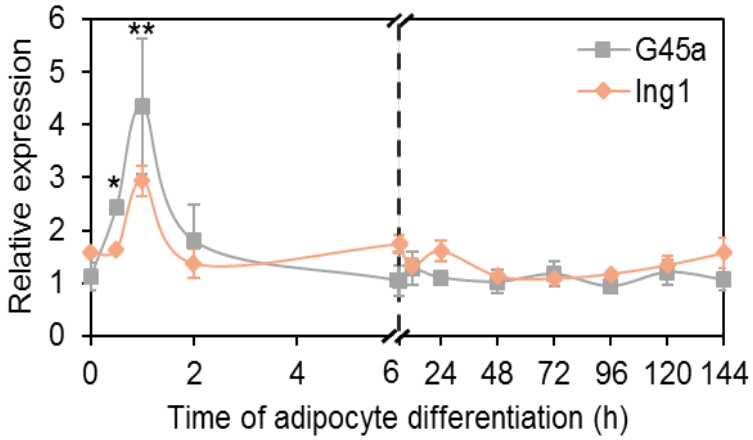

FIGURE 4.15 G45A AND ING1 EXPRESSION IS TRANSIENTLY INDUCED BY ADIPOGENIC STIMULI
Expression of G45a and Ing1 during the course of MEF to adipocyte differentiation. 3 independent WT MEF lines were differentiated along the adipogenic lineage, samples for qPCR were taken at indicated time points. Expression values were normalized to Gapdh and Tbp. Data is presented as mean ± s.d., * $p<0.05$, ** $p<0.01$ compared to start of differentiation (Student's t test).

Next, the capacity for adipogenic differentiation was analyzed in WT, G45a$^{-/-}$, Ing1$^{-/-}$ and G45a$^{-/-}$ Ing1$^{-/-}$ MEFs. First morphological changes of cells became apparent after 4-5 days of adipocyte differentiation and consisted of a condensation of nuclei as well as whole cells and the development of multiple lipid

droplets inside the cytoplasm. Lipid droplets expanded during the course of adipogenic differentiation. Differentiating cells at defined time points were fixed and stained with Oil Red O to visualize the accumulation of triglycerides and with Hematoxylin as a counterstain to indicate cell positions (Figure 4.16A).

Indeed, a significantly decreased percentage of G45a$^{-/-}$ Ing1$^{-/-}$ MEFs developed morphologically into adipocytes compared to WT MEFs (Figure 4.16A). In contrast to mouse *in vivo* phenotypes, this impaired MEF to adipocyte differentiation was fully penetrant in G45a/Ing1-deficient cells. A quantification of the cell culture area stained with Oil Red O revealed a decrease of approximately 60% in G45a$^{-/-}$ Ing1$^{-/-}$ at all analyzed time points (Figure 4.16B). This quantification aggregates two parameters: (1) The amount of MEFs developing into adipocytes and (2) the amount of lipids accumulating in individual cells. The percentage of MEFs developing into adipocytes was clearly reduced by a combined loss of G45a and Ing1, however the size of lipid droplets was difficult to quantify due to a frequent overlap of individual lipid droplets.

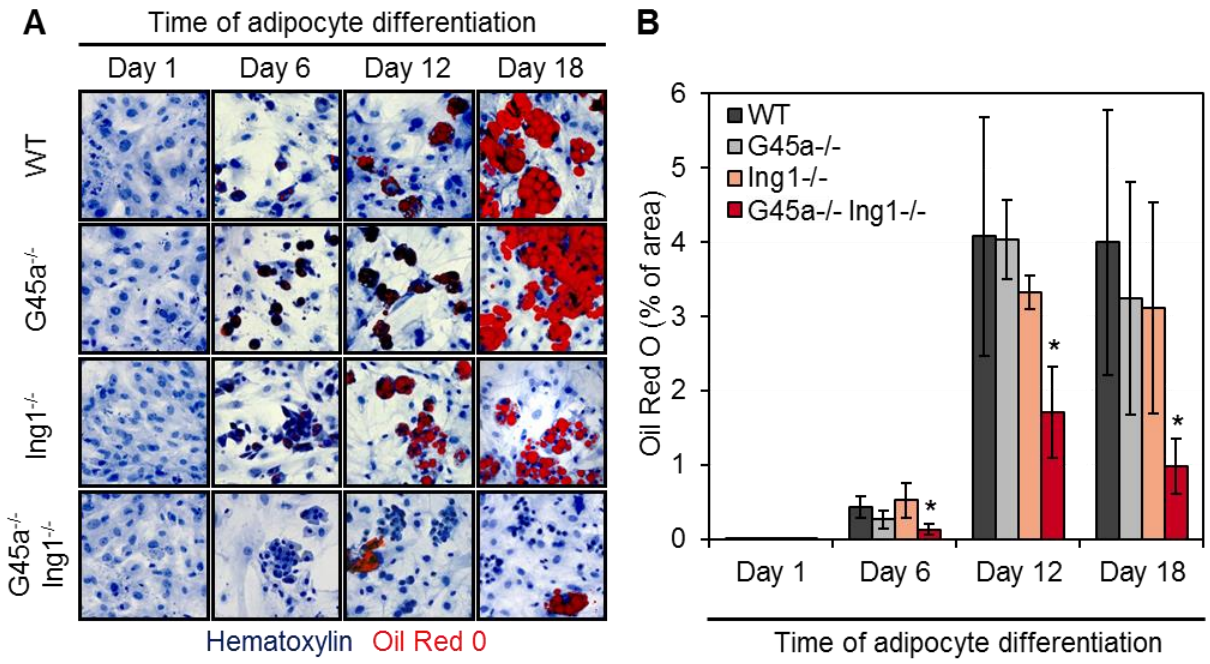

FIGURE 4.16 MEF TO ADIPOCYTE DIFFERENTIATION IS IMPAIRED BY LOSS OF G45A AND ING1
A Differentiation of MEFs to adipocytes using 3-4 independent MEF lines per genotype. Cells at indicated days of adipocyte differentiation were stained with Oil Red O (red) to visualize lipid droplets and Hematoxylin (blue) as a counterstain. **B** Quantification of stainings from (A). Areas with positive staining for Oil Red O were quantified in 9 overview pictures per MEF line and time point. Data is presented as mean of average stained area ± s.d., * $p<0.05$ compared to WT at same time point (t test).

To further characterize impaired adipogenic differentiation of G45a$^{-/-}$ Ing1$^{-/-}$ MEFs, RNA-seq was conducted in WT, G45a$^{-/-}$, Ing1$^{-/-}$ and G45a$^{-/-}$ Ing1$^{-/-}$ cells in biological triplicates at different time points of MEF to adipocyte differentiation.

At day 2 of differentiation, 311 genes were upregulated and 226 genes were downregulated at least 2.0-fold in G45a$^{-/-}$ Ing1$^{-/-}$ adipocytes. These genes represent early transcriptional changes in cells that do not yet show adipocyte-specific morphological changes. The amount of differentially expressed genes in cells deficient for Ing1 alone was approximately one third of the amount found by a combined loss of G45a and Ing1, with both gene sets showing a high overlap. Loss of G45a alone did not affect gene expression during MEF to adipocyte differentiation (Figure 4.17B). A heatmap of misexpressed genes in day 2 adipocytes shows that while many deregulated genes are shared between Ing1$^{-/-}$ and G45a$^{-/-}$ Ing1$^{-/-}$ adipocytes, a large proportion of misexpressed genes are uniquely present in G45a$^{-/-}$ Ing1$^{-/-}$ cells (Figure 4.17A). Again, these RNA-Seq results corroborate previous findings (Figure 4.4-4.10 and Figures 4.13-4.14) that loss of Ing1 alone already causes partial phenotypes, which are synergistically enhanced by additional loss of G45a.

Using the DAVID gene ontology annotation tool, deregulated genes in G45a$^{-/-}$ Ing1$^{-/-}$ adipocytes were classified into functional categories. Upregulated genes in G45a$^{-/-}$ Ing1$^{-/-}$ adipocytes (Figure 4.17D) were strongly enriched for genes involved in inflammatory responses, both innate and adaptive immunity, complement activation and wound healing. This finding could already be observed in untreated MEFs (data not shown), but contrasted with a strongly repressed expression of adaptive immunity-related genes found *in vivo* in white adipose tissue (Figure 4.13).

Since G45a$^{-/-}$ Ing1$^{-/-}$ MEFs differentiated poorly into adipocytes, genes downregulated by a loss of G45a and Ing1 were, as expected, strongly enriched for genes related to lipid and fatty acid metabolism, triglyceride synthesis and fat cell differentiation (Figure 4.17C). This confirmed the impaired adipocyte differentiation seen morphologically in G45a$^{-/-}$ Ing1$^{-/-}$ cells also on a molecular level. Analysis of overrepresented transcription factor binding sites in the promoters of downregulated genes using the oPOSSUM tool indicated a possible regulation by the PPARγ:RXRα dimer (Z-score 18.3) and C/EBPα (Z-Score 9.5) (data not shown). Both of these putative regulators of G45a$^{-/-}$ Ing1$^{-/-}$ downregulated genes are well-established pro-adipogenic transcription factors acting in a well-defined gene expression cascade. Thus, I concentrated on further elucidating a potential impairment of this pathway during adipocyte differentiation of G45a$^{-/-}$ Ing1$^{-/-}$ MEFs.

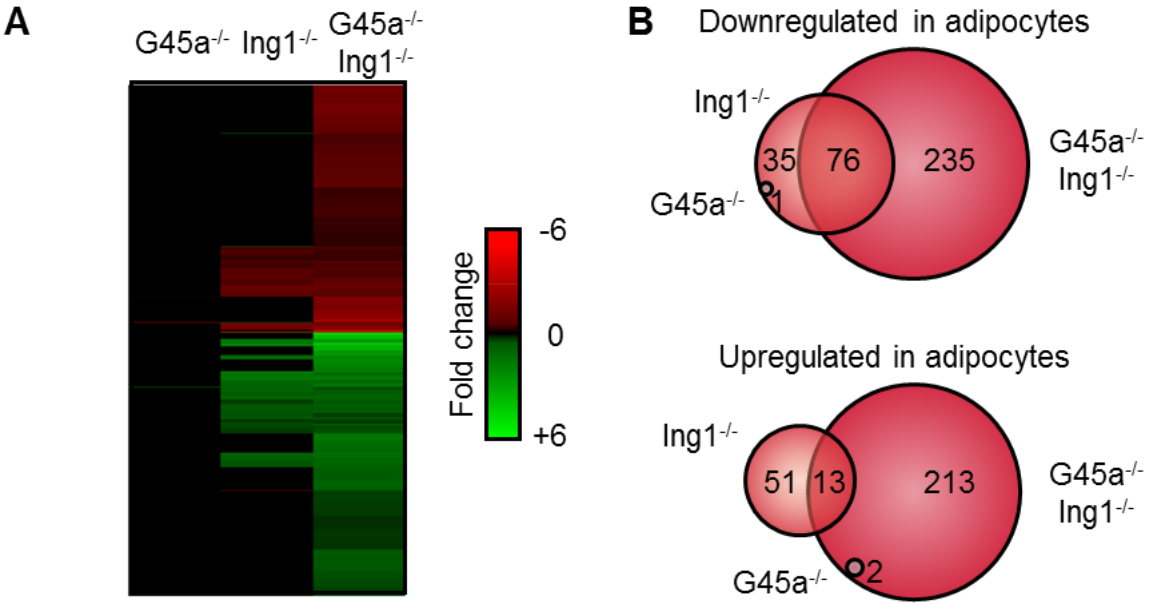

C

Downregulated in G45a$^{-/-}$Ing1$^{-/-}$ adipocytes

GO term	Gene count	p value
cellular lipid metabolic process	44	1.84E-18
fatty acid metabolic process	26	3.9E-16
lipid metabolic process	41	5.83E-14
regulation of lipid metabolic process	24	4.36E-13
neutral lipid metabolic process	14	6.72E-13
fat cell differentiation	14	1.37E-11
triglyceride biosynthetic process	6	7.16E-9

D

Upregulated in G45a$^{-/-}$Ing1$^{-/-}$ adipocytes

GO term	Gene count	p value
activation of immune response	12	3.29E-9
response to wounding	16	9.53E-7
complement activation	5	7.47E-6
innate immune response	11	8.33E-6
leukocyte activation	12	1.73E-5
inflammatory response	10	8.05E-5

FIGURE 4.17 G45A AND ING1 ARE NECESSARY FOR ESTABLISHING ADIPOCYTE-SPECIFIC GENE EXPRESSION DURING MEF TO ADIPOCYTE DIFFERENTIATION

RNA-seq of day 2 of MEF to adipocyte differentiation, analysis of 3 MEF lines per genotype. Sample preparation by Dr. Andrea Schäfer, bioinformatic analysis by Medhavi Mallick. **A** Heatmap of downregulated genes (red) and upregulated genes (green) in G45a$^{-/-}$ Ing1$^{-/-}$ adipocytes. Color intensities are proportional to strength of expression deregulation. **B** Venn Diagrams showing overlap of ≥ 2-fold up-and downregulated genes in day 2 adipocytes. Numbers in circles indicate numbers of deregulated genes in the respective genotype. **C** Gene ontology (GO) classification of genes downregulated ≥ 2-fold in G45a$^{-/-}$ Ing1$^{-/-}$ adipocytes compared to WT. **D** GO classification of genes upregulated ≥ 2-fold in G45a$^{-/-}$ Ing1$^{-/-}$ adipocytes compared to WT.

For this purpose, expression of factors involved in the well-studied [279-281] PPARγ and C/EBPα regulatory cascade was analyzed by qPCR at several time points during MEF-to-adipocyte differentiation in WT and knockout cells. [279-281]. First, adipogenic stimuli (Insulin, IBMX, Dexamethasone) induce the expression of early response genes via cAMP/PKA and glucocorticoid receptor pathways. Those early induced genes include Klf4, C/EBPβ and C/EBPδ. C/EBPβ and C/EBPδ proteins in turn bind to the promoters of the core adipogenic regulators PPARγ and C/EBPα, which, once expressed, form a positive feedback loop to enforce each other's expression. C/EBPα and especially PPARγ furthermore induce the expression of several effector genes, including Adiponectin, Leptin, and Fatty acid binding protein 4 (FABP4), to establish the mature adipocyte phenotype (Figure 4.18A). In agreement with previous reports [278], expression of the early induced factors Klf4, C/EBPβ and C/EBPδ increased quickly after presenting the adipogenic stimulus and peaked at 1-2h after onset of differentiation before returning to basal levels (Figure 4.18B-D). Loss of G45a, Ing1, or both did not impair the expression profile of any examined early induced gene (Figure 4.18B-D), indicating that G45a/Ing1 knockout cells responded normally to adipogenic stimuli with early marker gene induction.

The transcription factor C/EBPβ requires successive phosphorylation by first GSK3β and second p38 MAPK to translocate from the cytoplasm to the nucleus and to acquire DNA binding ability [282]. Since both G45a and Ing1 bind to p38 MAPK [211, 228] and affect MAPK signaling [226], I analyzed C/EBPβ localization during adipocyte differentiation by immunofluorescence as a proxy for C/EBPβ activity. In MEFs, C/EBPβ was localized ubiquitously in both nucleus and cytoplasm. This changed at 2h after onset of adipocyte differentiation, when nearly all C/EBPβ protein has translocated to the nucleus. After 12h of differentiation, a punctate staining pattern of C/EBPβ was visible in the nucleus. This corresponds to C/EBPβ binding to DNA, especially to centromeres [283]. Punctate staining patterns were reduced at 24h of differentiation and were absent at any later time points. At 4 days of adipocyte differentiation, C/EBPβ has partially relocated again to the cytoplasm, presumably having fulfilled its transcriptional function (Figure 4.18E). C/EBPβ localization was similar in WT cells and all analyzed knockout conditions. Thus, neither expression nor function of this early adipogenic factor was impaired in G45a$^{-/-}$ Ing1$^{-/-}$ cells, showing that the onset of adipogenic differentiation proceeds normally in cells deficient for G45a and Ing1.

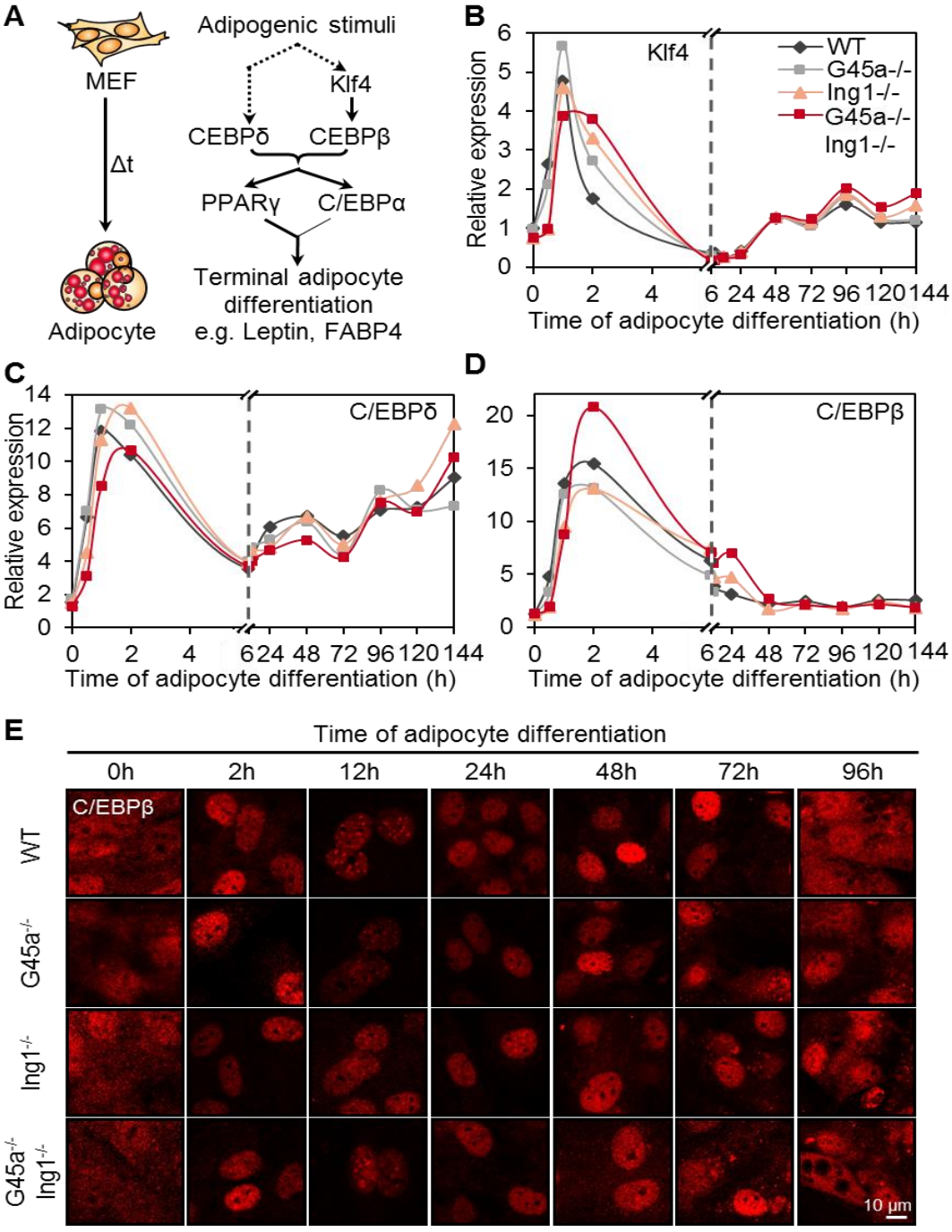

FIGURE 4.18 EARLY MARKERS OF ADIPOCYTE DIFFERENTIATION ARE UNAFFECTED BY LOSS OF G45A AND ING1

A Scheme of factors necessary for adipocyte differentiation with their temporal and causal relationship to each other. Adipogenic stimuli induce via different pathways the transcription factors C/EBPβ and C/EBPδ. Those two factors bind in concert to the promoters of the transcription factors C/EBPα and PPARγ. PPARγ and C/EBPα in turn reinforce each other's expression and induce a large number of effector genes, which establish adipocyte identity. **B-D** Expression of early adipogenic transcription factors Klf4, C/EBPδ, and C/EBPβ during MEF to adipocyte differentiation in WT and G45a/Ing1 knockout cells. n=3-4 MEF lines per genotype. s.d. not shown for clarity reasons. **E** Immunostaining of endogenous C/EBPβ protein during adipogenic differentiation of WT and G45a/Ing1 knockout MEFs.

Expression of PPARγ, a direct C/EBPβ and C/EBPδ target and master regulator of adipocyte differentiation, was induced 50- to 60-fold in WT cells during the time course of adipocyte differentiation. Importantly, PPARγ induction was diminished by approximately 50% at all analyzed time points by loss of G45a and Ing1 (Figure 4.19A).

Expression of all analyzed downstream targets of PPARγ, e.g. C/EBPα, Leptin and FABP4 similarly increased during adipocyte differentiation and followed the increase in PPARγ expression after specific time delays. Again, induction of all analyzed downstream targets of PPARγ was diminished by loss of G45a and Ing1, mirroring the effects seen for PPARγ expression. Loss of Ing1 alone had a partial effect on PPARγ and late adipogenic effector gene induction (Figure 4.19A), arguing, like the *in vivo* phenotypic data, for Ing1 being the driver of phenotypic changes, and G45a and Ing1 acting synergistically.

To further verify results obtained by qPCR, protein levels of C/EBPβ and PPARγ were analyzed during adipocyte differentiation. PPARγ protein was strongly reduced in G45a$^{-/-}$ Ing1$^{-/-}$ cells compared to WT cells (Figure 4.19B), consistent with its decreased mRNA expression (Figure 4.19A). C/EBPβ protein levels however remained unaffected by loss of G45a or Ing1, confirming both the mRNA expression results (Figure 4.18D) as well as immunofluorescence intensities for C/EBPβ during adipocyte differentiation (Figure 4.18E). Reduction of PPARγ expression in G45a$^{-/-}$ Ing1$^{-/-}$ cells was specific for MEF to adipocyte differentiation and did not occur in any other tested cell type or organ (Figure 4.19C). These findings suggest that genes affected by loss of G45a and Ing1 might by cell-type specific.

Taken together, the conducted analyses on pathways responsible for adipocyte differentiation suggest that loss of G45a and Ing1 cause a stop of the adipogenic cascade at the level of its master regulator PPARγ, making this gene a prime candidate for being a G45a and Ing1 target. Efforts to analyze whether PPARγ might be directly regulated by G45a and Ing1 however failed to provide positive evidence: (1) The promoter region of PPARγ was fully demethylated in both WT and G45a$^{-/-}$ Ing1$^{-/-}$ MEFs, and putative PPARγ enhancers did not show reproducible DNA methylation differences between the analyzed genotypes (data not shown). (2) Neither G45a nor Ing1 occupancy of PPARγ promoters or enhancers could be detected in MEFs or day 2 adipocytes, as analyzed by chromatin immunoprecipitation of overexpressed tagged G45a and Ing1 (data not shown). These analyses however do not exclude the possibility that G45a and Ing1 directly induce PPARγ expression by interacting with chromatin regions not analyzed here. Alternatively, PPARγ might be an indirect target of G45a and Ing1 that is regulated via an unknown mechanism.

C/EBPα, a PPARγ downstream target, forms a positive feedback loop with PPARγ. As C/EBPα's expression is also reduced in G45a$^{-/-}$ Ing1$^{-/-}$ adipocytes, it is a second candidate gene which might be directly regulated by G45a and Ing1. However, again no evidence was found for this hypothesis: (1) Similar to PPARγ, the C/EBPα promoter region was fully demethylated in both WT and G45a$^{-/-}$ Ing1$^{-/-}$ MEFs, and (2) no binding of G45a or Ing1 could be detected at the C/EBPα locus by chromatin immunoprecipitation (data not shown).

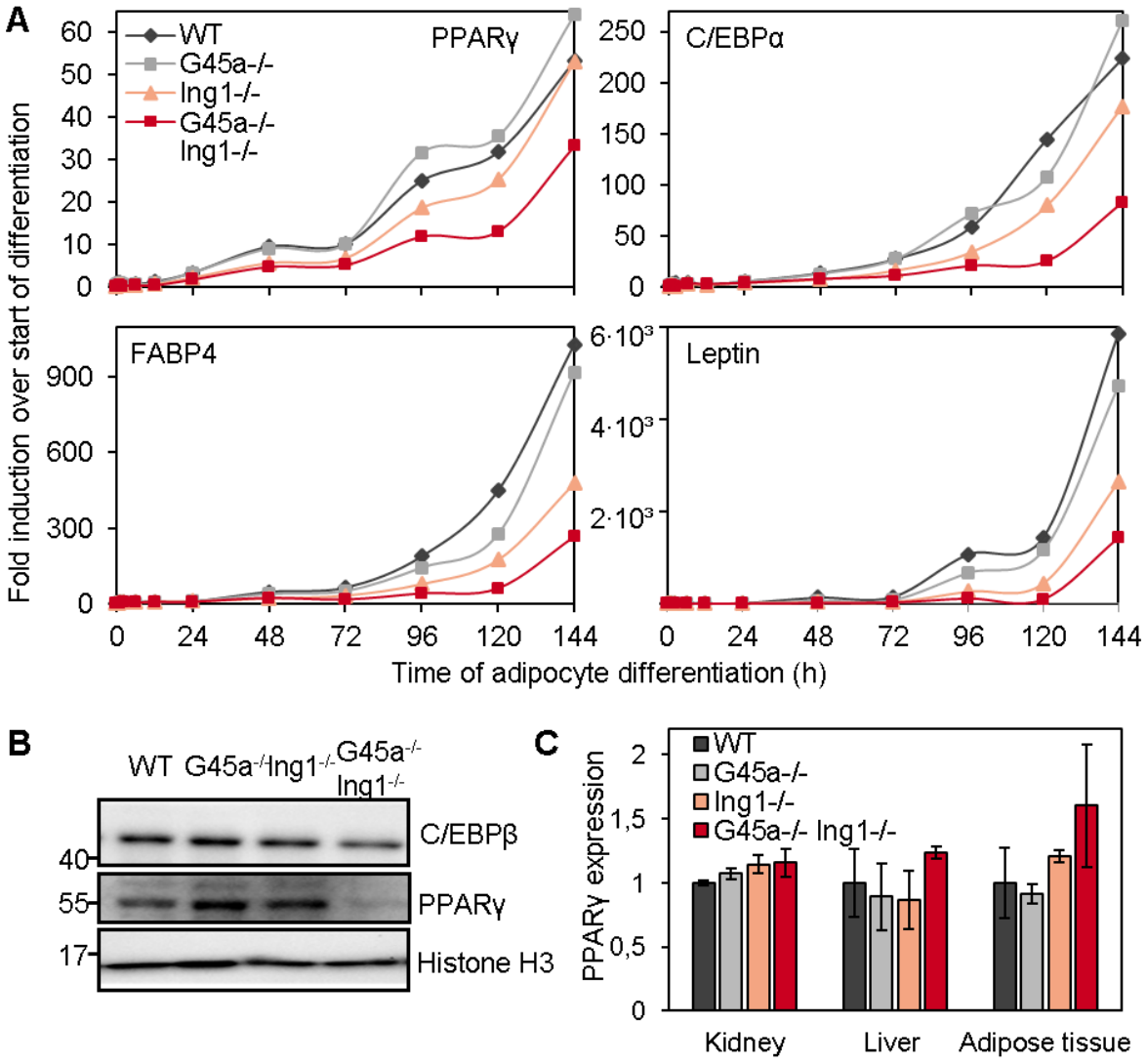

FIGURE 4.19 THE ADIPOGENIC CASCADE IS INTERRUPTED AT THE LEVEL OF PPARΓ EXPRESSION DURING DIFFERENTIATION OF G45A$^{-/-}$ ING1$^{-/-}$ MEFS.

A Gene expression analysis of PPARγ, C/EBPα, FABP4, and Leptin at indicated time points of MEF to adipocyte differentiation of WT and G45a/Ing1 knockout cells. n=3-4 independent MEF lines per genotype, s.d. not shown for clarity reasons. **B** Western Blot of C/EBPβ and PPARγ protein levels at day 6 (144h) of MEF to adipocyte differentiation, histone H3 used as loading control. Representative blot from 3 independent cell lines per genotype. **C** PPARγ expression in kidney, liver, and adipose tissue, taken from microarray data sets of 3 pools à 3 age- and sex-matched mice per genotype. WT expression levels set to 1 for each tissue. Data is presented as mean ± s.d.

To ascertain an acute role for G45a and Ing1 in adipocyte differentiation, rescue experiments with ectopically expressed G45a and Ing1 were of significant importance. For that purpose, human G45a and Ing1 (hG45a, hIng1b) were stably overexpressed during adipocyte differentiation of either WT or G45a$^{-/-}$ Ing1$^{-/-}$ MEFs using a retroviral transduction system [284, 285]. At day 4 of adipocyte differentiation, expression of adipogenic marker genes was induced as expected, with G45a$^{-/-}$ Ing1$^{-/-}$ cells showing a diminished induction. Introduction of hIng1b to the cells normalized adipogenic gene expression in G45a-and Ing1-deficient cells to WT levels, whereas overexpression of hG45a did not have an effect on gene expression (Figure 4.20A). These results demonstrate the acute requirement for at least Ing1 during adipocyte differentiation and rule out the possibility that loss of Ing1 might have led to non-reversible changes prior to adipocyte differentiation. A missing rescue by hG45a was unexpected, but could be explained, if for example human G45a cannot compensate for its mouse orthologue.

Moreover, overexpression of hIng1b induced adipogenic gene expression in MEFs already in the absence of adipogenic stimuli. Comparable to the knockout of Ing1, expression of the early adipogenic factors C/EBPβ and C/EBPδ was not affected by ectopic hIng1b expression. However, ectopic hIng1b induced PPARγ expression, and to a lesser degree expression of PPARγ target genes (Figure 4.20B). This demonstrated that Ing1 was not only necessary but also sufficient for induction of adipogenic gene expression. Since PPARγ showed the strongest observed induction, it might be a possible direct target of Ing1. The comparatively small induction of other adipogenic genes might either derive from an incubation time too short for stronger induction, or the requirement of further factors for their full induction.

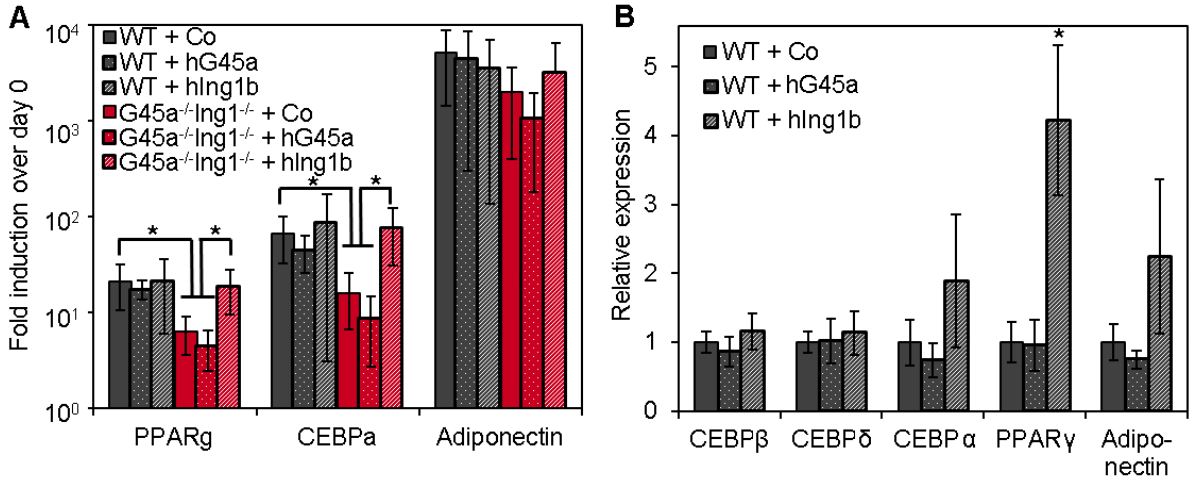

FIGURE 4.20 OVEREXPRESSION OF ING1 RESCUES G45A$^{-/-}$ ING1$^{-/-}$ ADIPOCYTE DIFFERENTIATION AND IS SUFFICIENT FOR INDUCING ADIPOGENIC GENE EXPRESSION
Human G45a (hG45a), human Ing1 (hIng1b), or empty vector (Co) were stably overexpressed in WT MEFs (grey bars) and G45a$^{-/-}$ Ing1$^{-/-}$ MEFs (red bars) using retroviral transduction. Following a Puromycin selection of successfully transduced cells, cells were harvested at different time points of adipocyte differentiation. Expression of indicated genes was analyzed by qPCR. n=3 independent MEF lines per genotype, data is presented as mean ± s.d., * $p<0.05$ (t test). **A** Expression of adipocyte marker genes in WT and G45a$^{-/-}$ Ing1$^{-/-}$ cells at day 4 of adipocyte differentiation. **B** Expression of adipocyte marker genes in undifferentiated WT MEFs following overexpression of indicated genes.

Following up on the finding that ectopic Ing1 expression induced PPARγ, I next analyzed whether PPARγ induction alone was sufficient to rescue the adipocyte differentiation defect of G45a$^{-/-}$ Ing1$^{-/-}$ MEFs. For this purpose, two approaches were used: (1) Overexpression of ectopic PPARγ and (2) activation of endogenous PPARγ protein by the PPAR ligand Rosiglitazone. While PPARγ overexpression had no significant effect on adipogenic gene expression in neither WT nor G45a$^{-/-}$ Ing1$^{-/-}$ cells (Figure 4.21A), treatment with Rosiglitazone induced adipocyte marker genes in all tested conditions (Figure 4.21B). This discrepancy could be potentially explained by either too low overexpression of PPARγ or the absence of sufficient endogenous PPARγ ligands to activate this nuclear hormone receptor. Rosiglitazone treatment elevated expression of adipocyte marker genes in G45a$^{-/-}$ Ing1$^{-/-}$ cells to WT levels (Figure 4.21B), suggesting that PPARγ activation can rescue the impaired adipocyte differentiation of G45a$^{-/-}$ Ing1$^{-/-}$ MEFs. These findings were corroborated by Oil Red O staining of developing adipocytes as a second readout of differentiation efficiency. Again, Rosiglitazone increased the percentage of adipocytes among G45a$^{-/-}$ Ing1$^{-/-}$ cells to WT levels, but also further boosted WT adipocyte differentiation (Figure 4.21C).

To assess whether impaired adipocyte differentiation of G45a$^{-/-}$ Ing1$^{-/-}$ MEFs was dependent on DNA demethylation, I analyzed whether enhancing DNA demethylation could rescue this differentiation defect. Similar to the above described approaches used for PPARγ, this was accomplished first by overexpression of human Tet1 and second by stimulating Tet activity using Vitamin C. Tet1 overexpression was technically challenging due to the large size of the Tet proteins and did not yield conclusive results (data not shown). However, treatment of differentiating MEFs with Vitamin C strongly enhanced adipocyte differentiation in both WT and G45a$^{-/-}$ Ing1$^{-/-}$ cells (Figure 4.21D). In G45a$^{-/-}$ Ing1$^{-/-}$ MEFs, Vitamin C treatment increased expression of adipocyte marker genes to levels encountered for standard differentiation of WT cells (Figure 4.21D). While these results are supportive of a potential role for DNA demethylation in adipocyte differentiation, further experiments are required to substantiate these findings, since Vitamin C modulates several further pathways besides DNA demethylation.

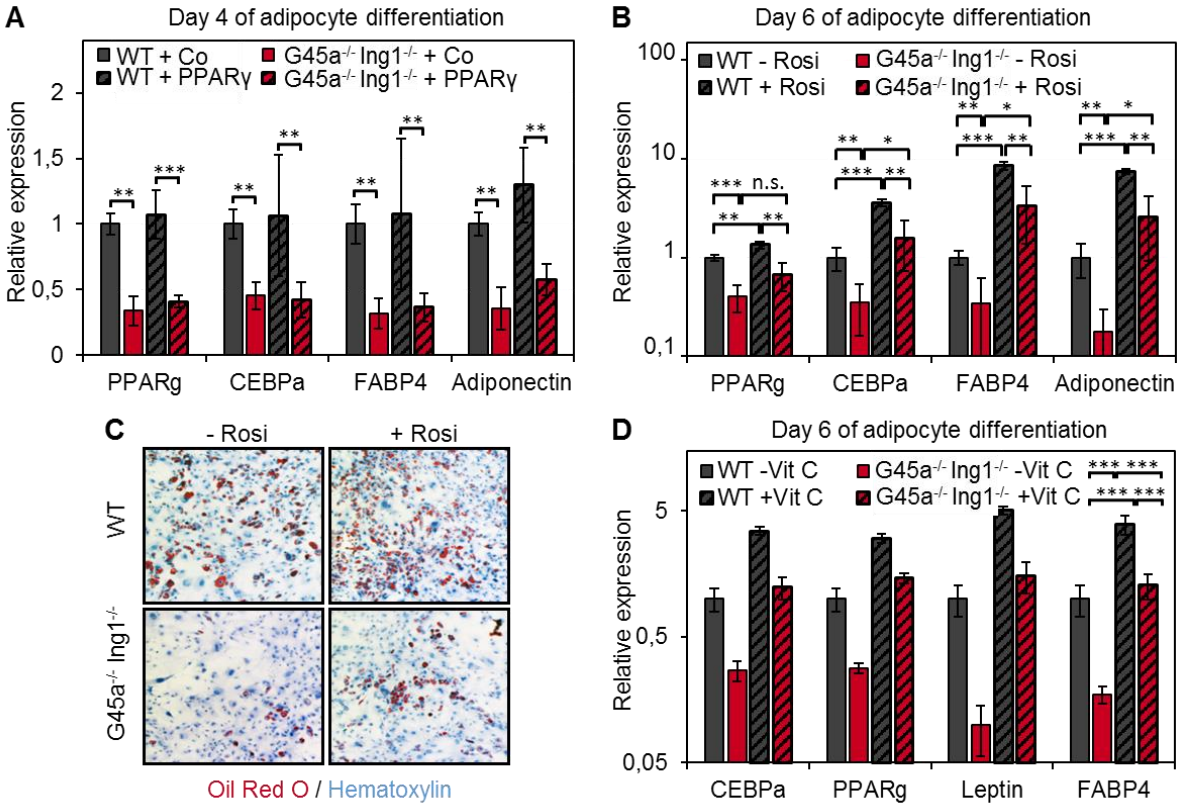

FIGURE 4.21 ROSIGLITAZONE AND VITAMIN C RESCUE G45A$^{-/-}$ ING1$^{-/-}$ ADIPOCYTE DIFFERENTIATION

A PPARγ or empty vector (Co) were stably overexpressed in WT MEFs (grey bars) and G45a$^{-/-}$ Ing1-/- MEFs (red bars) using retroviral transduction (n=3/genotype). Following Puromycin selection, MEFs were differentiated to adipocytes. Expression of indicated differentiation markers was analyzed by qPCR at day 4 of adipocyte differentiation. **B** WT and G45a$^{-/-}$ Ing1$^{-/-}$ MEFs (n=4/genotype) were differentiated to adipocytes in the presence of 0 µM or 0,5 µM of the PPARγ agonist Rosiglitazone (Rosi). qPCR analysis of gene expression was conducted at day 6 of adipocyte differentiation. **C** WT and G45a$^{-/-}$ Ing1$^{-/-}$ MEFs (n=3/genotype) were differentiated to adipocytes in the presence of 0 µM or 0,5 µM Rosiglitazone. 6 days after onset of differentiation, accumulated triglycerides were stained with Oil Red O. Cells were counterstained with Hematoxylin. **D** WT and G45a$^{-/-}$ Ing1$^{-/-}$ MEFs (n=3/genotype) were differentiated to adipocytes in the presence or absence of the Tet agonist 2-phospho-L-ascorbic acid (Vitamin C/Vit C; 10 µg/ml). Expression of adipocyte marker genes was analyzed by qPCR at day 6 of differentiation. Data is presented as mean ± s.d. * $p<0.05$, ** $p< 0.01$, *** $p<0.001$ (t test).

4.6 SEVERAL AGING-ASSOCIATED MOLECULAR PATHWAYS ARE UNLIKELY TO CONTRIBUTE TO PREMATURE AGING OF G45A$^{-/-}$ ING1$^{-/-}$ MICE

To summarize previous findings, white adipose tissue were chosen as a model system to identify cellular mechanisms that contribute to premature aging in G45a$^{-/-}$ Ing1$^{-/-}$ mice. In this model, a cell-intrinsic differentiation defect was revealed as a possible cause for the observed WAT hypotrophy. However, the precise molecular pathways leading to impaired adipocyte differentiation, WAT hypotrophy, and ultimately premature aging in G45a$^{-/-}$ Ing1$^{-/-}$ mice have not been addressed so far. Several molecular causes and consequences of natural and premature aging have been identified [20-24]. A potential occurrence of these hallmarks of aging was examined closer in knockout animals.

Stem cell exhaustion is a symptom of aging that according to current knowledge occurs in all adult stem cells [20]. Since adult stem cells are rare and thus challenging to directly observe *in vivo*, a common way of quantifying them is a colony formation assay (CFU-F) [286]. There, the capability of cells to continuously sustain proliferation, and thereby form colonies from single cells, is taken as an indicator of stem cell identity. CFU-F assays of WT, G45a$^{-/-}$, Ing1$^{-/-}$ and G45a$^{-/-}$ Ing1$^{-/-}$ MEFs demonstrated that a combined loss of G45a and Ing1 lead to an on average 42% reduction of cells being able to form colonies. This phenotype was already partially observed in MEFs lacking Ing1 alone, with 2 out of 4 Ing1$^{-/-}$ MEF lines displaying similar defects (Figure 4.22A,B).

Analysis of growth curves of WT and knockout MEFs further corroborated impaired cell proliferation, which was used as another proxy for mesenchymal stem cell functionality. When seeded at an identical cell density, Ing1$^{-/-}$ MEFs already showed a slightly reduced cell proliferation. This was exacerbated in MEFs lacking both G45a and Ing1, where an on average 41% decrease of cell proliferation was observed compared to WT cells (Figure 4.22C).

These assays provided first indirect indications of stem cell attrition in cells lacking G45a and Ing1 and opened up avenues to determine molecular pathways responsible for this phenotype.

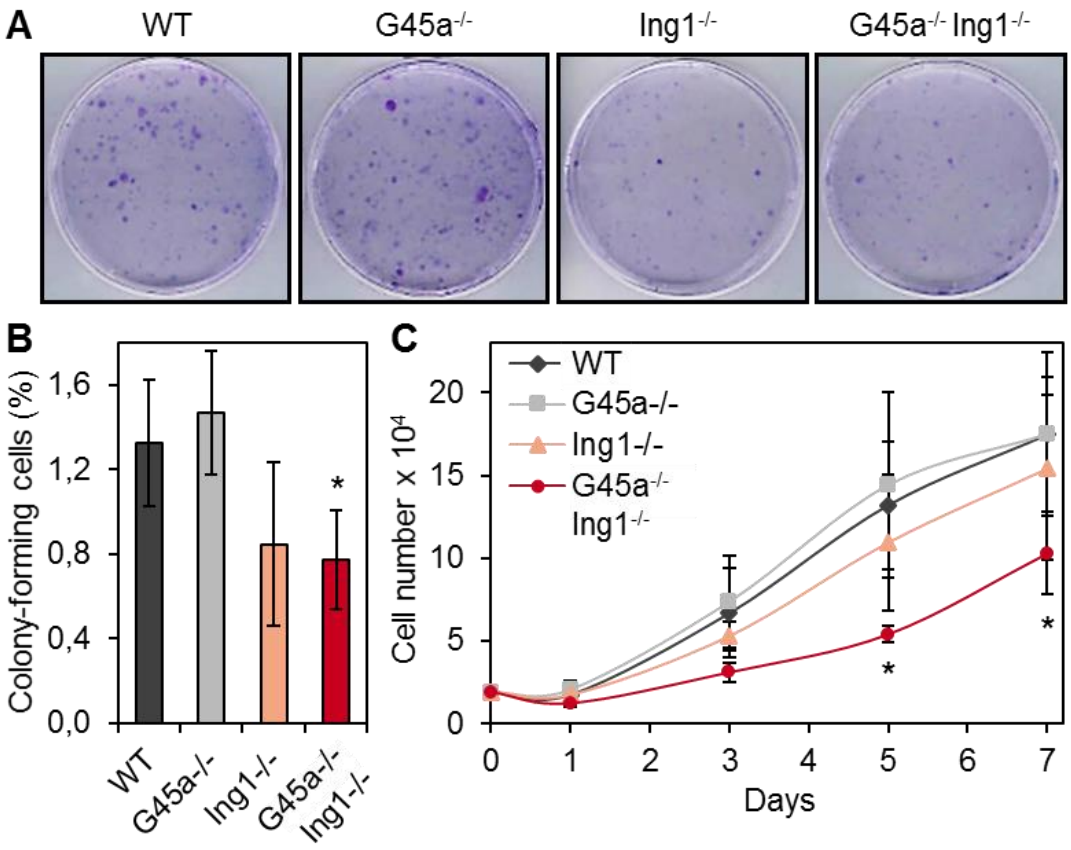

FIGURE 4.22 G45A$^{-/-}$ ING1$^{-/-}$ MEFS SHOW PHENOTYPES INDICATIVE OF STEM CELL EXHAUSTION
A Colony forming unit assay of WT and knockout MEFs. 2,5·10³ MEFs per 10 cm dish were seeded in technical triplicates (4 independent MEF lines per genotype), grown for 11 days and stained with Crystal Violet. **B** Quantification of (A) by normalizing colony number per dish to total number of seeded cells. Data presented as mean ± s.d., * $p<0.05$ compared to WT (t test). **C** Growth curves of 3 independent MEF lines per genotype seeded in technical triplicates. Total cell numbers were counted at indicated time points. Data presented as mean ± s.d., * $p<0.05$ compared to WT (t test). Panel C by Dominik Sebastian.

Stem cell attrition is an integrative consequence of nearly any known molecular mechanism of aging and is exacerbated by e.g. cellular senescence, deregulated pro-or anti-proliferative signaling pathways, cellular stress and telomere attrition [23, 283]. Thus, known causes of stem cell malfunction (and general aging) were investigated both in cell culture and *in vivo.*

On a cellular level, the poor proliferative capacity of G45a$^{-/-}$ Ing1$^{-/-}$ MEFs might be a consequence of a decreased rate of cell division, increased senescence, or increased apoptosis. Since both G45a and Ing1 are implicated in cell cycle regulation [193, 198, 224, 287], cell cycle profiles of WT, G45$^{-/-}$, Ing1$^{-/-}$ and G45a$^{-/-}$ Ing1$^{-/-}$ MEFs were assessed by flow cytometric analysis of cellular DNA content. Neither in steady-state conditions (Figure 4.23A) nor upon oxidative stress (data not shown) was a difference observed between WT and G45a- and Ing1- deficient MEFs. Correspondingly, senescence of G45a$^{-/-}$

Ing1$^{-/-}$ MEFs was indistinguishable from WT, as assessed by senescence-associated β-Galactosidase staining (Figure 4.23B) and Western Blot analysis of the senescence marker p16^{Ink4a} (Figure 4.23C). As both G45a and Ing1 are furthermore implicated in apoptosis [213, 288-290], Western Blot analyses were performed for Caspase-3 activation as an integrator of both extrinsic and intrinsic apoptotic pathways. However, no difference in Caspase-3 cleavage could be detected between WT and G45a-/Ing1-deficient MEFs (Figure 4.23D). Taken together, these analyses provide strong evidence against the involvement of altered cell cycle progression, senescence, or apoptosis in the observed reduction of cell proliferation of G45a$^{-/-}$ Ing1$^{-/-}$ MEFs.

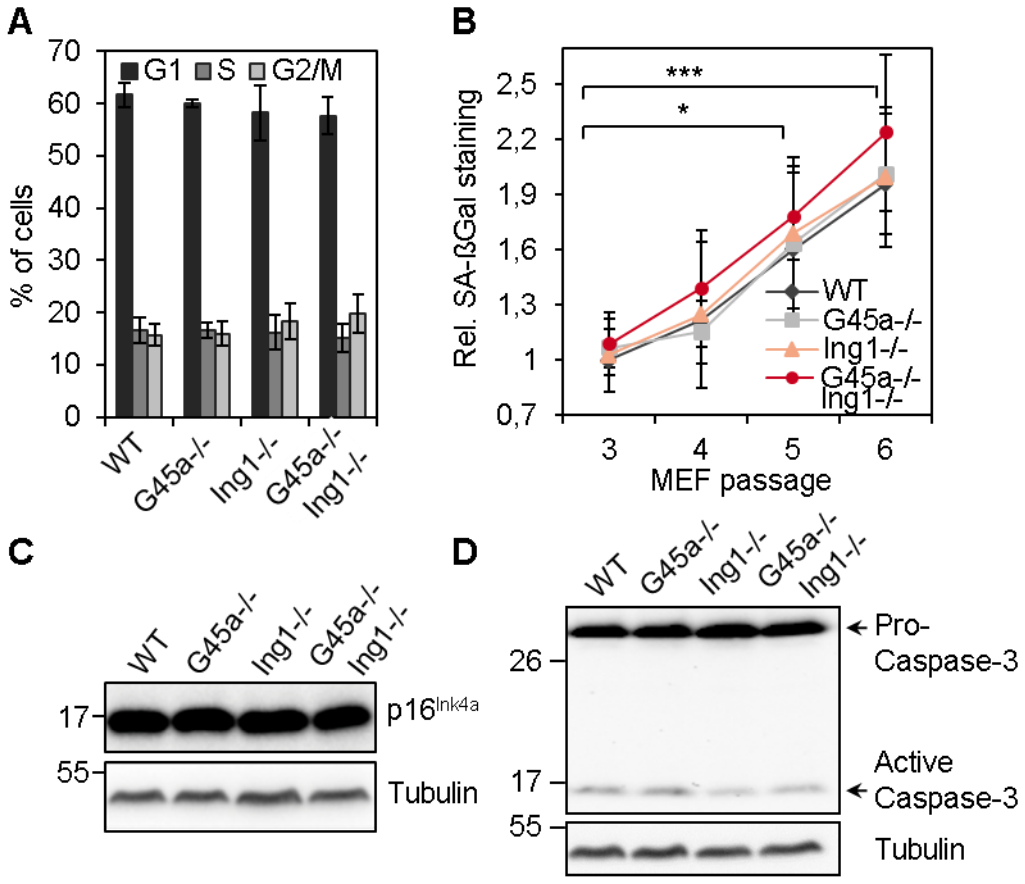

FIGURE 4.23 CELL CYCLE PPROGRESSION, SENESCENCE, AND APOPTOSIS ARE UNAFFECTED IN G45A$^{-/-}$ ING1$^{-/-}$ MEFS

A Cell cycle profile of passage 4 MEFs of indicated genotypes (n=3/genotype) measured by flow cytometric detection of propidium iodide stained cells. Data presented as mean ± s.d. **B** Senescence-associated β-Galactosidase (SA-βGal) assay of WT, G45a$^{-/-}$, Ing1$^{-/-}$, and G45a$^{-/-}$ Ing1$^{-/-}$ MEFs (n=3/genotype) of indicated passages. Data presented as mean ± s.d. * $p<0.05$, *** $p<0.001$ (t test). **C** Representative Western Blot of p16 protein levels in passage 6 MEFs of indicated genotypes**. D** Representative Western Blot of Caspase 3 protein levels in passage 6 MEFs of indicated genotypes. Data in Figure 4.23 by Dominik Sebastian.

Further contributors to premature aging might be an overactive immune system causing chronic low-grade inflammation [46, 48, 98]. As both G45a and Ing1 regulate immune responses [218, 266, 291], this possibility was closer examined. First, levels of 62 different cytokines were quantified in sera of WT, G45a$^{-/-}$, Ing1$^{-/-}$, and G45a$^{-/-}$ Ing1$^{-/-}$ mice using a cytokine antibody array. Five cytokines were found to be ≥ 2-fold downregulated, and four cytokines were ≥ 2-fold upregulated in G45a$^{-/-}$ Ing1$^{-/-}$ serum (Figure 4.24A). Upregulated cytokines included IL17, TARC/Ccl17, and TECK/Ccl25, which all function in T cell development and chemotaxis. Downregulated cytokines include GCSF, GM-CSF, CD40 and IL3, which participate in formation and activation of macrophages as well as other cells of the myeloid lineage. Taken together, these results point to an overstimulation of adaptive immunity concomitant with a decline in innate immune function in G45a$^{-/-}$ Ing1$^{-/-}$ mice. This was further corroborated by gene expression analysis of peritoneal macrophages, which showed a strong reduction in markers of M1 activation (Figure 4.24B), but not M2 activation (Figure 4.24C). Since M1 activation of macrophages is pro-inflammatory and associated with aging [292, 293], and M1 activation was reduced in G45a$^{-/-}$ Ing1$^{-/-}$ mice, increased inflammatory responses do not seem to contribute to G45a$^{-/-}$ Ing1$^{-/-}$ segmental progeria.

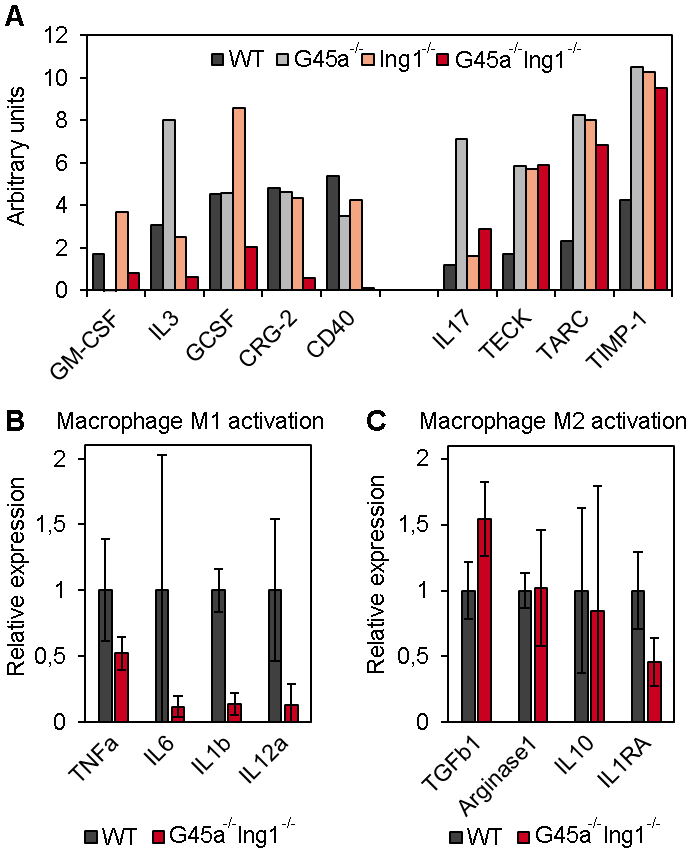

FIGURE 4.24 SKEWING OF MACROPHAGE LINEAGES IN G45A$^{-/-}$ ING1$^{-/-}$ MICE

A Protein concentrations of 3 pooled serum samples per genotype measured by a cytokine protein array. Signal intensities represent arbitrary units and are comparable only within the same protein. Left: Cytokines with ≥2-fold decreased abundance in G45a$^{-/-}$ Ing1$^{-/-}$ serum. Right: Cytokines with ≥2-fold increased abundance in G45a$^{-/-}$ Ing1$^{-/-}$ serum. **B** Expression of M1 macrophage markers in WT and G45a$^{-/-}$ Ing1$^{-/-}$ peritoneal macrophages measured by qPCR (n=3-4 mice/genotype). **C** Expression of M2 macrophage markers in WT and G45a$^{-/-}$ Ing1$^{-/-}$ peritoneal macrophages measured by qPCR (n=3-4 mice/genotype). Data presented as mean ± s.d.

Increased cellular senescence, a phenotype documented in G45a$^{-/-}$ Ing1$^{-/-}$ skin (Figure 4.6), is frequently accompanied by secretion of distinct pro-inflammatory factors – a phenomenon termed senescence-associated secretory phenotype (SASP) [90, 294, 295]. Several SASP factors were quantified in mouse serum using a cytokine antibody array, however no pronounced differences between WT and G45a$^{-/-}$ Ing1$^{-/-}$ sera were detected for any of those factors (Figure 4.25A).

A further molecular cause of aging is the excess generation of reactive oxygen species (ROS), primarily through electron leakage during dysfunctional mitochondrial respiration [38, 296, 297]. Using a commercial flow cytometry-based assay for quantification of superoxide (O_2^-, the most prevalent ROS) as well as other ROS, no difference in ROS quantity could be detected between WT and knockout MEFs at low passages (Figure 4.25B) or high passages (data not shown). On the contrary, expression of many antioxidant enzymes was elevated in G45a$^{-/-}$Ing1$^{-/-}$ and partially also in Ing1$^{-/-}$ mice (Figure 4.25C), hinting at improved defenses against oxidative stress in G45a- and Ing1-deficient cells.

p38 MAPK signaling, which is induced by ROS, has been linked to stem cell aging [298, 299]. Since both G45a and Ing1 are able to bind to p38 MAPK [211, 228] and G45a is a well-characterized positive modulator of p38 and JNK MAPK signaling [226, 227], I examined whether altered activation of any of the three main branches MAPK signaling (p38, JNK, Erk) could play a role in the premature aging phenotypes of G45a$^{-/-}$ Ing1$^{-/-}$ mice. A western blot for activated p38, JNK, and Erk in MEFs and differentiating adipocytes revealed no change in p38 or JNK activation, the two branches of MAPK signaling regulated by G45a (Figure 4.25D). Erk signaling was reduced in G45a$^{-/-}$ Ing1$^{-/-}$ adipocytes, however this might be a secondary consequence of G45a and Ing1 deficiency, since neither G45a nor Ing1 are known to directly regulate Erk signaling.

Telomere shortening is another powerful inducer of aging, causing cellular senescence and stem cell attrition [20, 300]. However, telomere length rather showed a slight but significant increase in G45a$^{-/-}$ and G45a$^{-/-}$ Ing1$^{-/-}$ liver (Figure 4.25E) and MEFs (data not shown). This could potentially be explained by reduced telomere erosion due to decreased cell proliferation.

Taken together, the above analyzed hallmarks of aging were either not affected in G45a$^{-/-}$ Ing1$^{-/-}$ mice or were even affected opposite to anticipated aging-related patterns, which might be for example due to compensatory regulatory mechanisms. Thus, these results excluded many aging-related mechanisms as a cause of segmental premature aging in G45a$^{-/-}$ Ing1$^{-/-}$ mice and allowed me to narrow down the molecular pathways affected by G45a and Ing1.

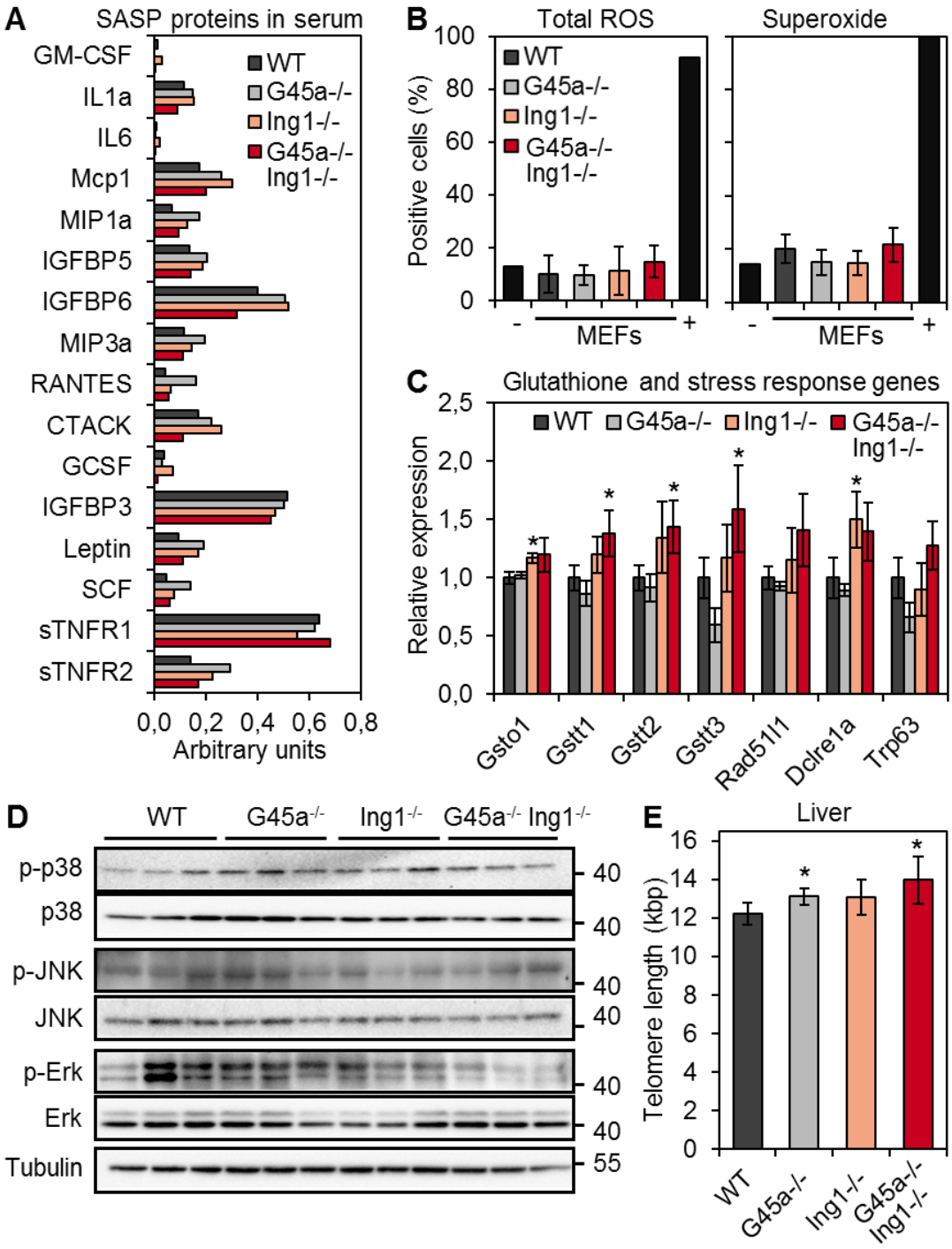

FIGURE 4.25 MANY AGING-ASSOCIATED PATHWAYS ARE UNAFFECTED BY LOSS OF G45A AND ING1

A Protein concentrations of 3 pooled serum samples per genotype measured by a cytokine protein array. Signal intensities represent arbitrary units and are comparable only within the same protein. **B** Quantification of superoxide and total reactive oxygen species (ROS) amounts by flow cytometry in low-passage MEFs (n=4 individual lines per genotype). An N-Acetyl -Cysteine treated negative control (-) and a Pyocyanine-treated positive control (+) served as calibration references. **C** Expression analysis of oxidative stress related genes in mouse livers (n=9 per genotype). Data presented as mean ± s.d., * $p<0.05$ (t test). **D** Western Blot analysis of activated p38, JNK and Erk MAPK in MEFs. **E** Telomere length in mouse livers (n=4 per genotype) measured by Southern Blot analysis. Data is presented as mean of average telomere length per genotype ± s.d., * $p<0.05$ (t test).

4.7 LOCAL DNA HYPERMETHYLATION AT PROMOTERS AND ENHANCERS OF G45A AND ING1 DEFICIENT MEFS

To examine a potential role for DNA demethylation in the G45a$^{-/-}$ Ing1$^{-/-}$ adipocyte differentiation and aging phenotypes, global DNA modification levels were measured in different organs by mass spectrometry. In testis, kidney, liver, and white adipose tissue of WT, G45a$^{-/-}$, Ing1$^{-/-}$ and G45a$^{-/-}$ Ing1$^{-/-}$ mice, about 4% of cytosines were methylated in all analyzed genotypes (Figure 4.26A). In contrast, global amounts of 5hmC differed between the examined tissues and ranged from 0.07% of total cytosine levels in testis to 0.3% of total cytosine levels in kidneys. Again, no significant differences in 5hmC amounts were detected between WT mice and mice lacking G45a, Ing1, or both (Figure 4.26B). Amounts of global 5fC in all analyzed tissues were two orders of magnitude below 5hmC amounts and on the limit of detection of the mass spectrometer. Consequently, measured 5fC levels showed large variance even between biological replicates and no definite conclusion concerning the impact of G45a and Ing1 on global 5fC levels could be reached (Figure 4.26C). 5caC levels were undetectable in the mass spectrometer and thus lay likely below global levels of 5fC in the analyzed organs and genotypes. In summary, no global differences in cytosine modifications could be detected between WT, G45a$^{-/-}$, Ing1$^{-/-}$, and G45a$^{-/-}$ Ing1$^{-/-}$ organs.

Since G45a and Ing1 are involved in gene specific rather than global DNA demethylation [140, 186, 236, 301], whole-genome bisulfite sequencing (WGBS-Seq) of a WT and a G45a$^{-/-}$ Ing1$^{-/-}$ mouse embryonic fibroblast (MEF) line was performed. WGBS-Seq generated 1.2 billion raw reads for WT and 0.8 billion raw reads for G45a$^{-/-}$ Ing1$^{-/-}$ MEFs. Read quality over the whole length of the reads remained satisfactory as judged by Phred quality scores being consistently over 30, translating to over 99.9% accurate base calling. Mapping of the raw reads to the NCBI37/mm9 assembly of the mouse genome yielded >75% uniquely mapped reads. This resulted in an on average 14-fold coverage of the genome, with 80% of the genome being covered at least 10-fold, and 50% of the genome showing greater than 20-fold coverage. According to recent coverage recommendations for whole-genome bisulfite sequencing [302], this should allow for accurate base-resolution estimates of DNA methylation levels and reliable identification of differentially methylated regions (DMRs).

Consistent with previous reports [168, 303], CpGs both in WT and G45a$^{-/-}$ Ing1$^{-/-}$ MEFs showed an approximately bimodal methylation pattern, with about 60% fully methylated sites, 7.3% fully unmethylated sites, and comparatively low percentages of CpGs with intermediate methylation levels (Figure 4.26D). Methylation levels of individual CpG sites were highly correlated between WT and G45a$^{-/-}$ Ing1$^{-/-}$ MEFs (R^2=0.87), showing that the overwhelming majority of CpGs had similar

methylation patterns in both genotypes (Figure 4.26E) and confirming the previous measurements of global 5mC levels by mass spectrometry.

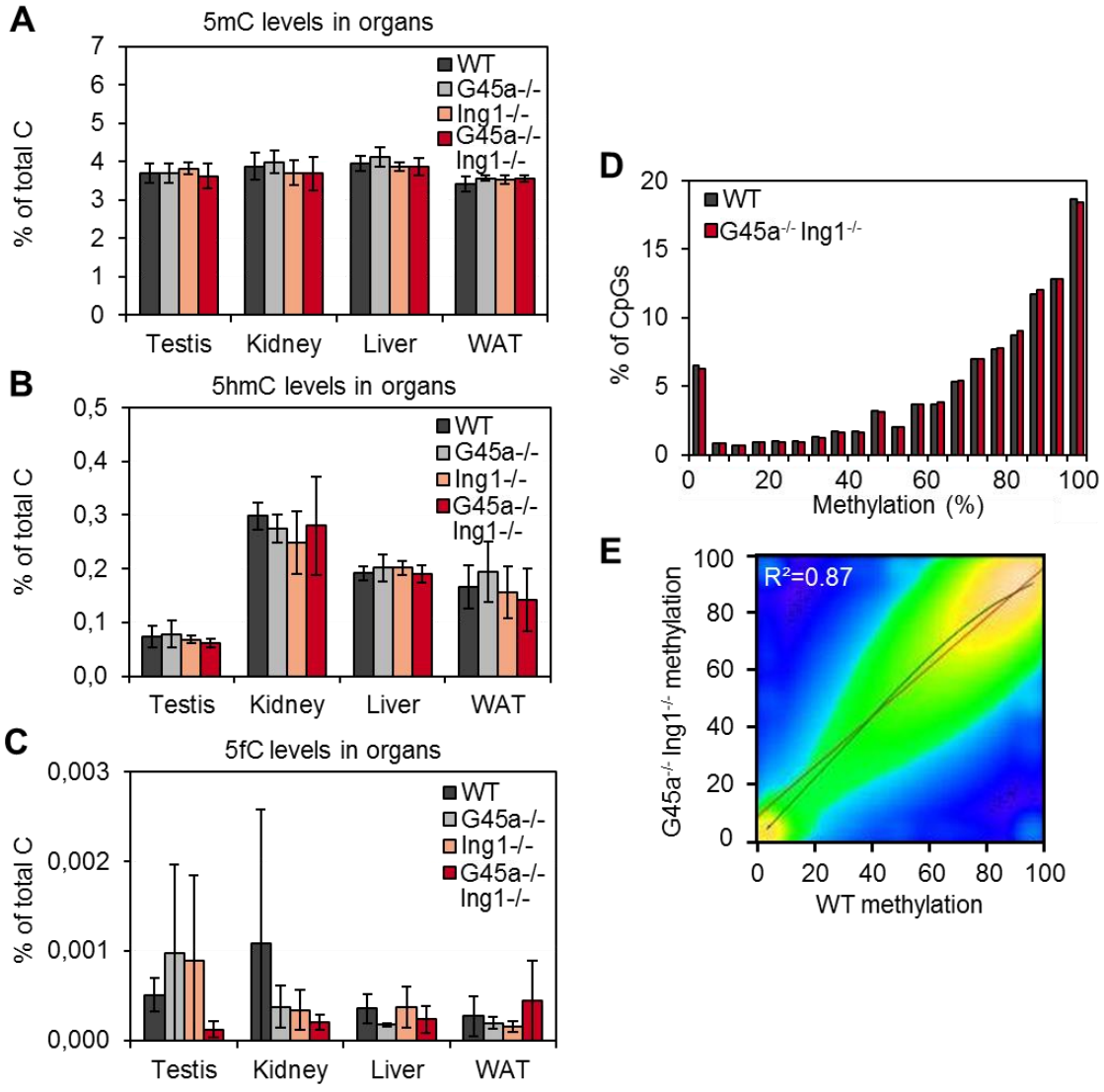

FIGURE 4.26 GLOBAL DNA METHYLATION LEVELS REMAIN UNCHANGED IN G45A$^{-/-}$ ING1$^{-/-}$ MICE
A-C Global 5mC levels (A), 5hmC levels (B), and 5fC levels (C) measured in DNA from testis, kidney, liver or white adipose tissue of mice of indicated genotypes. Data is presented as mean ± s.d. Mass spectrometer measurements performed by Dr. Michael Musheev. **D** Methylation of individual CpG sites of a WT and a G45a$^{-/-}$ Ing1$^{-/-}$ MEF line measured by WGBS-Seq. **E** Correlation of methylation levels at individual CpG sites in WT and G45a$^{-/-}$ Ing1$^{-/-}$ MEFs. Panels D and E by Medhavi Mallick.

After testing various algorithms, differentially methylated regions (DMRs) between WT and G45a$^{-/-}$ Ing1$^{-/-}$ MEFs were identified according to the following filtering criteria: (1) Minimum 10-fold read coverage of all CpGs, (2) minimum 25% methylation difference between WT and G45a$^{-/-}$ Ing1$^{-/-}$ MEFs

at individual CpGs, and (3) minimum 3 consecutive CpGs affected on both DNA strands. With these criteria, 886 DMRs were identified that were hypermethylated in G45a$^{-/-}$ Ing1$^{-/-}$ MEFs and 121 DMRs were found to be hypomethylated in G45a$^{-/-}$ Ing1$^{-/-}$ MEFs. While hypermethylated DMRs were located randomly across all 20 mouse chromosomes, the majority of hypomethylated DMRs clustered in short regions of chromosome 6 and 8, in less than 4Mb vicinity around the *Gadd45a* and *Ing1* gene loci, respectively. Likely, those hypomethylated DMRs were artefacts of incomplete backcrossing of G45a$^{-/-}$ Ing1$^{-/-}$ mice. Excluding DMRs around the *Gadd45a* and *Ing1* loci, 864 hypermethylated DMRs and only 53 hypomethylated DMRs remained in G45a$^{-/-}$ Ing1$^{-/-}$ MEFs (Figure 4.27A). This 16-fold bias of hyper- compared to hypomethylated DMRs in G45a- and Ing1 deficient cells is a strong hint towards an *in vivo* role for G45a and Ing1 in local, region-specific DNA demethylation. As examples, DMRs around the *Col1a2* (Figure 4.27B) and *Kitl* (Figure 4.27C) gene loci are depicted. These genes are crucial for mouse embryonic fibroblast function and contain DMRs that overlap with nearby gene regulatory histone marks.

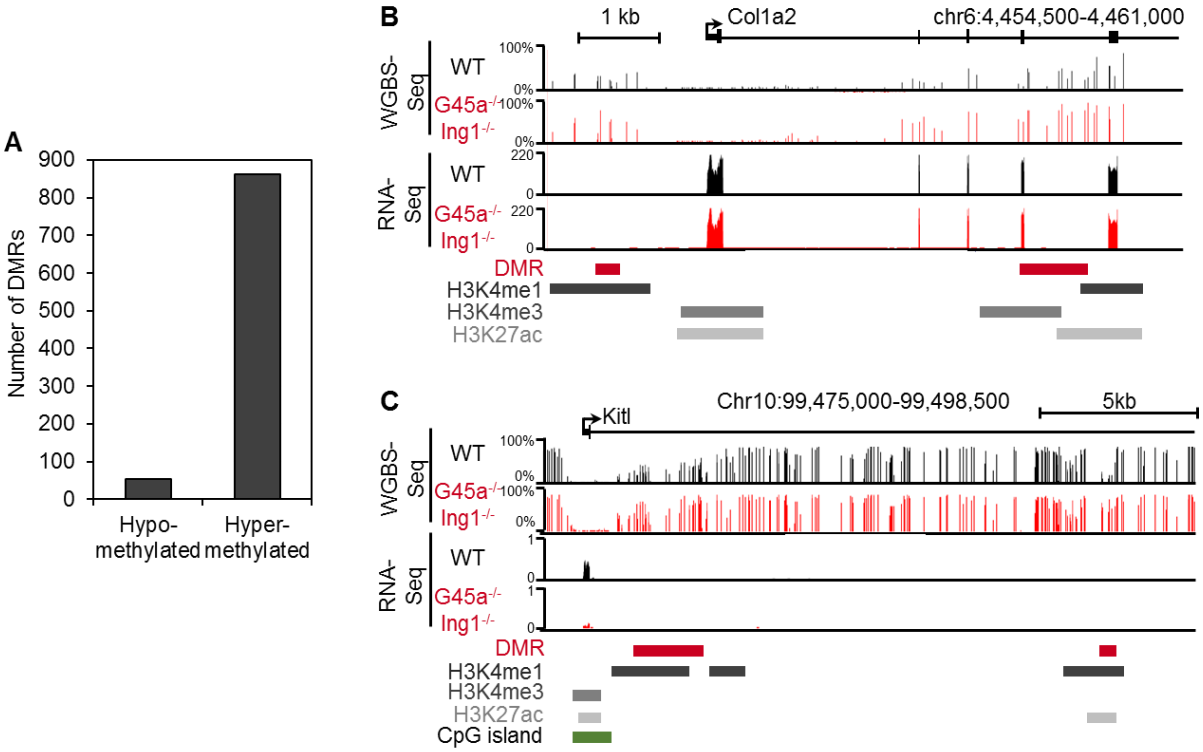

FIGURE 4.27 G45A$^{-/-}$ ING1$^{-/-}$ MEFS SHOW SPECIFIC LOCAL DNA HYPERMETHYLATION
A Amount of hyper-and hypomethylated differentially methylated regions (DMRs) in G45a$^{-/-}$ Ing1$^{-/-}$ MEFs identified by WGBS-Seq. **B,C** Example genomic regions showing WT and G45a$^{-/-}$ Ing1$^{-/-}$ MEF methylation at individual CpGs, WT and G45a$^{-/-}$ Ing1$^{-/-}$ MEF expression measured by RNA-Seq, identified DMRs, and their position relative to CpG islands and histone marks (taken from mouse ENCODE database). Panel A by Medhavi Mallick, panel B and C in cooperation with Medhavi Mallick.

I next assessed how technically and biologically reproducible the identified DMRs were. For this purpose, I employed methylation-sensitive PCR analysis (MS-PCR) as an independent method of quantifying DNA methylation levels. Using constitutively unmethylated (*Gapdh*) and imprinted regions (*Peg3*) as controls, the reliability and accuracy of this method was established (Figure 4.28A,C). Of 25 tested CpGs located in 18 different DMRs, hypermethylation in G45a$^{-/-}$ Ing1$^{-/-}$ cells was confirmed for 24 CpGs, when the same WT and G45$^{-/-}$ Ing1$^{-/-}$ DNA was used that was also analyzed by WGBS-Seq. CpG methylation levels measured by WGBS-Seq and MS-PCR correlated well, corroborating the reliability of both methods (Figure 4.28B). To assess biological reproducibility of DMRs, methylation levels of these 24 confirmed CpGs were additionally quantified in three independent MEF lines per genotype for WT, G45a$^{-/-}$, Ing1$^{-/-}$, and G45a$^{-/-}$ Ing1$^{-/-}$ MEFs. Only 6 of 24 tested CpGs were significantly hypermethylated also in independent G45a$^{-/-}$ Ing1$^{-/-}$ MEFs lines (Figure 4.28C). Thus, hypermethylation of only one fourth of examined CpGs seemed to be biologically reproducible. Neither MEFs deficient for G45a or Ing1 alone showed significantly altered methylation levels at most CpGs analyzed by MS-PCR (Figure 4.28C), indicating that G45a and Ing1 cooperate in DNA demethylation.

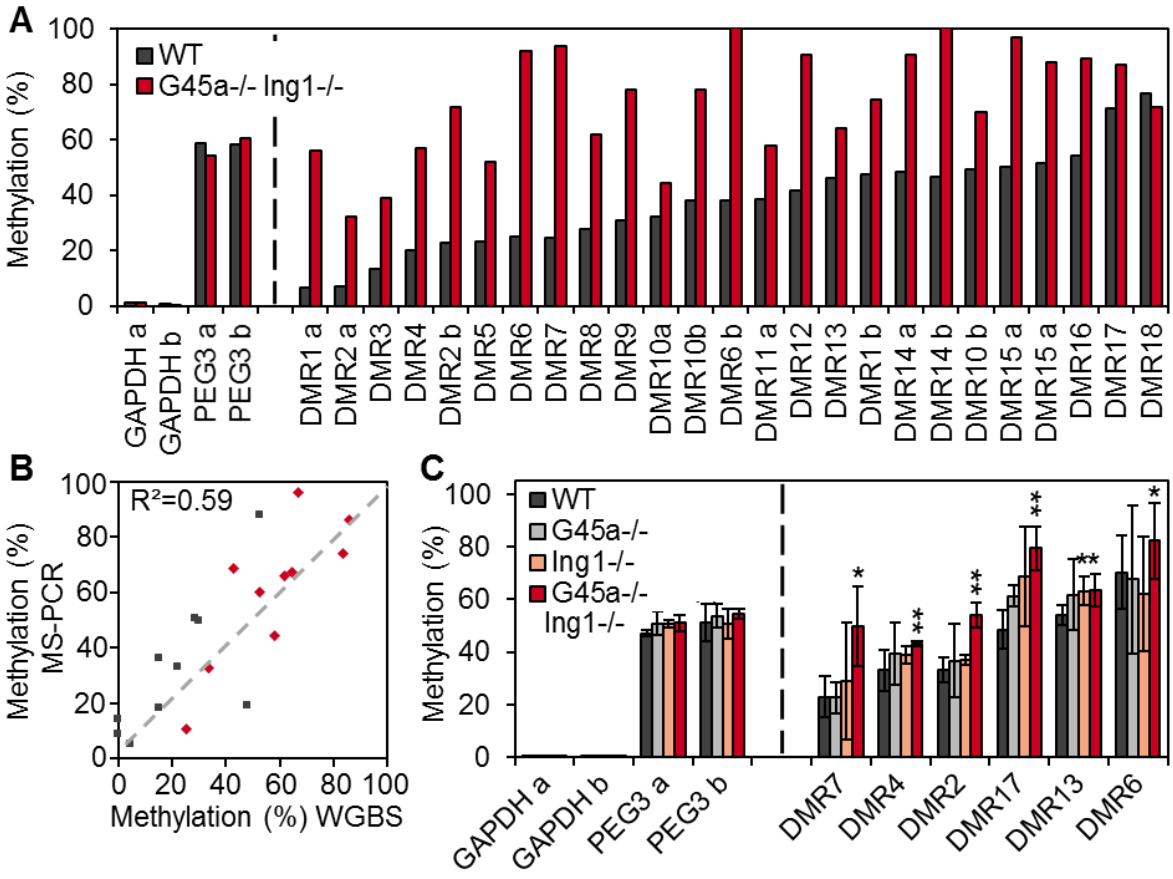

FIGURE 4.28 DIFFERENTIALLY METHYLATED REGIONS IN MEFS CAN BE VALIDATED BY MS-PCR
A Methylation levels at individual CpGs within the *Gapdh* promoter, the *Peg3* imprinted gene, and several DMRs in the WT and G45a$^{-/-}$ Ing1$^{-/-}$ MEF lines that were used for WGBS-Seq. Measurement by methylation-sensitive PCR (MS-PCR). **B** Correlation of DNA methylation levels at individual CpGs measured by WGBS-Seq and MS-PCR in WT MEFs (grey) and G45a$^{-/-}$ Ing1$^{-/-}$ MEFs (red). **C** Methylation levels at individual CpGs measured by MS-PCR in three independent WT, G45a$^{-/-}$, Ing1$^{-/-}$, and G45a$^{-/-}$ Ing1$^{-/-}$ MEF lines per genotype. Data is presented as mean ± s.d., * $p<0.05$, ** $p<0.01$ compared to WT (t test).

Further analyses concentrated on characterizing genomic regions in which DMRs were located. For this purpose, DMRs were cross-correlated with annotated features from public databases: Exons, introns, intergenic regions, 5'UTRs, promoters (defined as regions 2kb up- and downstream of transcription start sites), active promoters (defined by the presence of H3K4me3) and enhancers (defined by the presence of H3K4me1 and H3K27ac). In absolute numbers, the majority of DMRs overlapped with intronic and intergenic regions (Figure 4.29A). However, when normalized to the abundance of the examined features in the genome, hypermethylated DMRs were 13.4-fold enriched at enhancers. While DMRs were not overrepresented around promoters in general, they showed a 3.2-fold enrichment around active promoters (Figure 4.29B). These findings were further corroborated by analyzing the location of DMRs relative to the position of genomic features. Hypermethylated DMRs again were again strongly enriched around the enhancer marks H3K4me1 and H3K27ac, whereas no enrichments could be detected in relation to any other tested genomic feature (Figure 4.29C-E). DNA hypermethylation of enhancers in G45a$^{-/-}$ Ing1$^{-/-}$ MEFs is consistent with reports that attribute methylation changes across cell types specifically to enhancers and that show that enhancers are predominant sites of active DNA demethylation (see chapter 3.2.3 and figure 3.4).

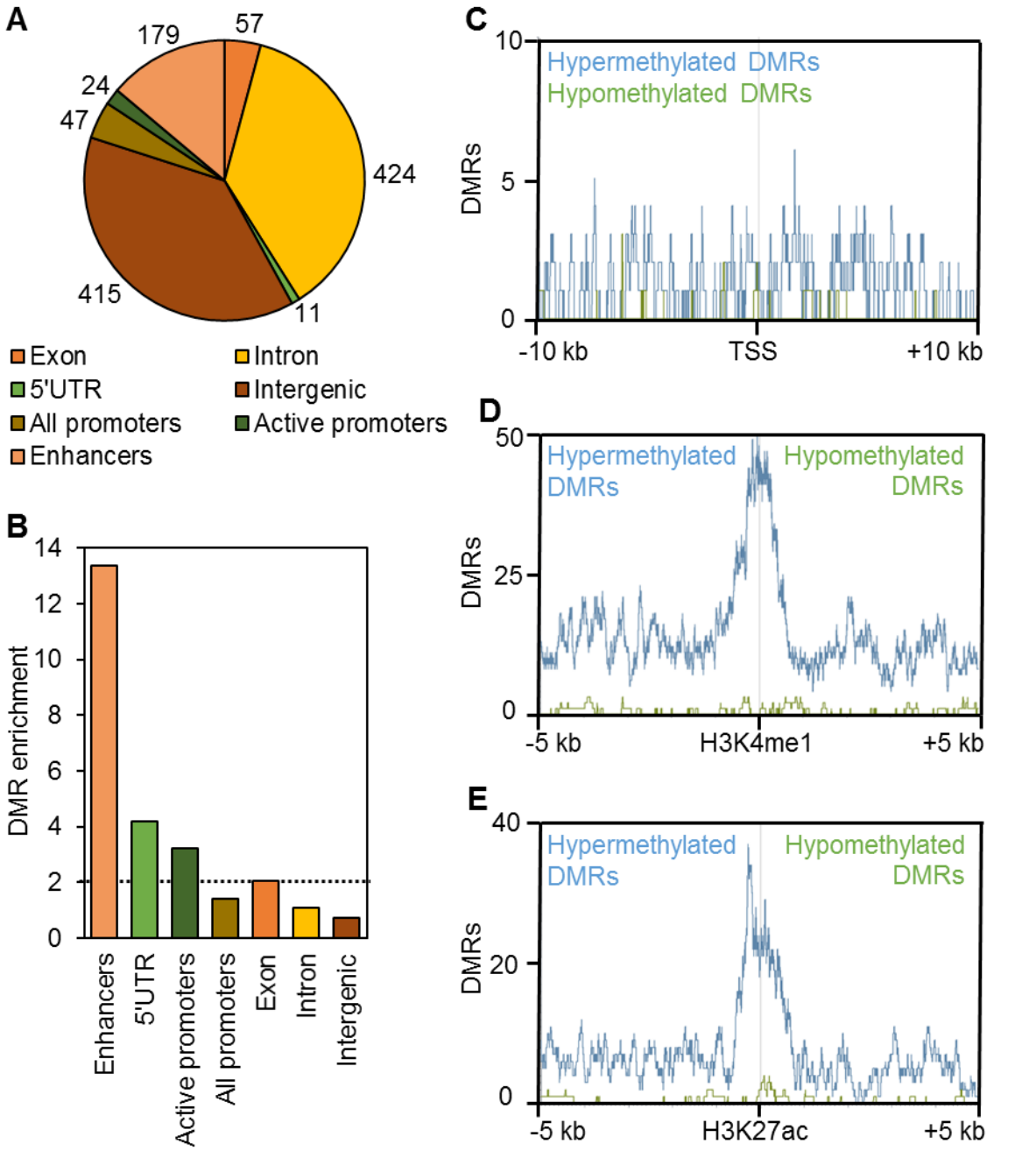

FIGURE 4.29 DIFFERENTIAL METHYLATION IN G45A$^{-/-}$ ING1$^{-/-}$ MEFS OCCURS PREFERENTIALLY AT ENHANCERS

A Numbers and percentages of DMRs overlapping with various genomic features: Exons, introns, 5'UTRs, Intergenic regions, promoters (± 2kb regions of transcription start sites), active promoters (defined by H3K4me3 occupancy), and enhancers (defined by H3K4me1 and H3K27ac occupancy). **B** Enrichment of DMRs from (A) normalized to the abundance and length of their correlated genomic features within the mouse genome. **C** Position of DMRs within a ± 10 kb distance from transcription start sites (TSS). **D** Position of DMRs within a ± 5 kb distance from the enhancer mark H3K4me1. **E** Position of DMRs within a ± 5 kb distance from the enhancer mark H3K27ac. Panels A and B in cooperation with Medhavi Mallick. Panels C-E by Medhavi Mallick.

Next, DMRs were associated with genes based on two criteria: (1) DMR location close to or within a given gene and (2) chromatin looping of intergenic DMRs to genes as assessed by a published Hi-C dataset [304]. The majority of DMR-associated genes was downregulated in G45a$^{-/-}$ Ing1$^{-/-}$ MEFs compared to WT (Figure 4.30A). Analysis of biological processes in which the DMR-associated genes are involved revealed an enrichment for extracellular matrix organization, cytoskeletal organization and several differentiation processes (Figure 4.30B). Genes linked to enhancer-associated DMRs regulate extracellular matrix functions and cellular differentiation, but are also specifically involved in regulation of fat cell differentiation (Figure 4.30C). With the majority of DMR-associated genes being downregulated, these results suggest impaired extracellular matrix secretion and impaired differentiation occurring as a result of aberrant DNA hypermethylation in G45a$^{-/-}$ Ing1$^{-/-}$ MEFs. Likely, locus-specific DNA hypermethylation might extend also to further cell types or organs in G45a$^{-/-}$ Ing1$^{-/-}$ mice. This might be correlated with aberrant expression of DMR-associated genes organism-wide, which ultimately could lead to the accelerated aging of G45a$^{-/-}$ Ing1$^{-/-}$ mice.

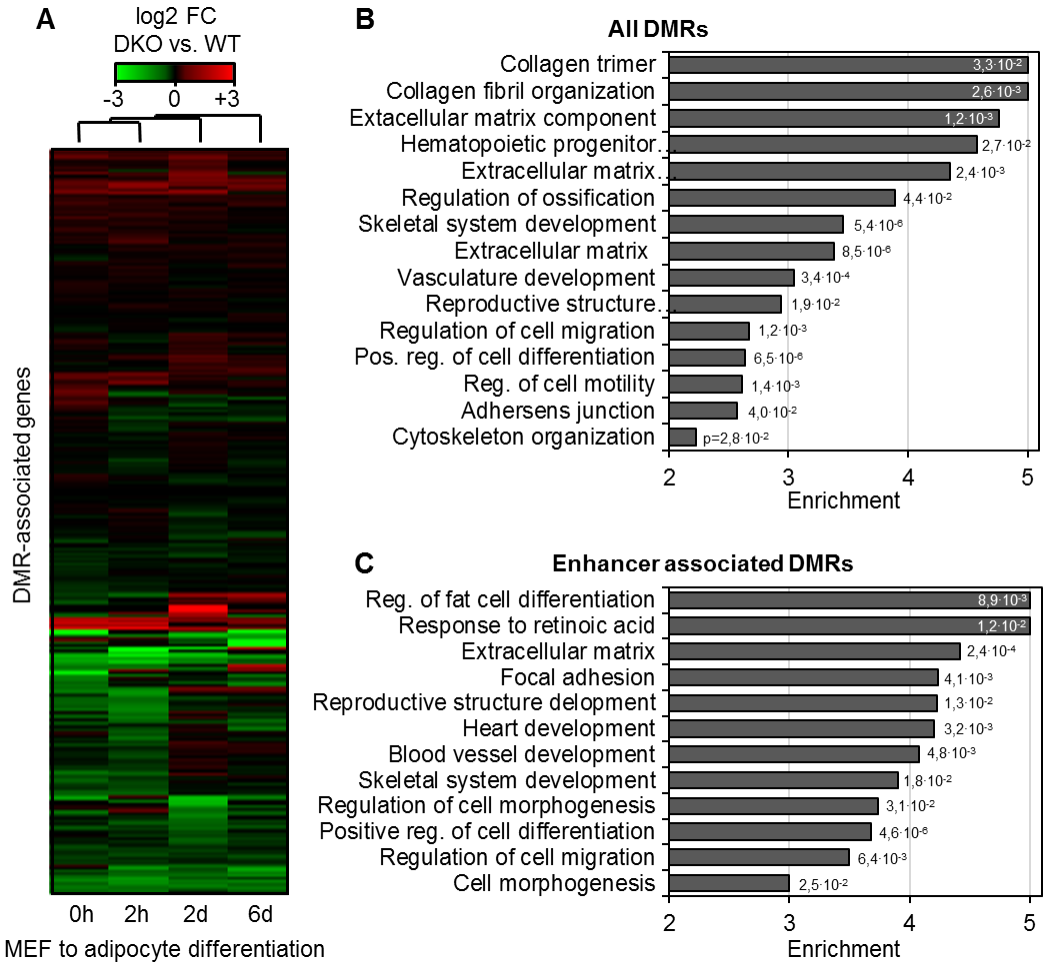

FIGURE 4.30 GENES ASSOCIATED WITH DMRS ARE FREQUENTLY DOWNREGULATED AND REGULATE FIBROBLAST-RELATED FUNCTIONS

A Heatmap of expression changes of DMR-associated genes at indicated timepoints of MEF to adipocyte differentiation. **B** Gene ontology enrichments of all DMR-associated genes. **C** Gene ontology enrichments of genes associated with DMRs localized in enhancer regions. Numbers next to bars denote p values of gene ontology terms. Panel A by Medhavi Mallick. Panels B and C in cooperation with Medhavi Mallick.

5. DISCUSSION

G45a is a multifunctional protein that in addition to its functions in MAPK signaling and DNA repair has also been implicated in DNA demethylation [131, 137, 139, 140]. The H3K4me3 reader Ing1 targets G45a to sites of DNA demethylation in cultured cells [186]. What physiological role the G45a-Ing1 interaction plays *in vivo* and which processes might be influenced by G45a- and Ing1-mediated DNA demethylation were unknown and the main focus of this thesis. Both G45a- and Ing1 single knockout mice have been described and have mild phenotypes with increased susceptibility to irradiation damage and lymphoma development [218, 230].

5.1 MOLECULAR ORIGINS OF NEURAL TUBE DEFECTS IN G45A-DEFICIENT MICE

In embryos, loss of G45a caused partially penetrant exencephaly, spina bifida and curly tails, each affecting approximately 15% of analyzed G45a-deficient embryos. While exencephaly has been shown to occur in G45a$^{-/-}$ mice at similar frequencies as observed in this study, spina bifida or curly tails were not reported before [230, 305]. All three of these G45a-driven embryonic phenotypes are caused by a failure to successfully complete neural tube closure [306].

A clear assignment of the molecular cause of neural tube defects in G45a-deficient mice is complicated by the multifunctional nature of G45a. However, potential molecular mechanisms can be narrowed down by matching G45a functions with known pathways that affect neural tube closure. Along the embryonic neural plate, there are three focal start points for neural tube closure, which are located at the hindbrain/cervical boundary, the forebrain/midbrain boundary and at the rostral tip of the embryo [306]. Different molecular pathways are involved in initiation and progression of neural tube closure at these start points. Only failure of neural tube closure initiated at the forebrain/midbrain boundary will cause exencephaly and spina bifida, thus narrowing down potentially affected pathways in G45a-mediated neural tube closure. Of proteins implicated in forebrain/midbrain boundary-initiated neural tube closure, in turn only 20% cause both exencephaly and spina bifida comparable to G45a$^{-/-}$ mice [307, 308]. The pathways these proteins are involved in include overactive Sonic hedgehog signaling and knockout of Protein Kinase A, which again indirectly causes Sonic hedgehog overactivation [307, 308]. Protein kinase A frequently activates p38 MAPK signaling [309]. Indeed, neural tube defects appear in mice deficient of many p38 MAPK signaling components [310-312], including the direct G45a target MAP3K4 [313, 314]. Thus, one likely mechanism of how G45a could be involved in

neural tube formation is activation of p38 signaling downstream of Protein Kinase A, leading to attenuation of Sonic hedgehog signaling.

Additionally to the mentioned signaling pathways, also mutation of many epigenetic factors impairs neural tube closure: Loss of either Dnmt3b, Dnmt3l, p300, CBP, or Sirtuin 1 cause exencephaly or spina bifida [307, 308]. Combined knockout of the 5mC oxidases Tet1 and Tet2 similarly leads to partially penetrant exencephaly [315]. Consequently, also aberrant DNA methylation is a possible mechanism for G45a-mediated neural tube defects. Crossing G45a mice with p53 [305], Cdkn1 [305] or Brca1 [316] mutant mice synergistically increases exencephaly. Since all of those proteins are required for DNA repair, this points to an involvement of DNA repair or DNA repair-mediated DNA demethylation in neural tube closure defects of G45a-deficient mice.

To distinguish between p38 MAPK signaling and DNA demethylation as molecular mechanisms of neural tube defects in G45a-deficient mice, further research is needed. A good starting point of further investigations would be the functional assessment of known pathways involved in neural tube closure by e.g. *in situ* hybridizations in affected G45a-deficient embryos.

5.2 MECHANISMS OF PREMATURE AGING IN G45A$^{-/-}$ ING1$^{-/-}$ MICE

Additionally to the observed neural tube and skeletal phenotypes, G45a$^{-/-}$ Ing1$^{-/-}$ mice exhibited a plethora of further symptoms, including a short life span, low body weight, failure to thrive, low body fat, kyphosis, bone marrow depletion, skin senescence, ovarian atrophy, reduced fertility, and reduced cellular proliferation. All observed phenotypes were partially penetrant, occurred with variable severity and seemed to arise independently of each other. In many cases, mice deficient of Ing1 alone showed a mild partial phenotype, making Ing1 the driver of phenotypical changes. In summary, all of the described symptoms are consistent with a segmental accelerated aging syndrome and are similar to phenotypes appearing in several other mouse models of premature aging [9, 37, 260].

Analogous to the neural and skeletal phenotypes discussed above, the multifunctional natures of G45a and Ing1 complicate the identification of causal molecular pathways of premature aging in G45a$^{-/-}$ Ing1$^{-/-}$ mice. Through analysis of known pathways involved in aging (see chapter 3.1.2), the premature aging phenotype of G45a$^{-/-}$ Ing1$^{-/-}$ mice was further molecularly characterized and the list of causative candidates considerably narrowed down.

Several pathways involved in physiological and premature aging were found to be unlikely candidates of aging for G45a- and Ing1 deficient mice. First, although unresolved low-grade inflammation can directly accelerate aging (see chapter 3.1.2.8), no signs of systemic inflammation were detected in

G45a$^{-/-}$ Ing1$^{-/-}$ mice. Immune gene expression was downregulated in liver and white adipose tissue microarrays (Figures 4.9 and 4.13), and no change in senescence-associated secretory phenotype proteins could be detected in mouse serum (Figure 4.26). Thus, the data point to a reduced immune response in G45a- and Ing1 deficient mice. Second, G45a$^{-/-}$ Ing1$^{-/-}$ mice showed telomere elongation, rather than a telomere shortening that has been correlated to aging (chapter 3.1.2.2). Telomere attrition should have most pronounced effects in fast proliferating tissues like skin, bone marrow or intestine. This contrasts with G45a$^{-/-}$ Ing1$^{-/-}$ phenotypes, which were most penetrant in adipose tissue and ovaries. Moreover, no indications of abnormal reactive oxygen species amounts or aberrant Wnt signaling activation were detected in G45a$^{-/-}$ Ing1$^{-/-}$ tissues. Lastly, G45a's role in p38 MAPK signaling is an unlikely mechanism of aging in the analyzed mice: Whereas loss of G45a leads to reduced p38 activation [225-227], the development of aging phenotypes has been correlated to increased p38 activity [298]. Nonetheless, p38 signaling might play a role by indirectly promoting nucleotide excision repair [317, 318] and thereby influencing DNA damage levels in G45a- and Ing1 deficient mice.

Both G45a and Ing1 are indirectly contributing to several DNA repair mechanisms including nucleotide excision repair and base excision repair [201, 206, 230, 231]. Defective DNA repair and consequently accumulating DNA damage are considered one of the causative mechanisms of premature aging [20]. Many proteins involved in nucleotide excision repair are linked to premature aging disorders [9, 10, 85, 319]. The strong phenotypic overlap of G45a$^{-/-}$ Ing1$^{-/-}$ mice with mice deficient for nucleotide excision repair proteins points to a potential contribution of unrepaired DNA damage also to the G45a$^{-/-}$ Ing1$^{-/-}$ premature aging phenotype. However, even in mice deficient of nucleotide excision repair proteins, the mechanism underlying premature aging is controversial, as most nucleotide excision repair proteins also play roles outside DNA repair. DNA mutation load in mice lacking those proteins is not necessarily increased [320]. Moreover, while e.g. Xpg deletion causes premature aging [321], a catalytically inactive Xpg mutant incapable of nucleotide excision repair does not age prematurely [322]. This argues for other Xpg functions like transcription regulation or scaffolding to be essential for its premature aging phenotype. Thus, notwithstanding a role for G45a and Ing1 in DNA repair, a similar reasoning might also hold true for G45a$^{-/-}$ Ing1$^{-/-}$ mice.

Analogously, mice lacking Thymidine DNA glycosylase (TDG) have defects in both DNA repair and DNA demethylation [138, 323]. Cortellino et al. and Cortazar et al. argue that defective DNA repair should cause highly variable phenotypes due to the stochastic nature of randomly occurring DNA damages. Thus, they argue, the synchronous and fully penetrant embryonic lethality of TDG-deficient mice must be attributed to defective DNA demethylation [138, 323]. However, phenotypes of Tet mutants show large variability as well: Tet1 mutant females are partially infertile [151], not all Tet2

mutants develop hematological disorders [324, 325], only a fraction of Tet1/2 double mutants show perinatal lethality [315], and imprinting defects their offspring are likewise only partially penetrant [152]. Hence for G45a$^{-/-}$ Ing1$^{-/-}$ mice, which show a likewise high phenotypic variability, both a DNA repair and DNA demethylation mediated phenotype could be envisioned. Since DNA repair and DNA demethylation processes are intertwined, differentiating between these two pathways is challenging.

An indication that defective DNA demethylation might contribute to the Gadd45a$^{-/-}$ Ing1$^{-/-}$ premature aging phenotypes comes from phenotypic overlaps of G45a$^{-/-}$ Ing1$^{-/-}$ mice with mice lacking Tet enzymes or Dnmts. Especially for Tet1/2 double knockout mice, a considerable phenotypic overlap to G45a$^{-/-}$ Ing1$^{-/-}$ mice can be observed (table 5.1). For example, G45a$^{-/-}$ Ing1$^{-/-}$ ovarian atrophy is similar to that observed in Tet1$^{-/-}$ mice, and both G45a$^{-/-}$ Ing1$^{-/-}$ and Tet1$^{-/-}$ female embryos show reduced expression of meiosis-related genes [151]. Conversely, Dnmt3b hypomorphic mice display overactivation of meiotic genes even in non-reproductive tissues [326]. During natural and premature ovarian aging, aberrant DNA methylation patterns and misexpression of Tet and Tdg have been reported [327]. These findings strongly indicate that meiotic genes are regulated by DNA methylation and that DNA hypermethylation in primordial germ cells could be causative for meiotic defects of G45a$^{-/-}$ Ing1$^{-/-}$ mice. An argument against a role of DNA demethylation in G45a$^{-/-}$ Ing1$^{-/-}$ premature aging comes from experiments in *Drosophila*, in which neuronal overexpression of Gadd45 is sufficient to prolong lifespan [179]. As *Drosophila* does not have significant DNA methylation, Gadd45a must act there via other pathways to extend lifespan.

	G45a$^{-/-}$ [230]	G45a$^{-/-}$ Ing1$^{-/-}$	Tet1$^{-/-}$ [151]	Tet1$^{-/-}$ Tet2$^{-/-}$ *[315]*	Dnmt3a$^{-/-}$ *[328]*
Execenphaly	x	x		x	
Memory defects	x[1]	ND	x [329]	ND	
Leukemia	x	ND		x	
Elongated telomeres		x		x [176]	x[2] [330]
Small body size		x	x	x	x
Ovarian atrophy		x	x	x	
Low body weight		x		x	x
Kyphosis		x			x

TABLE 5.1 COMPARISON OF PHENOTYPES IN MICE DEFICIENT OF DNA METHYLATION OR DNA DEMETHYLATION PROTEINS
x: Phenotype present; ND: not determined; [1] Beat Lutz lab, personal communication; [2] Combined knockout of Dnmt3a and Dnmt3b

Additionally to roles in DNA repair and DNA demethylation, both Gadd45a and Ing1 interact with proteins and pathways directly involved in aging. The nuclear envelop component Lamin A, whose

mutated version causes Hutchinson-Gilford progeria, is required for retaining Ing1 in the cell nucleus. In Lamin A mutant cells, Ing1 relocalizes to the cytoplasm and cannot exert its functions [196]. Therefore, the premature aging phenotype of Lamin A mutants can be at least partially attributed to Ing1 inactivation. Furthermore, Ing1 interacts with Sirtuin 1, which is implicated in longevity-regulating processes through deacetylation of several aging-related proteins [104]. Ing1-Sirtuin 1 interaction blocks deacetylation of p53 [199], but whether it has further consequences that are relevant for aging is not known. Gadd45a is connected to established aging mechanisms by being a downstream target of Igf1 signaling. Low levels of Igf1 promote longevity and induce Gadd45a expression via Foxo3a [209]. This could be part of the more widespread Igf1-mediated regulation of stress response genes that is aimed at reducing reactive oxygen species in the cell. Moreover, Gadd45a physically interacts with and inhibits mTOR, one of the central downstream mediators of Igf1 signaling [331]. As decreased mTOR activity, e.g. via caloric restriction or Rapamycin treatment, prolongs lifespan [73, 74], it is possible that loss of Gadd45a could conversely mediate premature aging via mTOR overactivation. However, whether Gadd45a and Ing1 contribute to aging and longevity through any of these proposed pathways requires further investigations. Similar to other premature aging mouse models [104, 332], also more than one molecular mechanism might play a role in $G45a^{-/-}$ $Ing1^{-/-}$ premature aging.

Whereas the contribution of DNA repair proteins to aging processes is well established [333-335], studies of the role of DNA methylation in aging remained mostly correlative. A direct role of DNA demethylation in the $G45a^{-/-}$ $Ing1^{-/-}$ phenotype would be the first direct evidence for a causal contribution of DNA demethylation processes to aging. However, to further dissect the causal mechanisms of premature aging in $G45a^{-/-}$ $Ing1^{-/-}$ mice, further research is required. Strong evidence for an epigenetic cause could be a successful rescue of the phenotype: Could enhanced DNA demethylation e.g. by treatment with the Tet activator Vitamin C or inhibiting DNA methylation via the Dnmt inhibitor Azacytidine rescue premature aging? Does boosting DNA repair mechanisms or reducing DNA damage (via e.g. antioxidants) ameliorate $G45a^{-/-}$ $Ing1^{-/-}$ aging phenotypes? A precedent for the ability of Vitamin C supplementation to rescue premature aging symptoms has been set in a mouse model of Werner syndrome, although neither the rationale nor the molecular mechanism of Vitamin C were stated in the study [336].

While Gadd45a and Ing1 have been recognized as proteins involved in cellular senescence, a role for them in organismal aging has not been described so far. Through combined knockout of both proteins, this study adds Gadd45a and Ing1 to the growing list of proteins implicated in aging and provides a starting point for potential Gadd45a- or Ing1-based strategies for prevention of age-related pathologies.

5.3 SELECTIVE REDUCTION OF ADIPOSE TISSUE DEPOTS AND WAT BROWNING IN G45A$^{-/-}$ ING1$^{-/-}$ MICE

As part of their premature aging phenotype, G45a$^{-/-}$ Ing1$^{-/-}$ mice displayed a systemic reduction of adipose tissue depots. Histologically, this is reflected by smaller adipocyte size and consequently decreased amounts of triglycerides stored per adipocyte. Moreover, islands within white adipose tissue depots of G45a$^{-/-}$ Ing1$^{-/-}$ mice have brown adipose tissue-like morphology, and brown adipocyte-associated gene expression signatures are observed in gene expression arrays of G45a$^{-/-}$ Ing1$^{-/-}$ white adipose tissue.

Adipose tissue hypotrophy as well as browning of white adipose tissue are characteristic symptoms of premature aging and are observed in many further mouse models of accelerated aging [85, 337-339]. For different premature aging models, adipose tissue hypotrophy has been attributed to cell-intrinsic mechanisms [270, 338, 340].

In G45a$^{-/-}$ Ing1$^{-/-}$ mice, theoretically different mechanisms could contribute to diminished white adipose tissue depots. Firstly, the observed browning of white adipose tissue leads to increased energy dissipation, which is further exacerbated by a shift towards catabolic gene expression observed in the liver (Figure 4.9). A higher energy usage could reduce the amounts of triglycerides available for storage in white adipose tissue. Secondly, reduced IGF-1 signaling could contribute to fat depletion in G45a$^{-/-}$ Ing1$^{-/-}$ mice. IGF-1 acts, similar to Insulin, as an anabolic signal to increase lipid storage. Consequently, the observed attenuation of the IGF-1 axis (Figure 4.10) might be a systemic signal limiting triglyceride storage in G45a$^{-/-}$ Ing1$^{-/-}$ mice. Thirdly, similar to other premature aging models [270, 338, 340], adipose tissue hypoplasia in G45a- and Ing1 deficient mice could be cell-intrinsic. The observed reduced potential of G45a$^{-/-}$ Ing1$^{-/-}$ MEFs to differentiate along the adipogenic lineage (Figures 4.16-4.19) provides strong evidence for a cell-intrinsic differentiation defect causing adipose tissue hypoplasia in mice deficient for G45a and Ing1. However, it cannot be excluded that systemic effects as described above further contribute to adipose tissue phenotypes.

The partial brown adipose tissue-like morphology of G45a$^{-/-}$ Ing1$^{-/-}$ WAT cannot be explained by an impaired differentiation towards white adipocytes, and different mechanisms could be responsible for WAT browning in G45a$^{-/-}$ Ing1$^{-/-}$ mice. As for WAT hypotrophy, secondary causes like decreased heat production or increased heat dissipation could play a role in WAT browning. For example, reduced adipose tissue content translates to reduced insulation against cold, potentially increasing the necessity for non-shivering thermogenesis and thus increased WAT browning. Reduced insulation against cold can furthermore be caused by skin atrophy or fur phenotypes and has been shown to be the primary

cause of WAT browning in a number of transgenic mice [341, 342]. Since decreased dermal thickness and skin cell senescence have been observed in G45a$^{-/-}$ Ing1$^{-/-}$ mice (Figure 4.6), this mechanism could provide a possible cause of WAT browning also for mice deficient of G45a and Ing1. Moreover, reduced heat production could be a consequence of muscle atrophy that occurs during aging. Mice are usually housed at 22°C, which exposes them to constant cold stress. Experiments to clarify whether WAT browning in G45a- and Ing1 deficient mice is due to the above described secondary causes would require mice to be housed at murine thermoneutrality at 30°C and to examine whether WAT browning still appears intrinsically in the absence of cold stress.

Molecular mechanisms of WAT browning have started to be elucidated, but knowledge about them is still incomplete [343, 344]. No factors of WAT browning have been identified that relate molecularly to Gadd45a or Ing1 functions. Two main pathways triggering WAT browning are β-adrenergic stimulation induced by cold stress, and reduced Insulin signaling. Both pathways coalesce on increasing cAMP levels and subsequent Protein Kinase A activation, which initiates expression of brown adipocyte genes. Further research is required to elucidate the molecular role of Gadd45a and Ing1 in these pathways.

Similar to other aging phenotypes, a pathway that can be excluded to cause WAT browning or impaired adipocyte differentiation in G45a$^{-/-}$ Ing1$^{-/-}$ mice is p38 MAPK signaling. p38 MAPK signaling promotes adipocyte differentiation [299] as well as WAT browning [345]. As G45a activates p38 signaling [225-227], loss of G45a and Ing1 should lead to decreased p38 signaling and thus the absence of a browning stimulus. Curiously, the opposite has been observed for the closely-related Gadd45a family member Gadd45g. In contrast to G45a and Ing1, Gadd45g promotes BAT development via p38 signaling [346]. In this process, Gadd45g acts downstream of cold-induced cAMP/Protein Kinase A to activate MAP3K4 and thus induce p38 signaling. Consequently, loss of Gadd45g results in reduced brown adipose tissue, highlighting opposite and non-redundant functions of Gadd45a and Gadd45g in adipose tissue biology.

Induction of WAT browning is a coveted and highly researched strategy for human weight reduction and combating the current obesity pandemic [272, 347, 348]. It promises an easier, more feasible and potentially faster way of weight reduction than a long-term conversion of eating habits towards a healthier diet. Inhibition of G45a, or especially Ing1 function, might be a potential approach to achieve WAT browning and slimming. However, any G45a- or Ing1 centered approach for this purpose will likely come with the tradeoff of accelerated aging and therefore does not represent a feasible strategy.

5.4 DNA HYPERMETHYLATION AND ITS POTENTIAL CONTRIBUTIONS TO AGING

In order to elucidate whether DNA demethylation defects could contribute to the G45a$^{-/-}$ Ing1$^{-/-}$ phenotypes, we analyzed the DNA methylome of WT and G45a$^{-/-}$ Ing1$^{-/-}$ MEFs. While no global DNA methylation differences were identified, G45a$^{-/-}$ Ing1$^{-/-}$ MEFs showed local DNA hypermethylation that was specifically enriched at enhancer regions. Enhancer hypermethylation was predominantly correlated with repression of associated genes and regulated genes involved in extracellular matrix functions, cytoskeletal organization, and cell migration. Thus, aberrant DNA hypermethylation in G45a$^{-/-}$ Ing1$^{-/-}$ MEFs was correlated with indicators of functional decline of fibroblasts, a process that is commonly observed in fibroblast aging. While few selected targets of G45a- and Ing1-mediated DNA demethylation have been previously identified in diverse cell types [140, 186, 236], this is the first study determining unbiasedly genome-wide targets of G45a-and Ing1-mediated DNA demethylation. The DNA hypermethylation observed at enhancer regions in G45a- and Ing1 deficient cells is consistent with published results that demonstrate that enhancers are especially prone to DNA methylation changes (see chapter 3.2.3). Comparable patterns of DNA hypermethylation were for example also observed for loss of Tet enzymes in embryonic stem cells [176].

Nonetheless, several caveats have to be kept in mind. Due to good genomic coverage in both WT and G45a$^{-/-}$ Ing1$^{-/-}$ MEF lines, the observed DNA methylation levels were technically reliable and fulfilled current quality recommendations for WGBS-Seq [302]. The identified DMRs could be well validated technically, but an unknown extent of biologically significant DMRs might have remained unidentified by the DMR filtering criteria. Thus, the true number of DMRs in the dataset may be larger than our conservative estimate that was employed on account of its low false discovery rate. For cost and data analysis reasons, DNA methylation levels of only a single WT and G45a$^{-/-}$ Ing1$^{-/-}$ MEF line could be analyzed in the here obtained depth and resolution. This makes the data vulnerable to cell line-specific effects. Indeed, while DMRs were highly reproducible using the same MEF lines as for WGBS-Seq, biological reproducibility in independent MEF lines dropped to approximately 25% of tested loci. Also, it is unclear why DMRs were strongly enriched for enhancers, when Ing1 is a reader of H3K4me3 marks [349] that do not occur in enhancer regions. ChIP-Seq of overexpressed Ing1 in myoblasts and myotubes demonstrated that in these cell lines, Ing1 is found exclusively at transcription start sites decorated with H3K4me3 [202]. This raises the question of how directly the DNA hypermethylation in DMRs is caused by loss of G45a and Ing1. Either ChIP-qPCR or ChIP-Seq analysis is required to confirm a direct binding of G45a and Ing1 at DMRs.

This study, along with others [350-352] correlates aging with the presence of local DNA hypermethylation. Any causal relationships of DNA hypo- or hypermethylation and aging remain to be

clarified, i.e. do DNA methylation changes arise as a byproduct of aging, or do DNA methylation changes causally contribute to the onset of aging symptoms?

Potentially, aging processes could lead to DNA methylation changes via aging-induced metabolic alterations. Caloric restriction has been tightly linked to delaying aging processes, with restriction of solely methionine consumption conferring nearly full life-extension effects of caloric restriction [353, 354]. Methionine is the substrate for generation of S-Adenosyl-Methionine, an important methyl group donor for various substrates, including DNA. Consequently, DNA methylation might be coupled to methionine availability. Similar to DNA methylation, also DNA demethylation could be coupled to metabolic processes. Tet proteins are dependent on the availability of their cofactor α-Ketoglutarate, an intermediate of the citric acid cycle. Thus, both DNA methylation and demethylation can be regulated by the levels of their metabolic cofactors, making them susceptible to age-related metabolic changes.

DNA methylation changes have the potential to causally contribute to the progression of aging. The global DNA hypomethylation observed during aging [114, 115] can lead to a derepression of transposable elements or lineage-inappropriate genes. Global DNA hypomethylation has been furthermore demonstrated to result in genomic instability and elevated mutation rates [355, 356]. Locally increased DNA methylation on the other side could repress either genes required for cell type specific functions or genes required for differentiation to specific lineages, leading to functional decline of tissues. DNA hypermethylation could furthermore repress longevity-associated genes that could have systemic effects on aging. In G45a$^{-/-}$ Ing1$^{-/-}$ MEFs, hypermethylated genomic regions are associated with genes important for functional integrity of fibroblasts, confirming that local DNA hypermethylation can be associated with functional decline during aging.

The identification of DNA methylation changes that contribute to aging has the potential to be used for combating age-related pathologies. Pollina et al. classified aging mechanisms into reversible and non-reversible ones [25]. Whereas e.g. DNA damage, telomere shortening or mitochondrial damage are non-reversible damages, altered cellular signaling or DNA methylation changes have the potential to be counteracted. Accordingly, reversible aging mechanisms such as DNA methylation changes are prime targets for combating age-associated symptoms and ameliorating pathologies in the aging population.

6. MATERIALS AND METHODS

6.1 EQUIPMENT AND MATERIALS

6.1.1 EQUIPMENT

-80°C freezer (Sanyo), -150°C freezer (Sanyo), agarose gel chambers (BioRad), automated tissue processor (Leica), bacterial incubators (Thermo Scientific), bacterial shaker (Infors), balances (Sartorius, Kern), Bioanalyzer (Agilent), Bioruptor (Diagenode), blotting apparatus (BioRad), cell counter (BioRad), cell culture incubators (Thermo Scientific), centrifuges (Heraeus), confocal microscopes (Leica), coverslips (Menzel), cryostat (Leica), glass slides (Thermo Scientific), heating blocks (Eppendorf), HiSeq 2500 sequencing system (Illumina), hybridization oven (Thermo Scientific), laminar flow hoods (Dometric), LightCycler 480 (Roche), LRS Fortessa Sorp flow cytometer (BD), magnetic stirrer (Heidolph), microcentrifuges (Heraeus), microplate reader (Tecan), microscope (Leica), microwave oven (Sharp), multidispenser pipette (Eppendorf), Nanodrop 2000 spectrophotometer (Thermo Scientific), Neon Transfection System (Invitrogen), orbital shaker (Neolab), PAGE minigel chambers (BioRad), PCR thermocyclers (Biometra), pH meter (Mettler Toledo), pipet boy (Integra), pipettes (Eppendorf), power supplies (BioRad), rotator (Neolab), rotary microtome (Leica), SpeedVac concentrator (Eppendorf), staining jars (Neolab), stereomicroscope (Leica), tissue embedding station (Leica), ultrapure water purification system (Millipore), ultrathurrax homogenator (IKA), UV photodocumentation system (BioRad), vortexer (Scientific industries), waterbaths (Neolab).

6.1.2 CHEMICALS

Chemicals from Sigma-Alrich: Acetic acid, Alcian Blue, Alizarin Red, ampicillin, boric acid, bovine serum albumin, bromphenol blue, chloroform, citric acid, crystal violet, DAPI, dithiothreitol, dexamethasone, dimethylsulfoxide, EDTA, ethanol, Eosin, glycerol, glycine, Harris' Hematoxylin, hydrochloric acid, Hoechst 33342, insulin, isobutylmethylxanthine (IBMX), isopropanol, L-ascorbic acid-2-phosphate, lithium chloride, $K_3[Fe(CN)_6$, $K_4[Fe(CN)_6$, magnesium chloride, ß-mercaptoethanol, methanol, Oil Red O, paraffin, polybrene, propidium iodide, puromycin, Rosiglitazone, skim milk powder, sodium chloride, sodium dodecyl sulfate, sodium hydroxide, sodium phosphate, sucrose, potassium hydroxide, RNAlater, TEMED, Tris base, Tris HCl, Tween-20, Triton X-100, xylol.

Further chemicals: Acrylamide (Roth), agarose (Biozym), chloroform (Roth), O.C.T. TissueTek (Weckert Labortechnik), dNTPs (Thermo Scientific, DMEM (Lonza), ethidium bromide (Roth, Sigma-

Aldrich), fetal bovine serum (Lonza), Immumount mounting medium (Thermo Scientific), nuclease-free water (Qiagen), paraformaldehyde (Merck), phenol (Roth), 100x Penicillin/Streptomycin (Lonza), protease inhibitor cocktail tablets (Roche), Roticlear (Roth), Qiazol (Qiagen), Trypsin (Lonza).

6.1.3 ENZYMES

HpaII (Promega), *HhaI* (Promega), *MspI* (Promega), *PvuII* (Promega), restriction endonucleases (NEB), Accuprime Taq polymerase system (Invitrogen), DNaseI (Qiagen, Roche), Proteinase K (Roche), RNaseA (Invitrogen), Superscript II reverse transcriptase (Invitrogen), *Taq* polymerase (homemade), T4 DNA ligase (Invitrogen).

6.1.4 ANTIBODIES

Target protein	Host species	Conjugate	Company	Order number
α-Tubulin	Mouse		Sigma	T5186
Caspase 3	Rabbit		Cell Signaling	9662
C/EBPβ	Rabbit		Santa Cruz	sc-150X
Erk	Rabbit		Cell Signaling	4695S
phospho-Erk	Mouse		Sigma	M8159
γH2.AX	Mouse		Millipore	05-636
Histone H3	Rabbit		Abcam	ab1791
JNK	Rabbit		Santa Cruz	sc-571
phospho-JNK	Rabbit		Cell Signaling	4668S
p38	Rabbit		Cell Signaling	9212S
phospho-p38	Rabbit		Cell Signaling	9211S
p16	Rabbit		Santa Cruz	sc-1207
PPARγ	Mouse		Abcam	ab41928
Mouse IgG	Goat	Horse radish peroxidase	Dianova	115-035-146
Rabbit IgG	Goat	Horse radish peroxidase	Dianova	111-035-144
Rabbit IgG	Goat	Alexa Fluor 546	Invitrogen	A11035
Mouse IgG	Goat	Alexa Fluor 488	Invitrogen	A11030

TABLE 6.2 PRIMARY AND SECONDARY ANTIBODIES

6.1.5 KITS

Cellular Senescence Assay kit (Cell Biolabs), DNeasy Blood & Tissue kit (Qiagen), Epitect Bisulfite kit (Qiagen), Mouse Cytokine Antibody array C series Array 3 (RayBiotech), PCR purification kit (Qiagen), Qiaprep Qiaprep Miniprep kit (Qiagen), Qiaprep Midiprep kit (Qiagen), Qiaquick Gel extraction kit (Qiagen), RNeasy Mini Kit (Qiagen), RNeasy 96 kit (Qiagen), Telo TAAGG telomere length assay kit (Roche), Total ROS/Superoxide Detection Kit (Enzo Life Sciences).

6.1.6 PLASMIDS

The retroviral expression vector pBABE-puro was obtained from Addgene (Plasmid #1764). pBABE-puro-HA-hGadd45a contains the N-terminally HA-tagged human Gadd45a sequence that was PCR amplified from pHA-hGadd45a [137] using primers with flanking *SnaBI* restriction sites and inserted into pBABE-puro into its *SnaBI* restriction site. pBABE-puro-Myc-hIng1b contains the N-terminally Myc-tagged human Ing1b sequence cloned from pCS2-Myc-hIng1b [186] into pBABE-puro using *EcoRI* and *SalI* restriction sites. pBABE-puro-Flag-mPPARγ contains the the N-terminally FLAG-tagged mouse PPARγ sequence that was PCR-amplified from pcDNA-Flag-PPARγ (Addgene Plasmid # 8895) using primers with flanking *EcoRI* and *SalI* restriction sites and inserted into pBABE-puro using its *EcoRI* and *SalI* restriction sites.

6.1.7 PRIMERS

Target gene	Forward primer sequence	Reverse primer sequence	UPL probe
Acadl	TGGGGACTTGCTCTCAACA	GGCCTGTGCAATTGGAGTA	103
Acadm	AGTACCCTGTGGAGAAGCTGAT	TCAATGTGCTCACGAGCTATG	110
Acadsb	TCCAGATAGGGAAACGAGAAAA	TCCCCAAAATATTAGTCTCTGGA	105
Acot3	GTGCACGAGCGTCACTTC	TCCAGGAAAGGGTCCAGTT	4
Acot4	ATGCTTCGACATCCAAAGGT	GGAAGCCATGATCAGACAGAC	17
Adiponectin	GGAGAGAAAGGAGATGCAGGT	CTTTCCTGCCAGGGGTTC	17
Aldh2	TGTTCGGGGACGTAAAAGAC	TGAGGATTTGCATCACTGGT	63
Arginase1	GAATCTGCATGGGCAACC	GAATCCTGGTACATCTGGGAAC	2
C/EBPa	AAACAACGCAACGTGGAGA	GCGGTCATTGTCACTGGTC	67
C/EBPb	TGATGCAATCCGGATCAA	CACGTGTGTTGCGTCAGTC	102
C/EBPd	CTTTTAGGTGGTTGCCGAAG	GCAACGAGGAATCAAGTTTCA	33
Cidea	TTCAAGGCCGTGTTAAGGA	CCTTTGGTGCTAGGCTTGG	46
C6	TCCAGTACTTGAGATGTTTACCAGA	TTGAGGCACGAGGTCCTT	109
Cox4i1	TCACTGCGCTCGTTCTGAT	CGATCGAAAGTATGAGGGATG	7
Cox5b	CTCCATGGCTTCTGGAGGT	GCCTTTGGAGGTAGCATATTGT	26
Cyp4a10	GTTCCAGCACAGGAGGATG	CAGCCGTTCCCATTTGTC	97
Cyp4a31	CAGCACCGGAAGATGCTAA	CAGCCGTTCCCATTTGTC	97
Cyt c	AACGTTCGTGGTGTTGACC	TTATGCTTGCCTCCCTTTTC	104
Dhrs4	GAGTGTGACTGGCATCGTGT	ATATCAATCCCCTGGTGACG	60
Elovl3	ACTTCGAGACGTTTCAGGACTTA	GACGACCACTATGAGAAATGAGC	25
Elovl4	ACGACACCGTGGAGTTCTATC	GCGGCCAGTCTGCTACAC	85
FABP4	AAGAGAAAACGAGATGGTGACAA	CTTGTGGAAGTCACGCCTTT	31
Gadd45a	GCTGCCAGCTGCTCAAC	TCGTCGTCTTCGTCAGCA	98
Gapdh	AGCTTGTCATCAACGGGAAG	TTTGATGTTAGTGGGGTCTCG	9
GhR	AGTAAATGAATCAAAATGGAAAGT	ATCTCACCCGCACTTCATGT	47
Hsd17b2	TCACCAAGCCAGAGCAGATA	GTTAACCACGGCCCACAGT	100
Idh3b	GCTGCGGCATCTCAATCT	CCATGTCTCGAGTCCGTACC	67

IL1b	AGTTGACGGACCCCAAAAG	AGCTGGATGCTCTCATCAGG	38
IL1RA	TCCTTCTCATCCTTCTGTTTCAT	GGTCTTCTGGTTAGTATCCCAGAT	34
IL10	CAGAGCCACATGCTCCTAGA	TGTCCAGCTGGTCCTTTGTT	41
IL12a	TCAGAATCACAACCATCAGCA	CGCCATTATGATTCAGAGACTG	49
IL6	GCTACCAAACTGGATATAATCAGG	CCAGGTAGCTATGGTACTCCAGA	6
Igf1	CTGCTTGCTCACCTTCACC	AGCCTGTGGGCTTGTTGA	22
Ing1	CCTCCTTCTTCGTGCAGATTG	TCTGGCGTTTGAACTTGTCATAG	17
InsR	GAGAATTTCCTTCACAATTCCATC	CACTTGCATGACGTCTCTCC	104
Irs1	CTATGCCAGCATCAGCTTCC	TTGCTGAGGTCATTTAGGTCTTC	71
Klf4	CGGGAAGGGAGAAGACACT	GAGTTCCTCACGCCAACG	62
Leptin	CAGGATCAATGACATTTCACACA	GCTGGTGAGGACCTGTTGAT	93
Mael	TGGCCACCTATTTACTGCAA	TCCATACGCTTCAAACACCA	106
Ndufab1	TGCAGATAAGAAGGATGTGTATGA	CTGTCAGTCGGCCACGAT	109
Ndufv1	GGGTGAGATGAAGACATCAGG	TCAGCATTCACCACCAGATACT	60
Pex19	TGCTGTACCCATCCCTGAA	GGAGGAGTGGAGTCCTGGT	50
Pex3	CAATGTGGAATTTTCTGAAACG	TCTGTCCATATTTTCCCAGGAT	104
Pgc1a	GAAAGGGCCAAACAGAGAGA	GTAAATCACACGGCGCTCTT	29
Plin1	AACGTGGTAGACACTGTGGTACA	TCTCGGAATTCGCTCTCG	64
PPARa	CACGCATGTGAAGGCTGTAA	GCTCCGATCACACTTGTCG	41
PPARg	CAAGCCCTTTACCACAGTTGA	CAGGTTCTACTTTGATCGCACTT	67
Prdm16	TCTCGGATCCCATCCTCA	GGAAGATCTTGCCACAGTACCT	12
Prdm9	GCCAGGAACTGGGCATTA	GGATGAATTTCTGTCCTTAGTTCT	60
Sycp1	CAGGTTGCTAATTCTGGCAGT	GCTCATTGGCTCTGAATTCTC	12
Sycp3	GGACAGCGACAGCTCACC	AAGGTGGCTTCCCAGATTTC	31
Tbp	GGGGAGCTGTGATGTGAAGT	CCAGGAAATAATTCTGGCTCA	97
Tex12	GAATCTCCGCTTGCGAGT	TCGGGTTTTACAAGGTGGTT	82
Tgfb1	TGGAGCAACATGTGGAACTC	GTCAGCAGCCGGTTACCA	72
Tnfa	TCTTCTCATTCCTGCTTGTGG	GGTCTGGGCCATAGAACTGA	49
Ucp1	GGCCTCTACGACTCAGTCCA	TAAGCCGGCTGAGATCTTGT	34
Ucp3	TACCCAACCTTGGCTAGACG	GTCCGAGGAGAGAGCTTGC	69

TABLE 6.3 QRT-PCR PRIMERS

Genomic region	Genomic coordinates	Primer sequence	UPL probe
Gapdh	chr6:125115169-125115257	**f:** CCTACGCAGGTCTTGCTGA	10
		r: TGACCTTGAGGTCTCCTTGG	
Peg3	chr7:6,683,069-6,683,210	f: AGTGGACCCACACTGAACC	26
		r: GAGAAGCGGAGAGATGTCCA	
DMR1	chr7:13489136-13489248	f: GGAATCCAGCCCTAGCTTTAC	42
		r: GCTCTCGCAGTTGGGCTA	
DMR2	chr11:49624657-49624751	f: TCCCTAGTGTGAGCCTTAGCC	102
		r: CACAGCAGCCCTCAAGATAA	
DMR3	chr13:113545830-113545918	f: ACCACGGAGCTGAGTCCTAA	53
		r: AGGAATCAGGAGACAACTATGGA	
DMR4	chr18:23940654-23940729	f: TGGTGGCTCACCCAGAGT	66
		r: GGCTGGTCTCTTGGGACA	
DMR5	chrX:166435106-166435188	f: ACACAGCGTGAACGACCAG	-
		GCCTGAGACGAATCAATGAAA	
DMR6	chr2:173091915-173092050	f: TTCCTCCTATGGCTGTGACC	33
		r: AAGGCGTGAATCATTTATTGGT	
DMR7	chr4:105314322-105314417	f: GTTCACTTCTTGAAGCTTTTCTCA	55
		r: CAACATGTTTATTCACATGGAGAGA	
DMR8	chr10:99495588-99495662	f: CATCCCTTCCAAACGTGTCT	-
		r: TCATGATGACTCCACACAGGA	
DMR9	chr2:118844243-118844321	f: CGATGAGTGTGTGAGCGAAT	-
		r: AGGAACAAGGGTAGCCAAGG	
DMR10	chrX:166435711-166435776	f: CCCTAGGTAGCGCAGTGAGT	-
		r: ACACGGGGTCTCTGTGTCTG	
DMR11	chr19: 38746596-38746995	f: TGGCAATCCTAACAAA	-
		r: GGCTCTGACACTGTGGTTGA	
DMR12	chr16:92449531-92449606	f: TGCGGTTAAAAGTCTCATGC	-
		r: ATTCGGAGCGTGTTGTTCTT	
DMR13	chr5:53794142-53794231	f: TGAGTGTGCTATGTGTCAGCAG	6
		r: AGGAAGCTAGTTCTACGAATCCAC	
DMR14	chr18:23940746-23940854	f: TTCTTTGTTTAACTTGTCATCTAGCC	9
		r: GGTTGGGAGACATAAGGACTCA	
DMR15	chr18:23940753-23940854	f: TTTAACTTGTCATCTAGCCTCAGC	9
		r: GGTTGGGAGACATAAGGACTCA	
DMR16	chr8:49394994-49395067	f: GGAAACCCAAGAGGGGAAA	-
		r: TCAGTGAAAAGATGTGTTCGAGA	
DMR17	chr6:4460009-4460109	f: TGGAAATAATTGTGAAGCAGTCA	-
		r: CACCGAAATGTAGCAAAAATG	

TABLE 6.4 METHYLATION-SPECIFIC PCR PRIMERS

6.1.8 BUFFERS AND SOLUTIONS

Solution	Components
Alcian Blue staining solution	15 mg Alcian Blue, 80 ml 95% Ethanol, 20 ml glacial acetic acid
DMEM+++	DMEM, 10% FBS, 10 mM L-Glutamine, 100U/ml Penicillin, 100U/ml Streptomycin
6x DNA loading buffer	60% (w/v) sucrose, 0.25% xylene cyanole, 0.25% bromphenol blue
dNTP mix	5 mM dATP, 5mM dCTP, 5mM dGTP, 5mM dTTP
Eosine-Phloxin staining solution	70% ethanol, 0.4% glacial acetic acid, 1g/l Eosine, 0.1g/l Phloxine B. Kept in dark.
4x Lämmli sample buffer	60 mM Tris-Cl pH 6.8, 2% sodium dodecyl sulfate, 10% glycerol, 5% β-mercaptoethanol, 0.01% bromophenol blue
Luria broth (LB)	10g bactotryptone, 5g yeast extract, 10g NaCl in 1l water, pH7.5, autoclaved
PBGNT	PBS, 0.5% BSA, 0.2% cold water fish gelatin, 0.5M NaCl, 0,1% Triton-X100
PBS	9.0 g/l NaCl, 144 mg/l KH_2PO_4, 795 mg/l Na_2HPO_4, sterile
RIPA buffer	150 mM NaCl, 1% Triton-X100, 0.5% sodium deoxycholate, 0.1 % sodium dodecyl sulfate, 50 mM Tris-HCl pH 8.0
SA-βGal staining solution	40 mM citric acid, 40 mM dibasic sodium phosphate, 5 mM $K_4[Fe(CN)_6]$, 5mM $K_3[Fe(CN)_6]$, 150 mM NaCl, 2 mM MgCl, 1 mg/ml X-Gal (5 -Bromo-4-chloro-3-indolyl-beta-D-galactopyranoside)
Tail lysis buffer	10 mM Tris, 5 mM EDTA, 300 mM sodium acetate, 1% Triton X-100, pH 8.0
10xTBE	1M Tris base, 1M boric acid, 20 mM EDTA, autoclaved
20x TBS	3M NaCl, 5.36 mM KCl, 1M Tris-HCl pH 7.4, autoclaved
TBS-T	1x TBS, 0.05% Tween 20
TE buffer	10 mM Tris-HCl pH 8.0, 10 mM EDTA, autoclaved

TABLE 6.5 BUFFERS AND SOLUTIONS

6.2 General molecular biology methods

General molecular biology methods including preparation of chemically competent XL1-blue *Escherichia coli* bacteria, plasmid amplification in *Escherichia coli*, spectrophotometric quantification of DNA and RNA, restriction digests, DNA ligations, PCR, agarose gel electrophoresis, and SDS-PAGE were carried out as previously described [357]. All used oligonucleotides were synthesized by Sigma Aldrich. Plasmid DNA was sequenced by GATC Biotech.

6.2.1 AMPLIFICATION AND PURIFICATION OF PLASMIDS FROM BACTERIA

For plasmid amplification, plasmids were transformed into *Escherichia coli* XL-1 blue chemically competent bacteria by a 45sec heatshock at 42°C, 2 min incubation on ice and subsequent incubation in LB containing an appropriate selection antibiotic overnight at 37°C. Plasmid DNA was purified from bacteria using Qiagen Miniprep or Midiprep kits according to the manufacturer's recommendation. DNA amount and purity were estimated on a Nanodrop 2000 spectrophotometer.

6.2.2 PROTEIN EXTRACTION AND WESTERN BLOT

Cultured cells were harvested either by Trypsin digestion or cell scraping, transferred into a 1.5 ml tube and pelleted by centrifugation for 5 min at 300g. Cell pellets were resuspended in 50-100 µl RIPA buffer. Cell disruption was achieved by 4 cycles of freezing in liquid nitrogen and thawing at 37°C, followed by sonication for 10 cycles 15 sec on/off, high setting, in a Bioruptor (Diagenode). After centrifugation of samples for 15 min at 21.000g at 4°C, cleared whole-cell lysates were transferred to a fresh tube.

Protein concentration was estimated by BCA assay. For this purpose, 2 µl of whole-cell lysate was incubated with 200 µl of bicinchoninic acid + 2% $Cu(II)SO_4$ at 37°C until the purple reaction product developed. Absorption at 562 nm was measured with an Infinite 200 Pro microplate reader (Tecan) and compared to a standard curve of bovine serum albumin samples with known protein concentrations that was run in parallel to samples of interest.

Defined protein amounts of whole-cell lysates were mixed with 6x Lämmli sample buffer and incubated for 5 min at 95°C. SDS-PAGE, transfer to polyvinylidene difluoride (PVDF) membranes and Western Blotting was performed according to standard protocols [357]. Signals were developed with SuperSignal West Pico Chemiluminescent Substrate (Thermo Scientific) and analyzed using a ChemiDoc (BioRad) with ImageLab software.

Primary antibodies used in this study were rabbit anti Histone H3 (1:10.000, Abcam ab1791), mouse anti α-Tubulin (1:10.000, Sigma, T5186), rabbit anti p38 (1:1.000, Cell Signaling 9212S), rabbit anti phospho-p38 (1:1.000, Cell Signaling 9211S), rabbit anti JNK (1:1.000, Santa Cruz sc-571), rabbit anti phospho-JNK (1:1.000, Cell Signaling 4668S), rabbit anti Erk (1:1.000, Cell Signaling 4695S), mouse anti phospho-Erk (1:1.000, Sigma M8159), rabbit anti C/EBPβ (1:1000, Santa Cruz sc-150X), mouse anti PPARγ (1:1.000, Abcam ab41928), rabbit anti Caspase 3 (1:1000, Cell Signaling 9662), and rabbit anti p16 (1:500, Santa Cruz sc-1207).

6.3 MOUSE EXPERIMENTAL PROCEDURES

6.3.1 MOUSE HANDLING

Gadd45a deficient mice were generated by the Fornace lab [230] and were a kind gift from M. Christine Hollander. Ing1 deficient mice were generated by the Gudkov lab [218] and were obtained from Jackson Laboratories. Both strains were backcrossed several generations into the C57BL6/N background and interbred to generate WT, Gadd45a$^{-/-}$, Ing1$^{-/-}$ and Gadd45a$^{-/-}$ Ing1$^{-/-}$ mice from homogenous genetic backgrounds. Mice were housed in accordance with national and international guidelines with *ad libidum* access to water and chow diet, exposure to on average 22.5°C room temperature, 63% humidity and a 12h/12h light-dark rhythm. Mice were sacrificed by CO_2 asphyxiation followed by cervical dislocation before experimental manipulation. All procedures were performed with approval of the ethical committees on animal care and use of the federal states of Baden-Württemberg and Rheinland-Pfalz, Germany.

6.3.2 ISOLATION OF MOUSE EMBRYONIC FIBROBLASTS (MEFS)

Timed mouse matings were set up overnight for embryo dissections and isolation of mouse embryonic fibroblasts. In case of successful detection of vaginal plugs in the females, the previous midnight was defined as the time of conception. Pregnant females were sacrificed 15.5 days post coitum. Uteri were isolated, quickly disinfected in 70% ethanol and kept in ice-cold PBS during the dissection procedure. Embryos were liberated from the uteri, and their placenta, amniotic sac, head, limbs and inner organs were removed. A genotyping sample was taken from the discarded tissues. The remaining embryo carcass was minced with a scalpel and transferred to a Falcon tube containing sterile glass beads and 2 ml 0.25% Trypsin + 100U DNaseI. After a 30 min incubation, trypsinization was stopped by adding 5 ml DMEM+++ with 20% FBS and transferring the cell suspension to a 10 cm cell culture dish containing 15 DMEM+++. Cells were incubated from here on at 37°C, 5% CO_2, 5% O_2. MEFs were passaged to 4x 10 cm plates after 24h, and frozen in FBS + 10% DMSO to 8 cryovials after additional 48h.

6.3.3 GENOTYPING

For genotyping of embryonic and adult mice, small biopsies (usually from the tail tip) were taken and digested overnight at 56°C in 100 µl tail lysis buffer with freshly added 0.5 mg/ml Proteinase K. Samples were diluted 1:20 with 10 mM Tris-HCl pH 8.5 and heat-inactivated for 10 min at 95°C. Genotypic PCR reactions were set up with 2 µl DNA sample, 2 µl PCR buffer (Fermentas), 1.5 mM-

2.0 mM $MgCl_2$, 250 nM -750 nM primers, 250 µM dNTPs and filled up to 20 µl with nuclease-free water.

Following PCR conditions were used:

PCR step	Temperature	Time	
Denaturation	95°C	5 min	
Denaturation	95°C	30 sec	Repeat 34x
Annealing	60-62,5°C	30 sec	
Elongation	72°C	45 sec	
Final elongation	72°C	5 min	

PCR samples were subjected to agarose gel electrophoresis according to standard protocols [357]. Primers and specific conditions for each genotyping PCR are listed in table 6.5.

Geno-typing	**Primers**	**Primer conc.**	**MgCl2 conc.**	**Annealing temp.**	**Expected PCR product size**
XY	Xist-fwd: ACCCGGTACTGTCAATGAGC Xist rev: TGGCATGATGGAATTGAGAA Sry fwd: GCAAAGCTGTGTTTTCAAGG Sry rev: AGAAACTGTTGCAGGGGTTG	375 nM 375 nM 250 nM 250 nM	1,5 mM	60°C	Female: 373 bp Male: 373 + 290 bp
G45a	Fwd: CCTCTGCTTACCTCTGCACAA Gadd45a-wt rev: GAAGACCTAGACAGCACGGTT Gadd45a-mut rev: AGAACGAGATCAGCAGCCTCT	250 nM 375 mM 250 nM	1,5 mM	62,5°C	Gadd45a-wt: 324 bp Gadd45a-mut: 211 bp
Ing1	Ing1-wt fwd: GCCACAATTGCCACAATTTC Ing1-mut fwd: CCTTCTATCGCCTTCTTGACG Rev: GTCTGTGTGGCATCATGGTC	750 nM 750 nM 750 nM	2,0 mM	61°C	Ing1-wt: 233 bp Ing1-mut: 200 bp

TABLE 6.6 GENOTYPING PCR CONDITIONS

6.3.4 ESTRUS CYCLE ANALYSIS

Estrus cycle phases were determined as previously described [262]. Pasteur pipettes containing approximately 0.5 ml room-temperature PBS were carefully inserted maximally 1-2 mm into vaginas of analyzed mice. Vaginas were gently flushed 1-3 times with PBS. A drop of fluid was placed on a glass slide and dried at room temperature. This procedure was repeated for 14 consecutive days.

Analysis of the estrus cycle phase was conducted using a light microscope at 100x magnification. Different estrus cycle phases were identified by the cell types found in vaginal smears. Estrus cycles were quantified based on the relative amount of cornified epithelial cells, which mark the estrus phase and are strongly reduced or absent in other phases of the estrus cycle.

6.3.5 ISOLATION OF PERITONEAL MACROPHAGES

Isolation of peritoneal macrophages was performed as described by Ray et al. [358]. In summary, abdomen of sacrificed mice were opened approximately 1 cm without injuring the peritoneum. With a 27G needle, 5ml of ice-cold PBS + 3% FBS + 100U/ml Penicillin/Streptomycin were slowly injected into the peritoneal cavity. The mouse abdomen was gently squeezed several times to detach peritoneal macrophages. Fluid containing abdominal cells was collected from the peritoneal cavity with a 25G needle and transferred to a Falcon tube. This cell suspension was centrifuged 8 min at 400g at 4°C, resuspended in 10 ml warm cell culture medium and cultured overnight at 37°C, 5% CO_2. Cell culture dishes were washed several times to remove non-attached cells. All attached cells were considered to be peritoneal macrophages.

6.3.6 QUANTIFICATION OF SERUM CYTOKINES

Blood from adult mice was collected by cardiac puncture after CO_2 asphyxiation. Collected blood was allowed to clot for 30 min at room temperature and centrifuged at 2.000g for 10 min at 4°C. The supernatant, i.e. the serum, was transferred to a fresh tube and stored at -20°C. For cytokine detection, 50 µl serum each of 3 animals per genotype was pooled and processed using a Mouse Cytokine Antibody array (C series, Array 3) from RayBiotech according to the manufacturer's recommendations. Both serum and antibody cocktail incubation steps were conducted overnight at 4°C. Signals were detected with a ChemiDoc Imager (BioRad) and analyzed with the accompanying ImageLab software. Background signals were substrated and technical duplicate values were averaged using Microsoft Excel.

6.3.7 QUANTIFICATION OF TELOMERE LENGTH

To determine telomere length in mice, liver tissues were extracted from ice and stored at -80°C in RNAlater buffer. After thawing, samples were transferred to 2ml Eppendorf tubes with 600 µl RLT buffer incl. 1% β-Mercaptoethanol and homogenized with an Ultrathurrax homogenator and genomic DNA was purified with a Qiagen Blood&Tissue kit according to the manufacturer's recommendations. Telomere length of 1,35 µg genomic DNA per mouse liver was analyzed by Southern Blot using the Telo TAAGG telomere length assay kit (Roche) according to the manufacturer's instructions. Signals were detected with a ChemiDoc Imager (Biorad) and analyzed as described for the Telo TAAGG kit using the Biorad ImageLab software.

6.4 CELL CULTURE

6.4.1 GENERAL CELL CULTURE TECHNIQUES

Mouse embryonic fibroblasts (MEFs) and Phoenix-Eco human embryonic kidney cells, which were frozen in FBS+10% DMSO, were quickly thawed in a waterbath and added to 10 ml DMEM+++ cell culture medium. The cell suspension was centrifuged 5 min at 300g, resuspended in 10 ml fresh DMEM+++ and plated on a 10 cm dish. Cells were cultured at 37°C, 5% CO_2 and 5% O_2 for MEFs, and 37°C, 5% CO_2 and 21% O_2 for Phoenix-Eco cells.

For passaging, MEFs were detached from their cell culture dishes by incubation with 0.25% Trypsin for 1 min at 37°C. Trypsinization was stopped by addition of 9x volume of DMEM+++ and cells were distributed to fresh cell culture dishes in a 1:4 to 1:5 ratio. Phoenix-Eco cells were handled similarly, but detached with 0.05% Trypsin and passaged in 1:8 to 1:10 ratio every 2-3 days.

For cryopreservation of cell lines, cells were detached from their culture dish with Trypsin, resuspended in DMEM+++ and pelleted for 5 min at 300g. Cells were resuspended in ice-cold FBS+10% DMSO, transferred to cryovials and slowly frozen to -80°C at a cooling rate of -1°C/min in freezing containers filled with isopropanol. Cells were transferred to -150°C for long-term storage.

6.4.2 DIFFERENTIATION OF MEFS TO ADIPOCYTES

$2 \cdot 10^5$ MEFs were seeded per well of a 6-well plate and cultured in 2 ml DMEM+++ per well for 48h. DMEM+++ was changed and the confluent MEFs were cultured for further 48h. Adipocyte differentiation was induced on hyperconfluent MEFs with DMEM+++ containing 500 mM IBMX, 1 µM Dexamethasone and 10 mM Insulin. In some experiments, 2 µM Rosiglitazone was added to the differentiation cocktail to enhance adipogenic differentiation. Adipocyte differentiation medium was changed every 2 days and differentiating cells were harvested at various time points up to 18 days of differentiation.

6.4.3 ELECTROPORATION

Electroporation of MEF cells was conducted using a Neon™ Transfection System (Invitrogen) according to the manufacturer's instructions. For each confluent 10 cm dish of MEFs, 20 µg plasmid was electroporated with 1 pulse of 1250 mV for 20 ms in a 100 µl Neon™ Tip. Two batches of electroporated MEFs were pooled to one 10 cm dish and incubated for 48h at 37°C, 5% O_2 before further analyses.

6.4.4 RETROVIRAL TRANSDUCTION

Stable retrovirus-producing cell lines were generated by transfection of the packaging cell line Phoenix-Eco (ATCC CRL-3214, a gift from Grummt Lab, DKFZ) with pBABE-Puro, pBABE-puro-HA-hGadd45a or pBABE-puro-Myc-hIng1b using Lipofectamine 2000 (Invitrogen) according to the manufacturer's suggestions and subsequent selection with 1 µg/ml Puromycin for at least 14 days. For MEF infection, supernatant of Phoenix-Eco cell lines was collected and passed through a 0.45 µm filter. Polybrene was added to a final concentration of 4 µg/ml. On 30-70% confluent MEFs, cell culture medium was replaced by 15 ml retrovirus-containing supernatant per 75cm² cell culture flask. MEFs were then spin-infected by centrifugation of cell culture flasks for 60 min at 1800 rpm, following an overnight incubation at 37°C. Successfully infected MEF cells were selected with 1 µg/ml Puromycin in DMEM+++ for 2-3 days and subsequently propagated in DMEM+++.

6.4.5 GROWTH CURVES OF MEFS

For growth curve analyses, MEFs were detached by trypsinization and collected in DMEM+++ for cell counting with a TC10 cell counter. $1.9 \cdot 10^4$ MEFs were seeded to wells of 12-well dishes in technical duplicates and cultured in 1ml DMEM+++ per well. Medium was changed every 2 days. At intervals of 1, 3, 5 and 7 days after cell seeding, MEFs were detached by trypsinization, centrifuged for 5 min at 300g, resuspended in 100 µl DMEM+++ and counted with a TC10 cell counter. Mean cell number per genotype and day of analysis were plotted along with the standard deviation per genotype.

6.4.6 COLONY FORMATION ASSAY

$2.5 \cdot 10^3$ MEFs per dish were seeded in technical triplicates to 10 cm dishes containing 10 ml DMEM+++. Cells were incubated for 12 days or until the appearance of clearly visible colonies. During colony growth, cell culture medium was changed every 3 days. Subsequently, culture dishes were washed in cold PBS and cells were fixed for 10 min in -20°C methanol. Dishes were stained 10 min at room temperature with 0.5% Crystal Violet in 25% methanol in water. Subsequently, dishes were washed 5x in water to remove excess staining solution. Stained dishes were dried at room temperature and scanned with a color scanner. Afterwards, stained dishes were stored at RT. Colonies were counted manually using a stereomicroscope, with colonies being defined as containing a minimum of 25 cells each.

6.4.7 FLUOROMETRIC QUANTIFICATION OF SENESCENCE-ASSOCIATED β-GALACTOSIDASE ACTIVITY

MEFs were seeded in triplicates on a 96-well plate (20,000 cells per well) and grown overnight. Activity of senescence-associated β-Galactosidase was determined using the 96-Well Cellular Senescence Assay kit (Cell Biolabs, CBA-231) according to manufacturer's instruction with the following modifications: Cell lysis was conducted for 10 min and clarification of the lysate was performed in the original multiwell plate. Fluorescence was normalized to protein concentration (determined by the BCA method, see 6.2.2) to give the relative senescence-associated β-Galactosidase activity. This assay was performed by Dominik Sebastian.

6.4.8 CELL CYCLE ANALYSIS VIA FLOW CYTOMETRY

MEFs were grown on a 6 cm cell culture dish to 80% confluence. After detachment with 0.25% Trypsin and neutralization with DMEM+++, cells were transferred to a 15 ml Falcon tube and centrifuged at 300g for 5 min. Cells were resuspended in 1 ml ice-cold PBS + 0.1% FBS and fixed by dropwise addition of 3 ml -20°C ethanol under constant vortexing. Fixed cells were stored at -20°C for at least 24h. For propidium iodide staining, fixed MEFs were washed 2x with ice-cold PBS before addition of 500 µl PI staining solution (PBS, 0.1 mg/ml propidium iodide, 0.1 mg/ml RNase A) and incubation for 3h at 4°C. Propidium iodide staining was analyzed using a LSR Fortessa Sorp flow cytometer. Cell debris and cell doublets were gated out, and propidium iodide signal was measured by excitation at 488 nm and absorption at 610/620 nm. Signals from 30000 cells were recorded and analyzed with ModFit cell cycle analysis software (Verity Software House).

6.4.9 QUANTIFICATION OF REACTIVE OXYGEN SPECIES VIA FLOW CYTOMETRY

Amounts of reactive oxygen species were measured in MEFs using the Total ROS/Superoxide Detection Kit (Enzo Life Sciences) according to the manufacturer's instructions. Presence of reactive oxygen species and superoxide anions were detected on a LSR-Fortessa Sorp flow cytometer. Cell debris and doublets were gated out, and unstained, N-acetylcysteine-treated negative control as well as pyocyanin-treated positive control cells were used for channel compensation corrections and population gating. Quantification of results was performed with FlowJo data analysis software (FlowJo LLC).

6.5 HISTOLOGY AND STAININGS

6.5.1 IMMUNOFLUORESCENCE STAINING

Coverslips, on which MEF cells have been cultured, were rinsed 2x with PBS before 30 min fixation in freshly prepared 4% paraformaldehyde in PBS at room temperature. Following a 5 min wash in PBS, neutralization of residual paraformaldehyde and permeabilization were performed by a 30 min incubation in 200 mM Glycine + 0.1% Triton X-100 in PBS. After blocking for 1h in PBGNT, coverslips were incubated overnight at 4°C in primary antibody (Santa Cruz sc-150X) diluted 1:200 in PBGNT. Coverslips were washed 3x 10 min in PBGNT and subsequently incubated with 1:1.000 diluted Alexa Fluor 546-coupled secondary antibody and 0.1 µg/ml DAPI in PBGNT for 1h at room temperature. After 3x 10 min additional washes in PBS, coverslips were mounted on glass slides with Immumount mounting medium. Immunofluorescence stainings were analyzed with a Leica SP5 confocal microscope and Leica LAS image software.

6.5.2 OIL RED O STAINING

Oil Red O staining was performed on either cells cultured on coverslips or tissue cryosections cut to 7-10 µm. Coverslips or tissue sections were washed in PBS and fixed for 30 min in 4% paraformaldehyde in PBS. After two washes in distilled water, slides were equilibrated for 5 min in 60% isopropanol. Oil Red O staining was conducted for 8 min (cells on coverslips) or 30 min (tissue sections) in freshly prepared and filtered staining solution consisting of 6 parts of 5g/l Oil Red O in isopropanol and 4 parts water. Background staining was removed by a 5 min incubation in 60% isopropanol. Following two short washes in water, samples were counterstained for 5-8 min with Harris' Hematoxylin. After two additional washes in water, samples were "blued" in 0.2% ammonium hydroxide solution, washed a last time in water and embedded in aqueous mounting medium. Samples were analyzed with a Leica DM2500 light microscope at 100x to 400x magnification. Micrographs were edited by adjusting brightness and contrast in Photoshop PS5.

Quantification of Oil Red O staining was performed on 9 randomly chosen micrographs per condition in biological triplicates. In Photoshop PS4, contrast of pictures was maximally increased five consecutive times to yield pictures composed of primary and secondary colors only. Lipids were represented by red, magenta and black colors, while nuclei were depicted in blue and cyan. Using the histogram function, the proportion of red, magenta and black pixels per total image was extracted. Mean values and standard deviations per condition were calculated, representing the Oil Red O stained area in percent.

6.5.3 CRYOCONSERVATION AND CRYOSECTIONING OF TISSUES

Tissues were dissected to a size of maximum 3mm in each dimension and fixed overnight in freshly prepared 4% paraformaldehyde in PBS. Following several washes for few hours in PBS, tissues were infiltrated overnight in 15% sucrose and subsequently in 30% sucrose. Tissues were immersed in O.C.T. TissueTek embedding medium in a mold and frozen using a slurry of dry ice and isopropanol. Cryoconserved blocks were stored at -80°C.

Sections of 5-10 µm diameter were produced with a Leica CS3050S cryostat chilled tissue-dependently to -35°C to -18°C. Sections were taken up on Superfrost Plus glass slides and dried for 2h at room temperature before long-term storage at -80°C.

6.5.4 SENESCENCE-ASSOCIATED B-GALACTOSIDASE STAINING

Senescence-associated ß-Galactosidase stainings were performed as described by Dimri et al. [359] and Debacq-Chainiaux et al. [360]. Briefly, cryosectioned tissue sections were taken from -80°C and thawed 10 min at RT. Slides were rinsed 2x 10 min in PBS at 4°C to remove O.C.T. TissueTek embedding medium. Samples were stained overnight at 37°C in freshly prepared SA-βGal staining solution adjusted to pH6. Subsequently, stained sections were washed 2x 10 min in PBS and mounted with aqueous mounting medium. Samples were examined and photographed using a Leica DM2500 light microscope. Senescence-associated ß-Galactosidase staining was quantified as percent of total area stained in Photoshop PS5 using iteratively increased image contrast and the histogram tool.

6.5.5 PARAFFIN EMBEDDING AND HEMATOXYLIN & EOSIN STAINING

Tissues were dissected and trimmed to pieces smaller than 3 mm in each dimension. Samples were transferred to an embedding cassette and fixed for 48h at 4°C in freshly prepared 4% paraformaldehyde in PBS.

Using a Leica TP1020 automated tissue processor, tissues were dehydrated by serial incubations in 70% ethanol (1h), 80% ethanol (1h), 95% ethanol (1h), and 100% ethanol (3x 1h). Subsequently, paraffin infiltration was performed by immersion of samples for 2x 1h in Roticlear, 2h in 58°C paraffin and a final 12h bath in 58°C paraffin. Paraffin-infiltrated tissues were embedded in molds and stored at 4°C until further use.

Sections of 5-10 µm thickness were produced with a Leica RM2255 rotary microtome. Sections were stretched for 1-2 min on a 42°C waterbath, after which they were taken up on Superfrost Plus glass slides. Residual water was evaporated for 2h on a 37°C heating plate. Optionally, glass slides were dried overnight vertically at 37°C. Afterwards, paraffin-embedded tissue sections were stored at 4°C.

For Hematoxylin & Eosin staining, sections were deparaffinized and rehydrated by sequential incubations in 2x 10 min Roticlear, 2x 5 min 100% ethanol, 2 min 95% ethanol, 2 min 70% ethanol and 5 min in distilled water. Hematoxylin staining was performed for approximately 8 min, after which samples were washed in distilled water until the water remained clear. Excess staining of sections was removed by 1-10 sec incubation in 1% hydrochloric acid in 70% ethanol and subsequent washes in distilled water. A blue hue of the Hematoxylin dye was achieved by a 10 sec treatment of sections with 0.2% ammonium hydroxide, followed by washes in distilled water. Sections were equilibrated to alcoholic solutions by 10 dips in 95% ethanol, after which Eosin staining was performed for maximum 30 sec with Eosine-Phloxin staining solution. Sections were finally dehydrated by sequential incubations of 5 min 95% ethanol, 2x 5 min 100% ethanol, and 2x 5 min Roticlear and embedded with a xylene-based mounting medium.

Hematoxylin & Eosin stained sections were photographed and analyzed using a Leica DM2500 light microscope. Changes of brightness and contrast in final images were made with Photoshop PS5.

6.5.6 ALCIAN BLUE AND ALIZARIN RED STAINING OF BONE

Adult mice were sacrificed by CO_2 asphyxiation. Mice were skinned, eviscerated and all excess adipose tissue was removed. After fixation for 5 days in 95% ethanol, cartilage was stained with Alcian Blue staining solution for 24h. Skeletons were rinsed and washed 2x 24h in 95% ethanol. After a quick rinse in water, samples were cleared by incubation in 2% potassium hydroxide solution for 5 days, with the potassium hydroxide solution being changed daily. Bone was stained with 50 mg/l Alizarin Red in 2% potassium hydroxide for 24h. After clearing the skeletons in 2% potassium hydroxide until excess tissue was removed, skeletons were processed through an increasing series of 20%, 40%, 60%, 80%, and 100 % glycerol for 24h each. Stained skeletons were stored in 100% glycerol at room temperature.

Pictures were taken with a digital camera by immersing skeletons in a broad, flat glass dish with 80% glycerol to avoid reflections. Excess tissue was manually removed, if necessary. Pictures were adjusted in Photoshop PS5 by changing brightness and contrast.

6.6 GENE EXPRESSION ANALYSIS

6.6.1 RNA ISOLATION, REVERSE TRANSCRIPTION AND QPCR

Tissues were excised from sacrificed animals and stored in RNAlater at -80°C (except for adipose tissue). For RNA isolation, up to 30 mg of tissue sample were transferred to a 2 ml tube containing 600 µl RLT buffer incl. 1% β-mercaptoethanol and homogenized with an Ultrathurrax homogenizer. Adipose tissue was collected and snap-frozen in liquid nitrogen until further use. For RNA isolation, samples were immersed in 1 ml Qiazol and homogenized with and Ultrathurrax homogenator. After 5 min incubation at room temperature, 200 µl chloroform was added and samples were shaken vigorously. Following centrifugation for 15 min at 12.000 rpm at 4°C, the upper, aqueous phase was transferred to a fresh tube. Cells grown in tissue culture were washed in PBS and resuspended in 600 µl RLT buffer incl. 1 % β -mercaptoethanol.

Subsequent steps of RNA isolation for all tissues and cells were performed using a Qiagen RNeasy Mini or Qiagen RNeasy 96-well kit according to the manufacturer's instructions, including the facultative on-column DNaseI digest step. RNA was eluted in 40 µl nuclease-free water and quantified on a Nanodrop 2000.

cDNA synthesis was conducted with Superscript II reverse transcriptase (Invitrogen) according to the manufacturer's instructions. Briefly, for each µg of RNA, 2 µl 5mM dNTPs and 2 µl 100 µM random primers were added in a final volume of 12µl. After denaturation for 5 min at 65°C, 4µl 5x FS buffer, 2µl 0.1M DTT, 1 µl Ribolock and 1 µl Superscript II Polymerase were added. Samples were incubated for 10 min at 25°C, 90 min at 42°C for cDNA synthesis and 5 min at 72°C for enzyme inactivation. Resulting cDNA was diluted 1:6 in water. For each batch of cDNA synthesis, negative control samples lacking either RNA or reverse transcriptase were included.

qPCR reactions were performed in technical duplicates using the Roche Universal probe library (UPL) system with a Roche Light Cycler 480 in a 384-well format. Per 11 µl qPCR reaction, 5 µl diluted cDNA, 5.5 µl 2x Probes Master, 0.05 µl 100 µM forward primer, 0.05 µl 100 µM reverse primer, 0.11 µl UPL probe and 0.28 µl water were combined. qPCRs were performed using the following PCR program:

PCR step	Temperature	Time	Ramp rate	
Denaturation	95°C	10 min	4.8 °C/sec	
Denaturation	95°C	10 sec	4.8 °C/sec	Repeat 50x
Annealing	60°C	20 sec	2.5 °C/sec	
Elongation + Signal acquisition	72°C	1 sec	4.8 °C/sec	
Cooling	4°C	1 sec	2.5 °C/sec	

UPL-compatible primers were designed using the Roche Assay Design center http://lifescience.roche.com/shop/en/mx/overviews/brand/universal-probe-library).

In case no UPL-compatible primers could be found, primers were designed using the Primer3 online tool (http://biotools.umassmed.edu/bioapps/primer3_www.cgi) and qPCR assays were run with the SYBR green system. For a 11 µl SYBR green reaction, 5 µl diluted cDNA, 5.5 µl 2x SYBR master, 0.05 µl 100 µM forward primer, 0.05 µl 100 µM reverse primer, and 0.4 µl water were combined. The following PCR program was used for signal detection with the Roche Light Cycler 480:

PCR step	Temperature	Time	Ramp rate	
Denaturation	95°C	10 min	4.8 °C/sec	
Denaturation	95°C	10 sec	4.8 °C/sec	Repeat 50x
Annealing	58°C	15 sec	2.5 °C/sec	
Elongation + Signal acquisition	72°C	10 sec	4.8 °C/sec	
Denaturation	95°C	10 min	4.8 °C/sec	
	58°C	1 min		
Melting curve + signal acquisition	97°C	1 sec	0.11 °C/sec	
Cooling	4°C	1 sec	2.5 °C/sec	

Initial evaluation of raw values was conducted using the Roche LightCycler analysis software and included a normalization for primer efficiencies. Resulting values were normalized to two housekeeping genes (mostly Gapdh and Tbp) and plotted with Microsoft Excel.

6.6.2 RNA EXPRESSION MICROARRAY

RNA from white adipose tissue, liver and kidney was purified as described in chapter 6.6.1. RNA integrity was determined with a RNA 6000 Nano kit on a Bioanalyzer (Agilent) and yielded RIN values ranging from 8.8 to 9.6, indicating suitable RNA quality without significant RNA degradation. 1.33 µg total RNA per tissue was pooled from 3 individual mice per genotype, and 3 pools per genotype were used for RNA expression microarray analysis. Samples were processed using a SurePrint G3 Mouse GE 8x60k microarray (Agilent) according to the manufacturer's recommendations, including cDNA synthesis, hybridization of cDNA to microarray chips, washing, and scanning of microarrays. Using this approach, 39.430 Entrez Gene RNAs and 16.251 lincRNAs could be detected. Data processing was performed with Chipster open source software (CSC) [361]. After background subtraction and signal intensity normalization, differentially expressed genes were

filtered at 1.2-fold or 1.5-fold differential expression and 10% false discovery rate using multiple testing correction. Results were visualized with heatmaps generated by hierarchical clustering in R and proportional Venn Diagrams generated with BioVenn (http://www.cmbi.ru.nl/cdd/ biovenn/index.php). Gene ontology analysis of differentially expressed genes was conducted with DAVID Gene Functional Annotation tool (david.abcc.ncifcrf.gov) [362].

Library preparation was performed by the IMB core facility genomics; Chipster analysis and heatmap generation was performed by Dr. Emil Karaulanov at the IMB core facility bioinformatics.

6.6.3 RNA SEQUENCING

RNA from MEFs and differentiating adipocytes was purified as described in chapter 6.6.1. Using an RNA 6000 Nano kit on a Bioanalyzer (Agilent), RNA integrity was assessed and deemed suitable with RIN values consistently above 9.5. 1 µg total RNA of biological triplicates from WT, Gadd45a$^{-/-}$, Ing1$^{-/-}$, and Gadd45a$^{-/-}$ Ing1$^{-/-}$ MEFs at 0h, 2h, 2d and 6d of adipogenic differentiation were submitted for further processing. Stranded mRNA libraries were prepared with a TruSeq Stranded mRNA Sample Prep Kit (Illumina) according to the manufacturer's recommendations and sequenced on a HiSeq2500 high-throughput sequencer (Illumina). Resulting reads had Phred quality scores of 33 to 40, translating in over 99.9% base calling accuracy. Raw reads could be mapped with >95% efficiency to the NCBI37/mm9 build of the mouse genome. Using the DESeq package in R [363], differentially expressed genes were identified at a false discovery rate of 5% and 2-fold differential expression compared to WT samples. Heatmaps of differentially expressed genes were generated by hierarchical clustering in R and proportional Venn Diagrams were produced with BioVenn (http://www.cmbi.ru.nl/cdd/biovenn/index.php). Gene ontology analysis was conducted with the DAVID Gene Functional Annotation tool (david.abcc.ncifcrf.gov) [362].

MEF differentiation and RNA isolation were performed by Dr. Andrea Schäfer. Quality controls, library preparation and sequencing were performed in the IMB core facility genomics. Bioinformatic analysis were performed in cooperation with Medhavi Mallick.

6.7 DNA METHYLATION ANALYSIS

6.7.1 MASS SPECTROMETRY ANALYSIS OF GENOMIC DNA

Genomic DNA was isolated using the Qiagen Blood and Tissue Kit according to the manufacturer's instructions and purified DNA was quantified with a Nanodrop spectrophotometer. 2 µg of genomic DNA were further cleaned from salt contaminations by ethanol precipitation [357] and resuspended in 10 µl nuclease-free water. Further steps were performed by Dr. Michael Musheev as described in Schomacher et al. (2015): NEIL DNA glycosylases coordinate substrate hand-over during oxidative DNA demethylation (submitted):

"DNA was degraded to nucleosides with nuclease P1 (Roche), snake venom phosphodiesterase (Worthington) and alkaline phosphatase (Fermentas) (Kellner, S. et al. Absolute and relative quantification of RNA modifications via biosynthetic isotopomers). An equal volume of isotopic standard mixture (15N3-C (Silantes), 2H3-5mC (TRC) and self-synthesized 15N3-5hmC, 15N3-5fC and 15N3-5caC) was added to the DNA and about 100 ng of total DNA was injected for LC-MS/MS analysis. Quantitative analysis was performed on an Agilent 1290 Infinity Binary LC system (Agilent technologies) using a ReproSil 100 C18 column (Jasco) coupled to an Agilent 6490 triple quadrupole mass spectrometer (Agilent technologies). Running buffers were 5 mM ammonium acetate pH 6.9 (A) and Acetonitrile (B). Separations were performed at a flow rate of 0.5 ml/min using the following gradient: 0% of solvent B from 0 min to 8 min, linear increase to 15% solvent B for the next 16 min. Washing and reconditioning of the column was performed with a flow rate of 1.0 ml/min with 15% solvent B for one minute and 100% buffer A for additional 5 min. During the last minute the flow rate was linearly decreased to the initial value of 0.5 ml/min. Quantification of highly abundant C and 5mC was performed using 100x diluted samples. The data were analyzed with the Agilent MassHunter Quantitative Analysis software version 26 B.05.02 (Agilent technologies) using isotopic standards to confirm the peak identity. Areas of the integrated peaks were exported into Microsoft Excel with which the areas were normalized to the area of the corresponding isotopic standard. Absolute values for the nucleosides were calculated using linear interpolation from a standard curve. Linear interpolation was performed using the two closely matching data points from the standard curve. Standards were spiked into the mixture of isotopic standards to normalize for ionization variability. The standard curve for every nucleoside was prepared to cover the amount of the corresponding nucleoside in the DNA sample analyzed. The linearity of standard curves over each region was monitored after every run and confirmed to be between 1-0.996 (R2-values) within a concentration range of at least two orders of magnitude. The technical standard deviation was < 7%. Standard curves were newly prepared with every new dataset."

6.7.2 METHYLATION SENSITIVE PCR (MS-PCR)

Methylation specific PCR takes advantage of the different sensitivity of restriction endonucleases to DNA methylation. While *MspI*, cutting at CCGG sequences, is insensitive to DNA methylation, its isoschizomere *HpaII* cuts only unmethylated DNA. *HhaI*, another methylation-sensitive restriction enzyme, cuts GCGC sequences only in their unmethylated state. *PvuII* was used to sterically relax genomic DNA by cutting in non-relevant sequence contexts.

Genomic DNA from cells or tissues was purified with a Qiagen Blood & Tissue kit according to the manufacturer's recommendations. For each genomic DNA sample, 4 reactions consisting of 100 ng DNA, 3 µl digestion buffer, 0.1 mg/ml BSA, 1 µl *PvuII* (Promega) and nuclease-free water up to a final volume of 29 µl were set up. Either 1 µl *HpaII (Promega)*, 1µl *MspI (Promega)*, 1µl *HhaI* (Promega) or 1 µl water were added. Restriction digests were incubated overnight a 37°C, subsequently diluted 1:5 in water and subjected to qPCR analysis of regions of interest (see chapter 6.6.1). Obtained values were normalized to *PvuII*-only control digests to estimate DNA methylation at examined CpGs.

Restriction enzymes	Promega Buffer
PvuII	Buffer B
PvuII + HpaII	Multicore
PvuII + MspI	Buffer C
PvuII + HhaI	Buffer B

6.7.3 WHOLE GENOME BISULFITE SEQUENCING

Genomic DNA was purified from early passage MEF cells with a DNeasy Blood & Tissue Kit (Qiagen) according to the manufacturer's instructions, and 5 µg genomic DNA per sample were submitted to DKFZ Genomics & Proteomics core facility for further processing. Genomic DNA was fragmented with a Covaris S2 ultrasonicator. For end repair of DNA fragments, the Paired End DNA Sample Prep kit (Illumina) was used. Adapter ligation was carried out with an Early Access Methylation Adapter Oligo kit (Illumina) and the Paired End DNA Sample Prep kit (Illumina). After size selection of fragments using the E-Gel electrophoresis system (Invitrogen), DNA was bisulfite converted with a EZ DNA Methylation kit (Zymo Research). PCR-amplified and purified products were subjected to 100 bp paired-end sequencing on an Illumina HiSeq2000 high throughput sequencer.

Processing and analysis of whole-genome bisulfite sequencing data was conducted by Medhavi Mallick.

7. REFERENCES

1. Roser, M. (2015). Life Expectancy.
2. Rose, M.R. (1994). The evolutionary biology of aging, (Oxford: Oxford University Press).
3. Finch, C.E. (2009). Update on slow aging and negligible senescence--a mini-review. Gerontology *55*, 307-313.
4. Gilbert, S.F., and Singer, S.R. (2006). Developmental Biology, 8th Edition, (Palgrave Macmillan).
5. Vanhooren, V., and Libert, C. (2013). The mouse as a model organism in aging research: usefulness, pitfalls and possibilities. Ageing research reviews *12*, 8-21.
6. Hasty, P., and Vijg, J. (2004). Accelerating aging by mouse reverse genetics: a rational approach to understanding longevity. Aging cell *3*, 55-65.
7. Guarente, L. (2011). Sirtuins, aging, and metabolism. Cold Spring Harbor symposia on quantitative biology *76*, 81-90.
8. de Boer, J., de Wit, J., van Steeg, H., Berg, R.J., Morreau, H., Visser, P., Lehmann, A.R., Duran, M., Hoeijmakers, J.H., and Weeda, G. (1998). A mouse model for the basal transcription/DNA repair syndrome trichothiodystrophy. Molecular cell *1*, 981-990.
9. de Boer, J., Andressoo, J.O., de Wit, J., Huijmans, J., Beems, R.B., van Steeg, H., Weeda, G., van der Horst, G.T., van Leeuwen, W., Themmen, A.P., et al. (2002). Premature aging in mice deficient in DNA repair and transcription. Science *296*, 1276-1279.
10. van der Pluijm, I., Garinis, G.A., Brandt, R.M., Gorgels, T.G., Wijnhoven, S.W., Diderich, K.E., de Wit, J., Mitchell, J.R., van Oostrom, C., Beems, R., et al. (2007). Impaired genome maintenance suppresses the growth hormone--insulin-like growth factor 1 axis in mice with Cockayne syndrome. PLoS biology *5*, e2.
11. Andressoo, J.O., Weeda, G., de Wit, J., Mitchell, J.R., Beems, R.B., van Steeg, H., van der Horst, G.T., and Hoeijmakers, J.H. (2009). An Xpb mouse model for combined xeroderma pigmentosum and cockayne syndrome reveals progeroid features upon further attenuation of DNA repair. Molecular and cellular biology *29*, 1276-1290.
12. Weeda, G., Donker, I., de Wit, J., Morreau, H., Janssens, R., Vissers, C.J., Nigg, A., van Steeg, H., Bootsma, D., and Hoeijmakers, J.H. (1997). Disruption of mouse ERCC1 results in a novel repair syndrome with growth failure, nuclear abnormalities and senescence. Current biology : CB *7*, 427-439.
13. Chen, D., Steele, A.D., Lindquist, S., and Guarente, L. (2005). Increase in activity during calorie restriction requires Sirt1. Science *310*, 1641.
14. Han, S., and Brunet, A. (2012). Histone methylation makes its mark on longevity. Trends in cell biology *22*, 42-49.
15. Wolkow, C.A., Kimura, K.D., Lee, M.S., and Ruvkun, G. (2000). Regulation of C. elegans life-span by insulinlike signaling in the nervous system. Science *290*, 147-150.
16. Mounkes, L.C., Kozlov, S., Hernandez, L., Sullivan, T., and Stewart, C.L. (2003). A progeroid syndrome in mice is caused by defects in A-type lamins. Nature *423*, 298-301.
17. Pendas, A.M., Zhou, Z., Cadinanos, J., Freije, J.M., Wang, J., Hultenby, K., Astudillo, A., Wernerson, A., Rodriguez, F., Tryggvason, K., et al. (2002). Defective prelamin A processing and muscular and adipocyte alterations in Zmpste24 metalloproteinase-deficient mice. Nature genetics *31*, 94-99.
18. Longo, V.D., and Kennedy, B.K. (2006). Sirtuins in aging and age-related disease. Cell *126*, 257-268.
19. Tyner, S.D., Venkatachalam, S., Choi, J., Jones, S., Ghebranious, N., Igelmann, H., Lu, X., Soron, G., Cooper, B., Brayton, C., et al. (2002). p53 mutant mice that display early ageing-associated phenotypes. Nature *415*, 45-53.

20. Lopez-Otin, C., Blasco, M.A., Partridge, L., Serrano, M., and Kroemer, G. (2013). The hallmarks of aging. Cell *153*, 1194-1217.
21. Oh, J., Lee, Y.D., and Wagers, A.J. (2014). Stem cell aging: mechanisms, regulators and therapeutic opportunities. Nature medicine *20*, 870-880.
22. Gonzalo, S. (2010). Epigenetic alterations in aging. Journal of applied physiology *109*, 586-597.
23. Signer, R.A., and Morrison, S.J. (2013). Mechanisms that regulate stem cell aging and life span. Cell stem cell *12*, 152-165.
24. Fraga, M.F., and Esteller, M. (2007). Epigenetics and aging: the targets and the marks. Trends in genetics : TIG *23*, 413-418.
25. Pollina, E.A., and Brunet, A. (2011). Epigenetic regulation of aging stem cells. Oncogene *30*, 3105-3126.
26. Kenyon, C.J. (2010). The genetics of ageing. Nature *464*, 504-512.
27. Gates, K.S. (2009). An overview of chemical processes that damage cellular DNA: spontaneous hydrolysis, alkylation, and reactions with radicals. Chemical research in toxicology *22*, 1747-1760.
28. Swenberg, J.A., Lu, K., Moeller, B.C., Gao, L., Upton, P.B., Nakamura, J., and Starr, T.B. (2011). Endogenous versus exogenous DNA adducts: their role in carcinogenesis, epidemiology, and risk assessment. Toxicological sciences : an official journal of the Society of Toxicology *120 Suppl 1*, S130-145.
29. Ciccia, A., and Elledge, S.J. (2010). The DNA damage response: making it safe to play with knives. Molecular cell *40*, 179-204.
30. Hoeijmakers, J.H. (2009). DNA damage, aging, and cancer. The New England journal of medicine *361*, 1475-1485.
31. Moskalev, A.A., Smit-McBride, Z., Shaposhnikov, M.V., Plyusnina, E.N., Zhavoronkov, A., Budovsky, A., Tacutu, R., and Fraifeld, V.E. (2012). Gadd45 proteins: relevance to aging, longevity and age-related pathologies. Ageing research reviews *11*, 51-66.
32. Kastan, M.B., Zhan, Q., el-Deiry, W.S., Carrier, F., Jacks, T., Walsh, W.V., Plunkett, B.S., Vogelstein, B., and Fornace, A.J., Jr. (1992). A mammalian cell cycle checkpoint pathway utilizing p53 and GADD45 is defective in ataxia-telangiectasia. Cell *71*, 587-597.
33. Zhan, Q., Chen, I.T., Antinore, M.J., and Fornace, A.J., Jr. (1998). Tumor suppressor p53 can participate in transcriptional induction of the GADD45 promoter in the absence of direct DNA binding. Molecular and cellular biology *18*, 2768-2778.
34. Moskalev, A.A., Shaposhnikov, M.V., Plyusnina, E.N., Zhavoronkov, A., Budovsky, A., Yanai, H., and Fraifeld, V.E. (2013). The role of DNA damage and repair in aging through the prism of Koch-like criteria. Ageing research reviews *12*, 661-684.
35. Jin, S., Zhao, H., Fan, F., Blanck, P., Fan, W., Colchagie, A.B., Fornace, A.J., Jr., and Zhan, Q. (2000). BRCA1 activation of the GADD45 promoter. Oncogene *19*, 4050-4057.
36. Le May, N., Egly, J.M., and Coin, F. (2010). True lies: the double life of the nucleotide excision repair factors in transcription and DNA repair. Journal of nucleic acids *2010*.
37. Trifunovic, A., Wredenberg, A., Falkenberg, M., Spelbrink, J.N., Rovio, A.T., Bruder, C.E., Bohlooly, Y.M., Gidlof, S., Oldfors, A., Wibom, R., et al. (2004). Premature ageing in mice expressing defective mitochondrial DNA polymerase. Nature *429*, 417-423.
38. Cui, H., Kong, Y., and Zhang, H. (2012). Oxidative stress, mitochondrial dysfunction, and aging. Journal of signal transduction *2012*, 646354.
39. Fan, W., Jin, S., Tong, T., Zhao, H., Fan, F., Antinore, M.J., Rajasekaran, B., Wu, M., and Zhan, Q. (2002). BRCA1 regulates GADD45 through its interactions with the OCT-1 and CAAT motifs. The Journal of biological chemistry *277*, 8061-8067.
40. Trifunovic, A., Hansson, A., Wredenberg, A., Rovio, A.T., Dufour, E., Khvorostov, I., Spelbrink, J.N., Wibom, R., Jacobs, H.T., and Larsson, N.G. (2005). Somatic mtDNA mutations cause aging

phenotypes without affecting reactive oxygen species production. Proceedings of the National Academy of Sciences of the United States of America *102*, 17993-17998.

41. Wada, T., and Penninger, J.M. (2004). Mitogen-activated protein kinases in apoptosis regulation. Oncogene *23*, 2838-2849.
42. Bluher, M., Kahn, B.B., and Kahn, C.R. (2003). Extended longevity in mice lacking the insulin receptor in adipose tissue. Science *299*, 572-574.
43. Hayflick, L., and Moorhead, P.S. (1961). The serial cultivation of human diploid cell strains. Experimental cell research *25*, 585-621.
44. Wang, M.C., O'Rourke, E.J., and Ruvkun, G. (2008). Fat metabolism links germline stem cells and longevity in C. elegans. Science *322*, 957-960.
45. Conboy, I.M., Conboy, M.J., Wagers, A.J., Girma, E.R., Weissman, I.L., and Rando, T.A. (2005). Rejuvenation of aged progenitor cells by exposure to a young systemic environment. Nature *433*, 760-764.
46. Adler, A.S., Sinha, S., Kawahara, T.L., Zhang, J.Y., Segal, E., and Chang, H.Y. (2007). Motif module map reveals enforcement of aging by continual NF-kappaB activity. Genes & development *21*, 3244-3257.
47. Zhang, G., Li, J., Purkayastha, S., Tang, Y., Zhang, H., Yin, Y., Li, B., Liu, G., and Cai, D. (2013). Hypothalamic programming of systemic ageing involving IKK-beta, NF-kappaB and GnRH. Nature *497*, 211-216.
48. Salminen, A., and Kaarniranta, K. (2009). NF-kappaB signaling in the aging process. Journal of clinical immunology *29*, 397-405.
49. Osorio, F.G., Barcena, C., Soria-Valles, C., Ramsay, A.J., de Carlos, F., Cobo, J., Fueyo, A., Freije, J.M., and Lopez-Otin, C. (2012). Nuclear lamina defects cause ATM-dependent NF-kappaB activation and link accelerated aging to a systemic inflammatory response. Genes & development *26*, 2311-2324.
50. Tilstra, J.S., Robinson, A.R., Wang, J., Gregg, S.Q., Clauson, C.L., Reay, D.P., Nasto, L.A., St Croix, C.M., Usas, A., Vo, N., et al. (2012). NF-kappaB inhibition delays DNA damage-induced senescence and aging in mice. The Journal of clinical investigation *122*, 2601-2612.
51. Jones, P.A. (2012). Functions of DNA methylation: islands, start sites, gene bodies and beyond. Nature reviews. Genetics *13*, 484-492.
52. He, Y.F., Li, B.Z., Li, Z., Liu, P., Wang, Y., Tang, Q., Ding, J., Jia, Y., Chen, Z., Li, L., et al. (2011). Tet-mediated formation of 5-carboxylcytosine and its excision by TDG in mammalian DNA. Science *333*, 1303-1307.
53. Rubinsztein, D.C., Marino, G., and Kroemer, G. (2011). Autophagy and aging. Cell *146*, 682-695.
54. Gidalevitz, T., Ben-Zvi, A., Ho, K.H., Brignull, H.R., and Morimoto, R.I. (2006). Progressive disruption of cellular protein folding in models of polyglutamine diseases. Science *311*, 1471-1474.
55. Calderwood, S.K., Murshid, A., and Prince, T. (2009). The shock of aging: molecular chaperones and the heat shock response in longevity and aging--a mini-review. Gerontology *55*, 550-558.
56. Morrow, G., Samson, M., Michaud, S., and Tanguay, R.M. (2004). Overexpression of the small mitochondrial Hsp22 extends Drosophila life span and increases resistance to oxidative stress. FASEB journal : official publication of the Federation of American Societies for Experimental Biology *18*, 598-599.
57. Walker, G.A., and Lithgow, G.J. (2003). Lifespan extension in C. elegans by a molecular chaperone dependent upon insulin-like signals. Aging cell *2*, 131-139.

58. Min, J.N., Whaley, R.A., Sharpless, N.E., Lockyer, P., Portbury, A.L., and Patterson, C. (2008). CHIP deficiency decreases longevity, with accelerated aging phenotypes accompanied by altered protein quality control. Molecular and cellular biology *28*, 4018-4025.
59. Gehrig, S.M., van der Poel, C., Sayer, T.A., Schertzer, J.D., Henstridge, D.C., Church, J.E., Lamon, S., Russell, A.P., Davies, K.E., Febbraio, M.A., et al. (2012). Hsp72 preserves muscle function and slows progression of severe muscular dystrophy. Nature *484*, 394-398.
60. Bjedov, I., Toivonen, J.M., Kerr, F., Slack, C., Jacobson, J., Foley, A., and Partridge, L. (2010). Mechanisms of life span extension by rapamycin in the fruit fly Drosophila melanogaster. Cell metabolism *11*, 35-46.
61. Harrison, D.E., Strong, R., Sharp, Z.D., Nelson, J.F., Astle, C.M., Flurkey, K., Nadon, N.L., Wilkinson, J.E., Frenkel, K., Carter, C.S., et al. (2009). Rapamycin fed late in life extends lifespan in genetically heterogeneous mice. Nature *460*, 392-395.
62. Eisenberg, T., Knauer, H., Schauer, A., Buttner, S., Ruckenstuhl, C., Carmona-Gutierrez, D., Ring, J., Schroeder, S., Magnes, C., Antonacci, L., et al. (2009). Induction of autophagy by spermidine promotes longevity. Nature cell biology *11*, 1305-1314.
63. Sahin, E., and DePinho, R.A. (2012). Axis of ageing: telomeres, p53 and mitochondria. Nature reviews. Molecular cell biology *13*, 397-404.
64. Bratic, A., and Larsson, N.G. (2013). The role of mitochondria in aging. The Journal of clinical investigation *123*, 951-957.
65. Katsimpardi, L., Litterman, N.K., Schein, P.A., Miller, C.M., Loffredo, F.S., Wojtkiewicz, G.R., Chen, J.W., Lee, R.T., Wagers, A.J., and Rubin, L.L. (2014). Vascular and neurogenic rejuvenation of the aging mouse brain by young systemic factors. Science *344*, 630-634.
66. Kanfi, Y., Naiman, S., Amir, G., Peshti, V., Zinman, G., Nahum, L., Bar-Joseph, Z., and Cohen, H.Y. (2012). The sirtuin SIRT6 regulates lifespan in male mice. Nature *483*, 218-221.
67. de la Calle-Mustienes, E., Glavic, A., Modolell, J., and Gomez-Skarmeta, J.L. (2002). Xiro homeoproteins coordinate cell cycle exit and primary neuron formation by upregulating neuronal-fate repressors and downregulating the cell-cycle inhibitor XGadd45-gamma. Mechanisms of development *119*, 69-80.
68. Hawley, S.A., Ross, F.A., Chevtzoff, C., Green, K.A., Evans, A., Fogarty, S., Towler, M.C., Brown, L.J., Ogunbayo, O.A., Evans, A.M., et al. (2010). Use of cells expressing gamma subunit variants to identify diverse mechanisms of AMPK activation. Cell metabolism *11*, 554-565.
69. Durieux, J., Wolff, S., and Dillin, A. (2011). The cell-non-autonomous nature of electron transport chain-mediated longevity. Cell *144*, 79-91.
70. Harkin, D.P., Bean, J.M., Miklos, D., Song, Y.H., Truong, V.B., Englert, C., Christians, F.C., Ellisen, L.W., Maheswaran, S., Oliner, J.D., et al. (1999). Induction of GADD45 and JNK/SAPK-dependent apoptosis following inducible expression of BRCA1. Cell *97*, 575-586.
71. Zhan, Q., Antinore, M.J., Wang, X.W., Carrier, F., Smith, M.L., Harris, C.C., and Fornace, A.J., Jr. (1999). Association with Cdc2 and inhibition of Cdc2/Cyclin B1 kinase activity by the p53-regulated protein Gadd45. Oncogene *18*, 2892-2900.
72. Sheng, N., Xie, Z., Wang, C., Bai, G., Zhang, K., Zhu, Q., Song, J., Guillemot, F., Chen, Y.G., Lin, A., et al. (2010). Retinoic acid regulates bone morphogenic protein signal duration by promoting the degradation of phosphorylated Smad1. Proceedings of the National Academy of Sciences of the United States of America *107*, 18886-18891.
73. Kapahi, P., Chen, D., Rogers, A.N., Katewa, S.D., Li, P.W., Thomas, E.L., and Kockel, L. (2010). With TOR, less is more: a key role for the conserved nutrient-sensing TOR pathway in aging. Cell metabolism *11*, 453-465.
74. Lapierre, L.R., and Hansen, M. (2012). Lessons from C. elegans: signaling pathways for longevity. Trends in endocrinology and metabolism: TEM *23*, 637-644.

75. Gupta, M., Gupta, S.K., Hoffman, B., and Liebermann, D.A. (2006). Gadd45a and Gadd45b protect hematopoietic cells from UV-induced apoptosis via distinct signaling pathways, including p38 activation and JNK inhibition. The Journal of biological chemistry *281*, 17552-17558.
76. Fontana, L., Partridge, L., and Longo, V.D. (2010). Extending healthy life span--from yeast to humans. Science *328*, 321-326.
77. Masoro, E.J. (2000). Caloric restriction and aging: an update. Experimental gerontology *35*, 299-305.
78. Yi, Y.W., Kim, D., Jung, N., Hong, S.S., Lee, H.S., and Bae, I. (2000). Gadd45 family proteins are coactivators of nuclear hormone receptors. Biochemical and biophysical research communications *272*, 193-198.
79. Li, Y., Zhao, M., Yin, H., Gao, F., Wu, X., Luo, Y., Zhao, S., Zhang, X., Su, Y., Hu, N., et al. (2010). Overexpression of the growth arrest and DNA damage-induced 45alpha gene contributes to autoimmunity by promoting DNA demethylation in lupus T cells. Arthritis and rheumatism *62*, 1438-1447.
80. Bongers, K.S., Fox, D.K., Ebert, S.M., Kunkel, S.D., Dyle, M.C., Bullard, S.A., Dierdorff, J.M., and Adams, C.M. (2013). Skeletal muscle denervation causes skeletal muscle atrophy through a pathway that involves both Gadd45a and HDAC4. American journal of physiology. Endocrinology and metabolism *305*, E907-915.
81. Li, S., Crenshaw, E.B., 3rd, Rawson, E.J., Simmons, D.M., Swanson, L.W., and Rosenfeld, M.G. (1990). Dwarf locus mutants lacking three pituitary cell types result from mutations in the POU-domain gene pit-1. Nature *347*, 528-533.
82. Flurkey, K., Papaconstantinou, J., Miller, R.A., and Harrison, D.E. (2001). Lifespan extension and delayed immune and collagen aging in mutant mice with defects in growth hormone production. Proceedings of the National Academy of Sciences of the United States of America *98*, 6736-6741.
83. Zhou, Y., Xu, B.C., Maheshwari, H.G., He, L., Reed, M., Lozykowski, M., Okada, S., Cataldo, L., Coschigamo, K., Wagner, T.E., et al. (1997). A mammalian model for Laron syndrome produced by targeted disruption of the mouse growth hormone receptor/binding protein gene (the Laron mouse). Proceedings of the National Academy of Sciences of the United States of America *94*, 13215-13220.
84. Holzenberger, M., Dupont, J., Ducos, B., Leneuve, P., Geloen, A., Even, P.C., Cervera, P., and Le Bouc, Y. (2003). IGF-1 receptor regulates lifespan and resistance to oxidative stress in mice. Nature *421*, 182-187.
85. Niedernhofer, L.J., Garinis, G.A., Raams, A., Lalai, A.S., Robinson, A.R., Appeldoorn, E., Odijk, H., Oostendorp, R., Ahmad, A., van Leeuwen, W., et al. (2006). A new progeroid syndrome reveals that genotoxic stress suppresses the somatotroph axis. Nature *444*, 1038-1043.
86. Schumacher, B., van der Pluijm, I., Moorhouse, M.J., Kosteas, T., Robinson, A.R., Suh, Y., Breit, T.M., van Steeg, H., Niedernhofer, L.J., van Ijcken, W., et al. (2008). Delayed and accelerated aging share common longevity assurance mechanisms. PLoS genetics *4*, e1000161.
87. Salvador, J.M., Mittelstadt, P.R., Belova, G.I., Fornace, A.J., Jr., and Ashwell, J.D. (2005). The autoimmune suppressor Gadd45alpha inhibits the T cell alternative p38 activation pathway. Nature immunology *6*, 396-402.
88. Bgatova, N., Dubatolova, T., Omelyanchuk, L., Plyusnina, E., Shaposhnikov, M., and Moskalev, A. (2015). Gadd45 expression correlates with age dependent neurodegeneration in Drosophila melanogaster. Biogerontology *16*, 53-61.
89. Freund, A., Orjalo, A.V., Desprez, P.Y., and Campisi, J. (2010). Inflammatory networks during cellular senescence: causes and consequences. Trends in molecular medicine *16*, 238-246.

90. Rodier, F., Coppe, J.P., Patil, C.K., Hoeijmakers, W.A., Munoz, D.P., Raza, S.R., Freund, A., Campeau, E., Davalos, A.R., and Campisi, J. (2009). Persistent DNA damage signalling triggers senescence-associated inflammatory cytokine secretion. Nature cell biology *11*, 973-979.
91. Tchkonia, T., Zhu, Y., van Deursen, J., Campisi, J., and Kirkland, J.L. (2013). Cellular senescence and the senescent secretory phenotype: therapeutic opportunities. The Journal of clinical investigation *123*, 966-972.
92. Baker, D.J., Wijshake, T., Tchkonia, T., LeBrasseur, N.K., Childs, B.G., van de Sluis, B., Kirkland, J.L., and van Deursen, J.M. (2011). Clearance of p16Ink4a-positive senescent cells delays ageing-associated disorders. Nature *479*, 232-236.
93. Geiger, H., de Haan, G., and Florian, M.C. (2013). The ageing haematopoietic stem cell compartment. Nature reviews. Immunology *13*, 376-389.
94. Liu, H., Fergusson, M.M., Castilho, R.M., Liu, J., Cao, L., Chen, J., Malide, D., Rovira, II, Schimel, D., Kuo, C.J., et al. (2007). Augmented Wnt signaling in a mammalian model of accelerated aging. Science *317*, 803-806.
95. Brack, A.S., Conboy, M.J., Roy, S., Lee, M., Kuo, C.J., Keller, C., and Rando, T.A. (2007). Increased Wnt signaling during aging alters muscle stem cell fate and increases fibrosis. Science *317*, 807-810.
96. Florian, M.C., Nattamai, K.J., Dorr, K., Marka, G., Uberle, B., Vas, V., Eckl, C., Andra, I., Schiemann, M., Oostendorp, R.A., et al. (2013). A canonical to non-canonical Wnt signalling switch in haematopoietic stem-cell ageing. Nature *503*, 392-396.
97. Lezzerini, M., and Budovskaya, Y. (2014). A dual role of the Wnt signaling pathway during aging in Caenorhabditis elegans. Aging cell *13*, 8-18.
98. Fearon, K.C., Glass, D.J., and Guttridge, D.C. (2012). Cancer cachexia: mediators, signaling, and metabolic pathways. Cell metabolism *16*, 153-166.
99. Petruzzelli, M., Schweiger, M., Schreiber, R., Campos-Olivas, R., Tsoli, M., Allen, J., Swarbrick, M., Rose-John, S., Rincon, M., Robertson, G., et al. (2014). A switch from white to brown fat increases energy expenditure in cancer-associated cachexia. Cell metabolism *20*, 433-447.
100. Elabd, C., Cousin, W., Upadhyayula, P., Chen, R.Y., Chooljian, M.S., Li, J., Kung, S., Jiang, K.P., and Conboy, I.M. (2014). Oxytocin is an age-specific circulating hormone that is necessary for muscle maintenance and regeneration. Nature communications *5*, 4082.
101. Egerman, M.A., Cadena, S.M., Gilbert, J.A., Meyer, A., Nelson, H.N., Swalley, S.E., Mallozzi, C., Jacobi, C., Jennings, L.L., Clay, I., et al. (2015). GDF11 Increases with Age and Inhibits Skeletal Muscle Regeneration. Cell metabolism *22*, 1-11.
102. Loffredo, F.S., Steinhauser, M.L., Jay, S.M., Gannon, J., Pancoast, J.R., Yalamanchi, P., Sinha, M., Dall'Osso, C., Khong, D., Shadrach, J.L., et al. (2013). Growth differentiation factor 11 is a circulating factor that reverses age-related cardiac hypertrophy. Cell *153*, 828-839.
103. Sinha, M., Jang, Y.C., Oh, J., Khong, D., Wu, E.Y., Manohar, R., Miller, C., Regalado, S.G., Loffredo, F.S., Pancoast, J.R., et al. (2014). Restoring systemic GDF11 levels reverses age-related dysfunction in mouse skeletal muscle. Science *344*, 649-652.
104. Houtkooper, R.H., Pirinen, E., and Auwerx, J. (2012). Sirtuins as regulators of metabolism and healthspan. Nature reviews. Molecular cell biology *13*, 225-238.
105. Satoh, A., Brace, C.S., Rensing, N., Cliften, P., Wozniak, D.F., Herzog, E.D., Yamada, K.A., and Imai, S. (2013). Sirt1 extends life span and delays aging in mice through the regulation of Nk2 homeobox 1 in the DMH and LH. Cell metabolism *18*, 416-430.
106. Brown, K., Xie, S., Qiu, X., Mohrin, M., Shin, J., Liu, Y., Zhang, D., Scadden, D.T., and Chen, D. (2013). SIRT3 reverses aging-associated degeneration. Cell reports *3*, 319-327.
107. Mostoslavsky, R., Chua, K.F., Lombard, D.B., Pang, W.W., Fischer, M.R., Gellon, L., Liu, P., Mostoslavsky, G., Franco, S., Murphy, M.M., et al. (2006). Genomic instability and aging-like phenotype in the absence of mammalian SIRT6. Cell *124*, 315-329.

108. Chen, I.T., Smith, M.L., O'Connor, P.M., and Fornace, A.J., Jr. (1995). Direct interaction of Gadd45 with PCNA and evidence for competitive interaction of Gadd45 and p21Waf1/Cip1 with PCNA. Oncogene *11*, 1931-1937.
109. Liu, B., Wang, Z., Zhang, L., Ghosh, S., Zheng, H., and Zhou, Z. (2013). Depleting the methyltransferase Suv39h1 improves DNA repair and extends lifespan in a progeria mouse model. Nature communications *4*, 1868.
110. de Magalhaes, J.P., Curado, J., and Church, G.M. (2009). Meta-analysis of age-related gene expression profiles identifies common signatures of aging. Bioinformatics *25*, 875-881.
111. Tsurumi, A., and Li, W.X. (2012). Global heterochromatin loss: a unifying theory of aging? Epigenetics : official journal of the DNA Methylation Society *7*, 680-688.
112. Oberdoerffer, P., and Sinclair, D.A. (2007). The role of nuclear architecture in genomic instability and ageing. Nature reviews. Molecular cell biology *8*, 692-702.
113. Fraga, M.F., Ballestar, E., Paz, M.F., Ropero, S., Setien, F., Ballestar, M.L., Heine-Suner, D., Cigudosa, J.C., Urioste, M., Benitez, J., et al. (2005). Epigenetic differences arise during the lifetime of monozygotic twins. Proceedings of the National Academy of Sciences of the United States of America *102*, 10604-10609.
114. Wilson, V.L., and Jones, P.A. (1983). DNA methylation decreases in aging but not in immortal cells. Science *220*, 1055-1057.
115. Shimoda, N., Izawa, T., Yoshizawa, A., Yokoi, H., Kikuchi, Y., and Hashimoto, N. (2014). Decrease in cytosine methylation at CpG island shores and increase in DNA fragmentation during zebrafish aging. Age *36*, 103-115.
116. Casillas, M.A., Jr., Lopatina, N., Andrews, L.G., and Tollefsbol, T.O. (2003). Transcriptional control of the DNA methyltransferases is altered in aging and neoplastically-transformed human fibroblasts. Molecular and cellular biochemistry *252*, 33-43.
117. Dennis, K., Fan, T., Geiman, T., Yan, Q., and Muegge, K. (2001). Lsh, a member of the SNF2 family, is required for genome-wide methylation. Genes & development *15*, 2940-2944.
118. Sun, L.Q., Lee, D.W., Zhang, Q., Xiao, W., Raabe, E.H., Meeker, A., Miao, D., Huso, D.L., and Arceci, R.J. (2004). Growth retardation and premature aging phenotypes in mice with disruption of the SNF2-like gene, PASG. Genes & development *18*, 1035-1046.
119. Wu, H., and Zhang, Y. (2014). Reversing DNA methylation: mechanisms, genomics, and biological functions. Cell *156*, 45-68.
120. Smith, Z.D., and Meissner, A. (2013). DNA methylation: roles in mammalian development. Nature reviews. Genetics *14*, 204-220.
121. Ebert, S.M., Dyle, M.C., Kunkel, S.D., Bullard, S.A., Bongers, K.S., Fox, D.K., Dierdorff, J.M., Foster, E.D., and Adams, C.M. (2012). Stress-induced skeletal muscle Gadd45a expression reprograms myonuclei and causes muscle atrophy. The Journal of biological chemistry *287*, 27290-27301.
122. Kriaucionis, S., and Heintz, N. (2009). The nuclear DNA base 5-hydroxymethylcytosine is present in Purkinje neurons and the brain. Science *324*, 929-930.
123. Tahiliani, M., Koh, K.P., Shen, Y., Pastor, W.A., Bandukwala, H., Brudno, Y., Agarwal, S., Iyer, L.M., Liu, D.R., Aravind, L., et al. (2009). Conversion of 5-methylcytosine to 5-hydroxymethylcytosine in mammalian DNA by MLL partner TET1. Science *324*, 930-935.
124. Ito, S., Shen, L., Dai, Q., Wu, S.C., Collins, L.B., Swenberg, J.A., He, C., and Zhang, Y. (2011). Tet proteins can convert 5-methylcytosine to 5-formylcytosine and 5-carboxylcytosine. Science *333*, 1300-1303.
125. Pfaffeneder, T., Hackner, B., Truss, M., Munzel, M., Muller, M., Deiml, C.A., Hagemeier, C., and Carell, T. (2011). The discovery of 5-formylcytosine in embryonic stem cell DNA. Angewandte Chemie *50*, 7008-7012.

126. Ma, D.K., Jang, M.H., Guo, J.U., Kitabatake, Y., Chang, M.L., Pow-Anpongkul, N., Flavell, R.A., Lu, B., Ming, G.L., and Song, H. (2009). Neuronal activity-induced Gadd45b promotes epigenetic DNA demethylation and adult neurogenesis. Science *323*, 1074-1077.
127. Zhang, L., Lu, X., Lu, J., Liang, H., Dai, Q., Xu, G.L., Luo, C., Jiang, H., and He, C. (2012). Thymine DNA glycosylase specifically recognizes 5-carboxylcytosine-modified DNA. Nature chemical biology *8*, 328-330.
128. Maiti, A., and Drohat, A.C. (2011). Thymine DNA glycosylase can rapidly excise 5-formylcytosine and 5-carboxylcytosine: potential implications for active demethylation of CpG sites. The Journal of biological chemistry *286*, 35334-35338.
129. Kohli, R.M., and Zhang, Y. (2013). TET enzymes, TDG and the dynamics of DNA demethylation. Nature *502*, 472-479.
130. Guo, J.U., Su, Y., Zhong, C., Ming, G.L., and Song, H. (2011). Hydroxylation of 5-methylcytosine by TET1 promotes active DNA demethylation in the adult brain. Cell *145*, 423-434.
131. Rai, K., Huggins, I.J., James, S.R., Karpf, A.R., Jones, D.A., and Cairns, B.R. (2008). DNA demethylation in zebrafish involves the coupling of a deaminase, a glycosylase, and gadd45. Cell *135*, 1201-1212.
132. Rai, K., Sarkar, S., Broadbent, T.J., Voas, M., Grossmann, K.F., Nadauld, L.D., Dehghanizadeh, S., Hagos, F.T., Li, Y., Toth, R.K., et al. (2010). DNA demethylase activity maintains intestinal cells in an undifferentiated state following loss of APC. Cell *142*, 930-942.
133. Popp, C., Dean, W., Feng, S., Cokus, S.J., Andrews, S., Pellegrini, M., Jacobsen, S.E., and Reik, W. (2010). Genome-wide erasure of DNA methylation in mouse primordial germ cells is affected by AID deficiency. Nature *463*, 1101-1105.
134. Bhutani, N., Brady, J.J., Damian, M., Sacco, A., Corbel, S.Y., and Blau, H.M. (2010). Reprogramming towards pluripotency requires AID-dependent DNA demethylation. Nature *463*, 1042-1047.
135. Rangam, G., Schmitz, K.M., Cobb, A.J., and Petersen-Mahrt, S.K. (2012). AID enzymatic activity is inversely proportional to the size of cytosine C5 orbital cloud. PloS one *7*, e43279.
136. Nabel, C.S., Jia, H., Ye, Y., Shen, L., Goldschmidt, H.L., Stivers, J.T., Zhang, Y., and Kohli, R.M. (2012). AID/APOBEC deaminases disfavor modified cytosines implicated in DNA demethylation. Nature chemical biology *8*, 751-758.
137. Barreto, G., Schafer, A., Marhold, J., Stach, D., Swaminathan, S.K., Handa, V., Doderlein, G., Maltry, N., Wu, W., Lyko, F., et al. (2007). Gadd45a promotes epigenetic gene activation by repair-mediated DNA demethylation. Nature *445*, 671-675.
138. Cortellino, S., Xu, J., Sannai, M., Moore, R., Caretti, E., Cigliano, A., Le Coz, M., Devarajan, K., Wessels, A., Soprano, D., et al. (2011). Thymine DNA glycosylase is essential for active DNA demethylation by linked deamination-base excision repair. Cell *146*, 67-79.
139. Li, Z., Gu, T.P., Weber, A.R., Shen, J.Z., Li, B.Z., Xie, Z.G., Yin, R., Guo, F., Liu, X., Tang, F., et al. (2015). Gadd45a promotes DNA demethylation through TDG. Nucleic Acids Res *43*, 3986-3997.
140. Arab, K., Park, Y.J., Lindroth, A.M., Schafer, A., Oakes, C., Weichenhan, D., Lukanova, A., Lundin, E., Risch, A., Meister, M., et al. (2014). Long noncoding RNA TARID directs demethylation and activation of the tumor suppressor TCF21 via GADD45A. Molecular cell *55*, 604-614.
141. Pastor, W.A., Aravind, L., and Rao, A. (2013). TETonic shift: biological roles of TET proteins in DNA demethylation and transcription. Nature reviews. Molecular cell biology *14*, 341-356.
142. Iqbal, K., Jin, S.G., Pfeifer, G.P., and Szabo, P.E. (2011). Reprogramming of the paternal genome upon fertilization involves genome-wide oxidation of 5-methylcytosine. Proceedings of the National Academy of Sciences of the United States of America *108*, 3642-3647.

143. Gu, T.P., Guo, F., Yang, H., Wu, H.P., Xu, G.F., Liu, W., Xie, Z.G., Shi, L., He, X., Jin, S.G., et al. (2011). The role of Tet3 DNA dioxygenase in epigenetic reprogramming by oocytes. Nature *477*, 606-610.
144. Inoue, A., and Zhang, Y. (2011). Replication-dependent loss of 5-hydroxymethylcytosine in mouse preimplantation embryos. Science *334*, 194.
145. Peat, J.R., Dean, W., Clark, S.J., Krueger, F., Smallwood, S.A., Ficz, G., Kim, J.K., Marioni, J.C., Hore, T.A., and Reik, W. (2014). Genome-wide bisulfite sequencing in zygotes identifies demethylation targets and maps the contribution of TET3 oxidation. Cell reports *9*, 1990-2000.
146. Nakamura, T., Arai, Y., Umehara, H., Masuhara, M., Kimura, T., Taniguchi, H., Sekimoto, T., Ikawa, M., Yoneda, Y., Okabe, M., et al. (2007). PGC7/Stella protects against DNA demethylation in early embryogenesis. Nature cell biology *9*, 64-71.
147. Shen, L., Inoue, A., He, J., Liu, Y., Lu, F., and Zhang, Y. (2014). Tet3 and DNA replication mediate demethylation of both the maternal and paternal genomes in mouse zygotes. Cell stem cell *15*, 459-470.
148. Ohno, R., Nakayama, M., Naruse, C., Okashita, N., Takano, O., Tachibana, M., Asano, M., Saitou, M., and Seki, Y. (2013). A replication-dependent passive mechanism modulates DNA demethylation in mouse primordial germ cells. Development *140*, 2892-2903.
149. Vincent, J.J., Huang, Y., Chen, P.Y., Feng, S., Calvopina, J.H., Nee, K., Lee, S.A., Le, T., Yoon, A.J., Faull, K., et al. (2013). Stage-specific roles for tet1 and tet2 in DNA demethylation in primordial germ cells. Cell stem cell *12*, 470-478.
150. Seisenberger, S., Andrews, S., Krueger, F., Arand, J., Walter, J., Santos, F., Popp, C., Thienpont, B., Dean, W., and Reik, W. (2012). The dynamics of genome-wide DNA methylation reprogramming in mouse primordial germ cells. Molecular cell *48*, 849-862.
151. Yamaguchi, S., Hong, K., Liu, R., Shen, L., Inoue, A., Diep, D., Zhang, K., and Zhang, Y. (2012). Tet1 controls meiosis by regulating meiotic gene expression. Nature *492*, 443-447.
152. Yamaguchi, S., Shen, L., Liu, Y., Sendler, D., and Zhang, Y. (2013). Role of Tet1 in erasure of genomic imprinting. Nature *504*, 460-464.
153. Dawlaty, M.M., Ganz, K., Powell, B.E., Hu, Y.C., Markoulaki, S., Cheng, A.W., Gao, Q., Kim, J., Choi, S.W., Page, D.C., et al. (2011). Tet1 is dispensable for maintaining pluripotency and its loss is compatible with embryonic and postnatal development. Cell stem cell *9*, 166-175.
154. Trowbridge, J.J., and Orkin, S.H. (2010). DNA methylation in adult stem cells: new insights into self-renewal. Epigenetics : official journal of the DNA Methylation Society *5*, 189-193.
155. Gan, H., Wen, L., Liao, S., Lin, X., Ma, T., Liu, J., Song, C.X., Wang, M., He, C., Han, C., et al. (2013). Dynamics of 5-hydroxymethylcytosine during mouse spermatogenesis. Nature communications *4*, 1995.
156. Calvanese, V., Fernandez, A.F., Urdinguio, R.G., Suarez-Alvarez, B., Mangas, C., Perez-Garcia, V., Bueno, C., Montes, R., Ramos-Mejia, V., Martinez-Camblor, P., et al. (2012). A promoter DNA demethylation landscape of human hematopoietic differentiation. Nucleic acids research *40*, 116-131.
157. Bock, C., Beerman, I., Lien, W.H., Smith, Z.D., Gu, H., Boyle, P., Gnirke, A., Fuchs, E., Rossi, D.J., and Meissner, A. (2012). DNA methylation dynamics during in vivo differentiation of blood and skin stem cells. Molecular cell *47*, 633-647.
158. Zhang, X., Ulm, A., Somineni, H.K., Oh, S., Weirauch, M.T., Zhang, H.X., Chen, X., Lehn, M.A., Janssen, E.M., and Ji, H. (2014). DNA methylation dynamics during ex vivo differentiation and maturation of human dendritic cells. Epigenetics & chromatin *7*, 21.
159. de la Rica, L., Rodriguez-Ubreva, J., Garcia, M., Islam, A.B., Urquiza, J.M., Hernando, H., Christensen, J., Helin, K., Gomez-Vaquero, C., and Ballestar, E. (2013). PU.1 target genes

undergo Tet2-coupled demethylation and DNMT3b-mediated methylation in monocyte-to-osteoclast differentiation. Genome biology *14*, R99.

160. Feng, J., Shao, N., Szulwach, K.E., Vialou, V., Huynh, J., Zhong, C., Le, T., Ferguson, D., Cahill, M.E., Li, Y., et al. (2015). Role of Tet1 and 5-hydroxymethylcytosine in cocaine action. Nature neuroscience *18*, 536-544.
161. Guo, J.U., Ma, D.K., Mo, H., Ball, M.P., Jang, M.H., Bonaguidi, M.A., Balazer, J.A., Eaves, H.L., Xie, B., Ford, E., et al. (2011). Neuronal activity modifies the DNA methylation landscape in the adult brain. Nature neuroscience *14*, 1345-1351.
162. Gavin, D.P., Sharma, R.P., Chase, K.A., Matrisciano, F., Dong, E., and Guidotti, A. (2012). Growth arrest and DNA-damage-inducible, beta (GADD45b)-mediated DNA demethylation in major psychosis. Neuropsychopharmacology : official publication of the American College of Neuropsychopharmacology *37*, 531-542.
163. Song, C.X., and He, C. (2013). Potential functional roles of DNA demethylation intermediates. Trends in biochemical sciences *38*, 480-484.
164. Meissner, A., Mikkelsen, T.S., Gu, H., Wernig, M., Hanna, J., Sivachenko, A., Zhang, X., Bernstein, B.E., Nusbaum, C., Jaffe, D.B., et al. (2008). Genome-scale DNA methylation maps of pluripotent and differentiated cells. Nature *454*, 766-770.
165. Koh, K.P., and Rao, A. (2013). DNA methylation and methylcytosine oxidation in cell fate decisions. Current opinion in cell biology *25*, 152-161.
166. Ziller, M.J., Gu, H., Muller, F., Donaghey, J., Tsai, L.T., Kohlbacher, O., De Jager, P.L., Rosen, E.D., Bennett, D.A., Bernstein, B.E., et al. (2013). Charting a dynamic DNA methylation landscape of the human genome. Nature *500*, 477-481.
167. Yearim, A., Gelfman, S., Shayevitch, R., Melcer, S., Glaich, O., Mallm, J.P., Nissim-Rafinia, M., Cohen, A.H., Rippe, K., Meshorer, E., et al. (2015). HP1 is involved in regulating the global impact of DNA methylation on alternative splicing. Cell reports *10*, 1122-1134.
168. Stadler, M.B., Murr, R., Burger, L., Ivanek, R., Lienert, F., Scholer, A., van Nimwegen, E., Wirbelauer, C., Oakeley, E.J., Gaidatzis, D., et al. (2011). DNA-binding factors shape the mouse methylome at distal regulatory regions. Nature *480*, 490-495.
169. Neri, F., Incarnato, D., Krepelova, A., Rapelli, S., Anselmi, F., Parlato, C., Medana, C., Dal Bello, F., and Oliviero, S. (2015). Single-Base Resolution Analysis of 5-Formyl and 5-Carboxyl Cytosine Reveals Promoter DNA Methylation Dynamics. Cell reports.
170. Song, C.X., Szulwach, K.E., Dai, Q., Fu, Y., Mao, S.Q., Lin, L., Street, C., Li, Y., Poidevin, M., Wu, H., et al. (2013). Genome-wide profiling of 5-formylcytosine reveals its roles in epigenetic priming. Cell *153*, 678-691.
171. Shen, L., Wu, H., Diep, D., Yamaguchi, S., D'Alessio, A.C., Fung, H.L., Zhang, K., and Zhang, Y. (2013). Genome-wide analysis reveals TET- and TDG-dependent 5-methylcytosine oxidation dynamics. Cell *153*, 692-706.
172. Neri, F., Incarnato, D., Krepelova, A., Rapelli, S., Pagnani, A., Zecchina, R., Parlato, C., and Oliviero, S. (2013). Genome-wide analysis identifies a functional association of Tet1 and Polycomb repressive complex 2 in mouse embryonic stem cells. Genome biology *14*, R91.
173. Wen, L., Li, X., Yan, L., Tan, Y., Li, R., Zhao, Y., Wang, Y., Xie, J., Zhang, Y., Song, C., et al. (2014). Whole-genome analysis of 5-hydroxymethylcytosine and 5-methylcytosine at base resolution in the human brain. Genome biology *15*, R49.
174. Feldmann, A., Ivanek, R., Murr, R., Gaidatzis, D., Burger, L., and Schubeler, D. (2013). Transcription factor occupancy can mediate active turnover of DNA methylation at regulatory regions. PLoS genetics *9*, e1003994.
175. Yu, M., Hon, G.C., Szulwach, K.E., Song, C.X., Zhang, L., Kim, A., Li, X., Dai, Q., Shen, Y., Park, B., et al. (2012). Base-resolution analysis of 5-hydroxymethylcytosine in the mammalian genome. Cell *149*, 1368-1380.

176. Lu, F., Liu, Y., Jiang, L., Yamaguchi, S., and Zhang, Y. (2014). Role of Tet proteins in enhancer activity and telomere elongation. Genes & development *28*, 2103-2119.
177. Mohn, F., Weber, M., Rebhan, M., Roloff, T.C., Richter, J., Stadler, M.B., Bibel, M., and Schubeler, D. (2008). Lineage-specific polycomb targets and de novo DNA methylation define restriction and potential of neuronal progenitors. Molecular cell *30*, 755-766.
178. Ji, H., Ehrlich, L.I., Seita, J., Murakami, P., Doi, A., Lindau, P., Lee, H., Aryee, M.J., Irizarry, R.A., Kim, K., et al. (2010). Comprehensive methylome map of lineage commitment from haematopoietic progenitors. Nature *467*, 338-342.
179. Plyusnina, E.N., Shaposhnikov, M.V., and Moskalev, A.A. (2011). Increase of Drosophila melanogaster lifespan due to D-GADD45 overexpression in the nervous system. Biogerontology *12*, 211-226.
180. Gilsbach, R., Preissl, S., Gruning, B.A., Schnick, T., Burger, L., Benes, V., Wurch, A., Bonisch, U., Gunther, S., Backofen, R., et al. (2014). Dynamic DNA methylation orchestrates cardiomyocyte development, maturation and disease. Nature communications *5*, 5288.
181. Gifford, C.A., Ziller, M.J., Gu, H., Trapnell, C., Donaghey, J., Tsankov, A., Shalek, A.K., Kelley, D.R., Shishkin, A.A., Issner, R., et al. (2013). Transcriptional and epigenetic dynamics during specification of human embryonic stem cells. Cell *153*, 1149-1163.
182. Heyn, H., Li, N., Ferreira, H.J., Moran, S., Pisano, D.G., Gomez, A., Diez, J., Sanchez-Mut, J.V., Setien, F., Carmona, F.J., et al. (2012). Distinct DNA methylomes of newborns and centenarians. Proceedings of the National Academy of Sciences of the United States of America *109*, 10522-10527.
183. Raddatz, G., Hagemann, S., Aran, D., Sohle, J., Kulkarni, P.P., Kaderali, L., Hellman, A., Winnefeld, M., and Lyko, F. (2013). Aging is associated with highly defined epigenetic changes in the human epidermis. Epigenetics & chromatin *6*, 36.
184. Rakyan, V.K., Down, T.A., Maslau, S., Andrew, T., Yang, T.P., Beyan, H., Whittaker, P., McCann, O.T., Finer, S., Valdes, A.M., et al. (2010). Human aging-associated DNA hypermethylation occurs preferentially at bivalent chromatin domains. Genome research *20*, 434-439.
185. McClay, J.L., Aberg, K.A., Clark, S.L., Nerella, S., Kumar, G., Xie, L.Y., Hudson, A.D., Harada, A., Hultman, C.M., Magnusson, P.K., et al. (2014). A methylome-wide study of aging using massively parallel sequencing of the methyl-CpG-enriched genomic fraction from blood in over 700 subjects. Human molecular genetics *23*, 1175-1185.
186. Schäfer, A., Karaulanov, E., Stapf, U., Doderlein, G., and Niehrs, C. (2013). Ing1 functions in DNA demethylation by directing Gadd45a to H3K4me3. Genes & development *27*, 261-273.
187. Garkavtsev, I., Kazarov, A., Gudkov, A., and Riabowol, K. (1996). Suppression of the novel growth inhibitor p33ING1 promotes neoplastic transformation. Nature genetics *14*, 415-420.
188. Shi, X., and Gozani, O. (2005). The fellowships of the INGs. Journal of cellular biochemistry *96*, 1127-1136.
189. Russell, M., Berardi, P., Gong, W., and Riabowol, K. (2006). Grow-ING, Age-ING and Die-ING: ING proteins link cancer, senescence and apoptosis. Experimental cell research *312*, 951-961.
190. Ludwig, S., Klitzsch, A., and Baniahmad, A. (2011). The ING tumor suppressors in cellular senescence and chromatin. Cell & bioscience *1*, 25.
191. Campos, E.I., Chin, M.Y., Kuo, W.H., and Li, G. (2004). Biological functions of the ING family tumor suppressors. Cellular and molecular life sciences : CMLS *61*, 2597-2613.
192. Feng, X., Hara, Y., and Riabowol, K. (2002). Different HATS of the ING1 gene family. Trends in cell biology *12*, 532-538.
193. Soliman, M.A., and Riabowol, K. (2007). After a decade of study-ING, a PHD for a versatile family of proteins. Trends in biochemical sciences *32*, 509-519.
194. Guerillon, C., Larrieu, D., and Pedeux, R. (2013). ING1 and ING2: multifaceted tumor suppressor genes. Cellular and molecular life sciences : CMLS *70*, 3753-3772.

195. Tallen, G., and Riabowol, K. (2014). Keep-ING balance: tumor suppression by epigenetic regulation. FEBS letters *588*, 2728-2742.
196. Han, X., Feng, X., Rattner, J.B., Smith, H., Bose, P., Suzuki, K., Soliman, M.A., Scott, M.S., Burke, B.E., and Riabowol, K. (2008). Tethering by lamin A stabilizes and targets the ING1 tumour suppressor. Nature cell biology *10*, 1333-1340.
197. Pena, P.V., Hom, R.A., Hung, T., Lin, H., Kuo, A.J., Wong, R.P., Subach, O.M., Champagne, K.S., Zhao, R., Verkhusha, V.V., et al. (2008). Histone H3K4me3 binding is required for the DNA repair and apoptotic activities of ING1 tumor suppressor. Journal of molecular biology *380*, 303-312.
198. Garkavtsev, I., Grigorian, I.A., Ossovskaya, V.S., Chernov, M.V., Chumakov, P.M., and Gudkov, A.V. (1998). The candidate tumour suppressor p33ING1 cooperates with p53 in cell growth control. Nature *391*, 295-298.
199. Kataoka, H., Bonnefin, P., Vieyra, D., Feng, X., Hara, Y., Miura, Y., Joh, T., Nakabayashi, H., Vaziri, H., Harris, C.C., et al. (2003). ING1 represses transcription by direct DNA binding and through effects on p53. Cancer research *63*, 5785-5792.
200. Leung, K.M., Po, L.S., Tsang, F.C., Siu, W.Y., Lau, A., Ho, H.T., and Poon, R.Y. (2002). The candidate tumor suppressor ING1b can stabilize p53 by disrupting the regulation of p53 by MDM2. Cancer research *62*, 4890-4893.
201. Ceruti, J.M., Ogara, M.F., Menendez, C., Palmero, I., and Canepa, E.T. (2013). Inhibitor of growth 1 (ING1) acts at early steps of multiple DNA repair pathways. Molecular and cellular biochemistry *378*, 117-126.
202. Cheng, J., Blum, R., Bowman, C., Hu, D., Shilatifard, A., Shen, S., and Dynlacht, B.D. (2014). A role for H3K4 monomethylation in gene repression and partitioning of chromatin readers. Molecular cell *53*, 979-992.
203. Cheung, K.J., Jr., Mitchell, D., Lin, P., and Li, G. (2001). The tumor suppressor candidate p33(ING1) mediates repair of UV-damaged DNA. Cancer research *61*, 4974-4977.
204. Berardi, P., Russell, M., El-Osta, A., and Riabowol, K. (2004). Functional links between transcription, DNA repair and apoptosis. Cellular and molecular life sciences : CMLS *61*, 2173-2180.
205. Wong, R.P., Lin, H., Khosravi, S., Piche, B., Jafarnejad, S.M., Chen, D.W., and Li, G. (2011). Tumour suppressor ING1b maintains genomic stability upon replication stress. Nucleic acids research *39*, 3632-3642.
206. Kuo, W.H., Wang, Y., Wong, R.P., Campos, E.I., and Li, G. (2007). The ING1b tumor suppressor facilitates nucleotide excision repair by promoting chromatin accessibility to XPA. Experimental cell research *313*, 1628-1638.
207. Carrier, F., Georgel, P.T., Pourquier, P., Blake, M., Kontny, H.U., Antinore, M.J., Gariboldi, M., Myers, T.G., Weinstein, J.N., Pommier, Y., et al. (1999). Gadd45, a p53-responsive stress protein, modifies DNA accessibility on damaged chromatin. Molecular and cellular biology *19*, 1673-1685.
208. Maeda, T., Hanna, A.N., Sim, A.B., Chua, P.P., Chong, M.T., and Tron, V.A. (2002). GADD45 regulates G2/M arrest, DNA repair, and cell death in keratinocytes following ultraviolet exposure. The Journal of investigative dermatology *119*, 22-26.
209. Tran, H., Brunet, A., Grenier, J.M., Datta, S.R., Fornace, A.J., Jr., DiStefano, P.S., Chiang, L.W., and Greenberg, M.E. (2002). DNA repair pathway stimulated by the forkhead transcription factor FOXO3a through the Gadd45 protein. Science *296*, 530-534.
210. Smith, M.L., Kontny, H.U., Zhan, Q., Sreenath, A., O'Connor, P.M., and Fornace, A.J., Jr. (1996). Antisense GADD45 expression results in decreased DNA repair and sensitizes cells to u.v.-irradiation or cisplatin. Oncogene *13*, 2255-2263.

211. Gordon, P.M., Soliman, M.A., Bose, P., Trinh, Q., Sensen, C.W., and Riabowol, K. (2008). Interspecies data mining to predict novel ING-protein interactions in human. BMC genomics *9*, 426.
212. Mihara, M., Erster, S., Zaika, A., Petrenko, O., Chittenden, T., Pancoska, P., and Moll, U.M. (2003). p53 has a direct apoptogenic role at the mitochondria. Molecular cell *11*, 577-590.
213. Bose, P., Thakur, S., Thalappilly, S., Ahn, B.Y., Satpathy, S., Feng, X., Suzuki, K., Kim, S.W., and Riabowol, K. (2013). ING1 induces apoptosis through direct effects at the mitochondria. Cell death & disease *4*, e788.
214. Gomez-Cabello, D., Callejas, S., Benguria, A., Moreno, A., Alonso, J., and Palmero, I. (2010). Regulation of the microRNA processor DGCR8 by the tumor suppressor ING1. Cancer research *70*, 1866-1874.
215. Ohmori, M., Nagai, M., Tasaka, T., Koeffler, H.P., Toyama, T., Riabowol, K., and Takahara, J. (1999). Decreased expression of p33ING1 mRNA in lymphoid malignancies. American journal of hematology *62*, 118-119.
216. Tallen, G., Kaiser, I., Krabbe, S., Lass, U., Hartmann, C., Henze, G., Riabowol, K., and von Deimling, A. (2004). No ING1 mutations in human brain tumours but reduced expression in high malignancy grades of astrocytoma. International journal of cancer. Journal international du cancer *109*, 476-479.
217. Kameyama, K., Huang, C.L., Liu, D., Masuya, D., Nakashima, T., Sumitomo, S., Takami, Y., Kinoshita, M., and Yokomise, H. (2003). Reduced ING1b gene expression plays an important role in carcinogenesis of non-small cell lung cancer patients. Clinical cancer research : an official journal of the American Association for Cancer Research *9*, 4926-4934.
218. Kichina, J.V., Zeremski, M., Aris, L., Gurova, K.V., Walker, E., Franks, R., Nikitin, A.Y., Kiyokawa, H., and Gudkov, A.V. (2006). Targeted disruption of the mouse ing1 locus results in reduced body size, hypersensitivity to radiation and elevated incidence of lymphomas. Oncogene *25*, 857-866.
219. Garate, M., Campos, E.I., Bush, J.A., Xiao, H., and Li, G. (2007). Phosphorylation of the tumor suppressor p33(ING1b) at Ser-126 influences its protein stability and proliferation of melanoma cells. FASEB journal : official publication of the Federation of American Societies for Experimental Biology *21*, 3705-3716.
220. Yu, L., Thakur, S., Leong-Quong, R.Y., Suzuki, K., Pang, A., Bjorge, J.D., Riabowol, K., and Fujita, D.J. (2013). Src regulates the activity of the ING1 tumor suppressor. PloS one *8*, e60943.
221. Gong, W., Russell, M., Suzuki, K., and Riabowol, K. (2006). Subcellular targeting of p33ING1b by phosphorylation-dependent 14-3-3 binding regulates p21WAF1 expression. Molecular and cellular biology *26*, 2947-2954.
222. Satpathy, S., Nabbi, A., and Riabowol, K. (2013). RegulatING chromatin regulators: post-translational modification of the ING family of epigenetic regulators. The Biochemical journal *450*, 433-442.
223. Satpathy, S., Guerillon, C., Kim, T.S., Bigot, N., Thakur, S., Bonni, S., Riabowol, K., and Pedeux, R. (2014). SUMOylation of the ING1b tumor suppressor regulates gene transcription. Carcinogenesis *35*, 2214-2223.
224. Jin, S., Tong, T., Fan, W., Fan, F., Antinore, M.J., Zhu, X., Mazzacurati, L., Li, X., Petrik, K.L., Rajasekaran, B., et al. (2002). GADD45-induced cell cycle G2-M arrest associates with altered subcellular distribution of cyclin B1 and is independent of p38 kinase activity. Oncogene *21*, 8696-8704.
225. Mita, H., Tsutsui, J., Takekawa, M., Witten, E.A., and Saito, H. (2002). Regulation of MTK1/MEKK4 kinase activity by its N-terminal autoinhibitory domain and GADD45 binding. Mol Cell Biol *22*, 4544-4555.

226. Takekawa, M., and Saito, H. (1998). A family of stress-inducible GADD45-like proteins mediate activation of the stress-responsive MTK1/MEKK4 MAPKKK. Cell *95*, 521-530.
227. Miyake, Z., Takekawa, M., Ge, Q., and Saito, H. (2007). Activation of MTK1/MEKK4 by GADD45 through induced N-C dissociation and dimerization-mediated trans autophosphorylation of the MTK1 kinase domain. Molecular and cellular biology *27*, 2765-2776.
228. Bulavin, D.V., Kovalsky, O., Hollander, M.C., and Fornace, A.J., Jr. (2003). Loss of oncogenic H-ras-induced cell cycle arrest and p38 mitogen-activated protein kinase activation by disruption of Gadd45a. Molecular and cellular biology *23*, 3859-3871.
229. Hildesheim, J., Belova, G.I., Tyner, S.D., Zhou, X., Vardanian, L., and Fornace, A.J., Jr. (2004). Gadd45a regulates matrix metalloproteinases by suppressing DeltaNp63alpha and beta-catenin via p38 MAP kinase and APC complex activation. Oncogene *23*, 1829-1837.
230. Hollander, M.C., Sheikh, M.S., Bulavin, D.V., Lundgren, K., Augeri-Henmueller, L., Shehee, R., Molinaro, T.A., Kim, K.E., Tolosa, E., Ashwell, J.D., et al. (1999). Genomic instability in Gadd45a-deficient mice. Nature genetics *23*, 176-184.
231. Smith, M.L., Ford, J.M., Hollander, M.C., Bortnick, R.A., Amundson, S.A., Seo, Y.R., Deng, C.X., Hanawalt, P.C., and Fornace, A.J., Jr. (2000). p53-mediated DNA repair responses to UV radiation: studies of mouse cells lacking p53, p21, and/or gadd45 genes. Mol Cell Biol *20*, 3705-3714.
232. Gupta, M., Gupta, S.K., Balliet, A.G., Hollander, M.C., Fornace, A.J., Hoffman, B., and Liebermann, D.A. (2005). Hematopoietic cells from Gadd45a- and Gadd45b-deficient mice are sensitized to genotoxic-stress-induced apoptosis. Oncogene *24*, 7170-7179.
233. Hall, H., Vorherr, T., and Schachner, M. (1995). Characterization of a 21 amino acid peptide sequence of the laminin G2 domain that is involved in HNK-1 carbohydrate binding and cell adhesion. Glycobiology *5*, 435-441.
234. Vieyra, D., Loewith, R., Scott, M., Bonnefin, P., Boisvert, F.M., Cheema, P., Pastyryeva, S., Meijer, M., Johnston, R.N., Bazett-Jones, D.P., et al. (2002). Human ING1 proteins differentially regulate histone acetylation. The Journal of biological chemistry *277*, 29832-29839.
235. Jung, H.J., Kim, E.H., Mun, J.Y., Park, S., Smith, M.L., Han, S.S., and Seo, Y.R. (2007). Base excision DNA repair defect in Gadd45a-deficient cells. Oncogene *26*, 7517-7525.
236. Schmitz, K.M., Schmitt, N., Hoffmann-Rohrer, U., Schäfer, A., Grummt, I., and Mayer, C. (2009). TAF12 recruits Gadd45a and the nucleotide excision repair complex to the promoter of rRNA genes leading to active DNA demethylation. Molecular cell *33*, 344-353.
237. Engel, N., Tront, J.S., Erinle, T., Nguyen, N., Latham, K.E., Sapienza, C., Hoffman, B., and Liebermann, D.A. (2009). Conserved DNA methylation in Gadd45a(-/-) mice. Epigenetics : official journal of the DNA Methylation Society *4*, 98-99.
238. Jin, S.G., Guo, C., and Pfeifer, G.P. (2008). GADD45A does not promote DNA demethylation. PLoS genetics *4*, e1000013.
239. Le May, N., Fradin, D., Iltis, I., Bougneres, P., and Egly, J.M. (2012). XPG and XPF endonucleases trigger chromatin looping and DNA demethylation for accurate expression of activated genes. Molecular cell *47*, 622-632.
240. Sen, G.L., Reuter, J.A., Webster, D.E., Zhu, L., and Khavari, P.A. (2010). DNMT1 maintains progenitor function in self-renewing somatic tissue. Nature *463*, 563-567.
241. Zhang, R.P., Shao, J.Z., and Xiang, L.X. (2011). GADD45A protein plays an essential role in active DNA demethylation during terminal osteogenic differentiation of adipose-derived mesenchymal stem cells. The Journal of biological chemistry *286*, 41083-41094.
242. Matrisciano, F., Dong, E., Gavin, D.P., Nicoletti, F., and Guidotti, A. (2011). Activation of group II metabotropic glutamate receptors promotes DNA demethylation in the mouse brain. Molecular pharmacology *80*, 174-182.

243. Leach, P.T., Poplawski, S.G., Kenney, J.W., Hoffman, B., Liebermann, D.A., Abel, T., and Gould, T.J. (2012). Gadd45b knockout mice exhibit selective deficits in hippocampus-dependent long-term memory. Learning & memory *19*, 319-324.
244. Kaufmann, L.T., Gierl, M.S., and Niehrs, C. (2011). Gadd45a, Gadd45b and Gadd45g expression during mouse embryonic development. Gene expression patterns : GEP *11*, 465-470.
245. Hoffman, B., and Liebermann, D.A. (2007). Role of gadd45 in myeloid cells in response to hematopoietic stress. Blood cells, molecules & diseases *39*, 344-347.
246. Liebermann, D.A., and Hoffman, B. (2007). Gadd45 in the response of hematopoietic cells to genotoxic stress. Blood cells, molecules & diseases *39*, 329-335.
247. Kaufmann, L.T., and Niehrs, C. (2011). Gadd45a and Gadd45g regulate neural development and exit from pluripotency in Xenopus. Mechanisms of development *128*, 401-411.
248. Ijiri, K., Zerbini, L.F., Peng, H., Correa, R.G., Lu, B., Walsh, N., Zhao, Y., Taniguchi, N., Huang, X.L., Otu, H., et al. (2005). A novel role for GADD45beta as a mediator of MMP-13 gene expression during chondrocyte terminal differentiation. J Biol Chem *280*, 38544-38555.
249. Ju, S., Zhu, Y., Liu, L., Dai, S., Li, C., Chen, E., He, Y., Zhang, X., and Lu, B. (2009). Gadd45b and Gadd45g are important for anti-tumor immune responses. European journal of immunology *39*, 3010-3018.
250. Cai, Q., Dmitrieva, N.I., Ferraris, J.D., Michea, L.F., Salvador, J.M., Hollander, M.C., Fornace, A.J., Jr., Fenton, R.A., and Burg, M.B. (2006). Effects of expression of p53 and Gadd45 on osmotic tolerance of renal inner medullary cells. American journal of physiology. Renal physiology *291*, F341-349.
251. Peretz, G., Bakhrat, A., and Abdu, U. (2007). Expression of the Drosophila melanogaster GADD45 homolog (CG11086) affects egg asymmetric development that is mediated by the c-Jun N-terminal kinase pathway. Genetics *177*, 1691-1702.
252. Giannakou, M.E., and Partridge, L. (2004). The interaction between FOXO and SIRT1: tipping the balance towards survival. Trends in cell biology *14*, 408-412.
253. Clavel, S., Siffroi-Fernandez, S., Coldefy, A.S., Boulukos, K., Pisani, D.F., and Derijard, B. (2010). Regulation of the intracellular localization of Foxo3a by stress-activated protein kinase signaling pathways in skeletal muscle cells. Molecular and cellular biology *30*, 470-480.
254. Lal, A., Abdelmohsen, K., Pullmann, R., Kawai, T., Galban, S., Yang, X., Brewer, G., and Gorospe, M. (2006). Posttranscriptional derepression of GADD45alpha by genotoxic stress. Molecular cell *22*, 117-128.
255. Gao, M., Li, X., Dong, W., Jin, R., Ma, H., Yang, P., Hu, M., Li, Y., Hao, Y., Yuan, S., et al. (2013). Ribosomal protein S7 regulates arsenite-induced GADD45alpha expression by attenuating MDM2-mediated GADD45alpha ubiquitination and degradation. Nucleic acids research *41*, 5210-5222.
256. Kovalsky, O., Lung, F.D., Roller, P.P., and Fornace, A.J., Jr. (2001). Oligomerization of human Gadd45a protein. The Journal of biological chemistry *276*, 39330-39339.
257. Bradley, J.P., Levine, J.P., Roth, D.A., McCarthy, J.G., and Longaker, M.T. (1996). Studies in cranial suture biology: IV. Temporal sequence of posterior frontal cranial suture fusion in the mouse. Plastic and reconstructive surgery *98*, 1039-1045.
258. Gerhard, G.S., and Kasales, C.J. (2003). Aging and kyphosis. The journals of gerontology. Series A, Biological sciences and medical sciences *58*, 968.
259. Vogel, H., Lim, D.S., Karsenty, G., Finegold, M., and Hasty, P. (1999). Deletion of Ku86 causes early onset of senescence in mice. Proceedings of the National Academy of Sciences of the United States of America *96*, 10770-10775.
260. Cao, J., Venton, L., Sakata, T., and Halloran, B.P. (2003). Expression of RANKL and OPG correlates with age-related bone loss in male C57BL/6 mice. Journal of bone and mineral

research : the official journal of the American Society for Bone and Mineral Research *18*, 270-277.

261. Saxon, S.V., Perkins, E.A., and Etten, M.J. (2009). Physical Change and Aging: A Guide for the Helping Professions, Fifth Edition 5Edition, (Springer Publishing Company).
262. Caligioni, C.S. (2009). Assessing reproductive status/stages in mice. Current protocols in neuroscience / editorial board, Jacqueline N. Crawley ... [et al.] *Appendix 4*, Appendix 4I.
263. Goldenberg, R.L., Grodin, J.M., Rodbard, D., and Ross, G.T. (1973). Gonadotropins in women with amenorrhea. The use of plasma follicle-stimulating hormone to differentiate women with and without ovarian follicles. American journal of obstetrics and gynecology *116*, 1003-1012.
264. Burger, H.G., Hale, G.E., Robertson, D.M., and Dennerstein, L. (2007). A review of hormonal changes during the menopausal transition: focus on findings from the Melbourne Women's Midlife Health Project. Human reproduction update *13*, 559-565.
265. Lapiere, C.M. (1990). The ageing dermis: the main cause for the appearance of 'old' skin. The British journal of dermatology *122 Suppl 35*, 5-11.
266. Salvador, J.M., Hollander, M.C., Nguyen, A.T., Kopp, J.B., Barisoni, L., Moore, J.K., Ashwell, J.D., and Fornace, A.J., Jr. (2002). Mice lacking the p53-effector gene Gadd45a develop a lupus-like syndrome. Immunity *16*, 499-508.
267. Laviola, L., Natalicchio, A., and Giorgino, F. (2007). The IGF-I signaling pathway. Current pharmaceutical design *13*, 663-669.
268. Osorio, F.G., Navarro, C.L., Cadinanos, J., Lopez-Mejia, I.C., Quiros, P.M., Bartoli, C., Rivera, J., Tazi, J., Guzman, G., Varela, I., et al. (2011). Splicing-directed therapy in a new mouse model of human accelerated aging. Science translational medicine *3*, 106ra107.
269. Kondratov, R.V., Kondratova, A.A., Gorbacheva, V.Y., Vykhovanets, O.V., and Antoch, M.P. (2006). Early aging and age-related pathologies in mice deficient in BMAL1, the core componentof the circadian clock. Genes & development *20*, 1868-1873.
270. Compe, E., Drane, P., Laurent, C., Diderich, K., Braun, C., Hoeijmakers, J.H., and Egly, J.M. (2005). Dysregulation of the peroxisome proliferator-activated receptor target genes by XPD mutations. Molecular and cellular biology *25*, 6065-6076.
271. Peinado, J.R., Quiros, P.M., Pulido, M.R., Marino, G., Martinez-Chantar, M.L., Vazquez-Martinez, R., Freije, J.M., Lopez-Otin, C., and Malagon, M.M. (2011). Proteomic profiling of adipose tissue from Zmpste24-/- mice, a model of lipodystrophy and premature aging, reveals major changes in mitochondrial function and vimentin processing. Molecular & cellular proteomics : MCP *10*, M111 008094.
272. Harms, M., and Seale, P. (2013). Brown and beige fat: development, function and therapeutic potential. Nature medicine *19*, 1252-1263.
273. Nishimura, S., Manabe, I., and Nagai, R. (2009). Adipose tissue inflammation in obesity and metabolic syndrome. Discovery medicine *8*, 55-60.
274. Lumeng, C.N., and Saltiel, A.R. (2011). Inflammatory links between obesity and metabolic disease. The Journal of clinical investigation *121*, 2111-2117.
275. Inazumi, T., Shirata, N., Morimoto, K., Takano, H., Segi-Nishida, E., and Sugimoto, Y. (2011). Prostaglandin E(2)-EP4 signaling suppresses adipocyte differentiation in mouse embryonic fibroblasts via an autocrine mechanism. Journal of lipid research *52*, 1500-1508.
276. Hakim-Weber, R., Krogsdam, A.M., Jorgensen, C., Fischer, M., Prokesch, A., Bogner-Strauss, J.G., Bornstein, S.R., Hansen, J.B., Madsen, L., Kristiansen, K., et al. (2011). Transcriptional regulatory program in wild-type and retinoblastoma gene-deficient mouse embryonic fibroblasts during adipocyte differentiation. BMC research notes *4*, 157.
277. Baudry, A., Yang, Z.Z., and Hemmings, B.A. (2006). PKBalpha is required for adipose differentiation of mouse embryonic fibroblasts. Journal of cell science *119*, 889-897.

278. Darlington, G.J., Ross, S.E., and MacDougald, O.A. (1998). The role of C/EBP genes in adipocyte differentiation. The Journal of biological chemistry *273*, 30057-30060.
279. Gregoire, F.M., Smas, C.M., and Sul, H.S. (1998). Understanding adipocyte differentiation. Physiological reviews *78*, 783-809.
280. Rosen, E.D., and MacDougald, O.A. (2006). Adipocyte differentiation from the inside out. Nature reviews. Molecular cell biology *7*, 885-896.
281. Tang, Q.Q., and Lane, M.D. (2012). Adipogenesis: from stem cell to adipocyte. Annual review of biochemistry *81*, 715-736.
282. Tang, Q.Q., Gronborg, M., Huang, H., Kim, J.W., Otto, T.C., Pandey, A., and Lane, M.D. (2005). Sequential phosphorylation of CCAAT enhancer-binding protein beta by MAPK and glycogen synthase kinase 3beta is required for adipogenesis. Proceedings of the National Academy of Sciences of the United States of America *102*, 9766-9771.
283. Tang, Q.Q., and Lane, M.D. (1999). Activation and centromeric localization of CCAAT/enhancer-binding proteins during the mitotic clonal expansion of adipocyte differentiation. Genes & development *13*, 2231-2241.
284. Morgenstern, J.P., and Land, H. (1990). Advanced mammalian gene transfer: high titre retroviral vectors with multiple drug selection markers and a complementary helper-free packaging cell line. Nucleic acids research *18*, 3587-3596.
285. Pear, W.S., Nolan, G.P., Scott, M.L., and Baltimore, D. (1993). Production of high-titer helper-free retroviruses by transient transfection. Proceedings of the National Academy of Sciences of the United States of America *90*, 8392-8396.
286. Friedenstein, A.J., Chailakhjan, R.K., and Lalykina, K.S. (1970). The development of fibroblast colonies in monolayer cultures of guinea-pig bone marrow and spleen cells. Cell and tissue kinetics *3*, 393-403.
287. Wang, X.W., Zhan, Q., Coursen, J.D., Khan, M.A., Kontny, H.U., Yu, L., Hollander, M.C., O'Connor, P.M., Fornace, A.J., Jr., and Harris, C.C. (1999). GADD45 induction of a G2/M cell cycle checkpoint. Proceedings of the National Academy of Sciences of the United States of America *96*, 3706-3711.
288. Salvador, J.M., Brown-Clay, J.D., and Fornace, A.J., Jr. (2013). Gadd45 in stress signaling, cell cycle control, and apoptosis. Advances in experimental medicine and biology *793*, 1-19.
289. Mak, S.K., and Kultz, D. (2004). Gadd45 proteins induce G2/M arrest and modulate apoptosis in kidney cells exposed to hyperosmotic stress. The Journal of biological chemistry *279*, 39075-39084.
290. Scott, M., Bonnefin, P., Vieyra, D., Boisvert, F.M., Young, D., Bazett-Jones, D.P., and Riabowol, K. (2001). UV-induced binding of ING1 to PCNA regulates the induction of apoptosis. Journal of cell science *114*, 3455-3462.
291. Salerno, D.M., Tront, J.S., Hoffman, B., and Liebermann, D.A. (2012). Gadd45a and Gadd45b modulate innate immune functions of granulocytes and macrophages by differential regulation of p38 and JNK signaling. Journal of cellular physiology *227*, 3613-3620.
292. Lee, D.C., Ruiz, C.R., Lebson, L., Selenica, M.L., Rizer, J., Hunt, J.B., Jr., Rojiani, R., Reid, P., Kammath, S., Nash, K., et al. (2013). Aging enhances classical activation but mitigates alternative activation in the central nervous system. Neurobiology of aging *34*, 1610-1620.
293. Lumeng, C.N., Liu, J., Geletka, L., Delaney, C., Delproposto, J., Desai, A., Oatmen, K., Martinez-Santibanez, G., Julius, A., Garg, S., et al. (2011). Aging is associated with an increase in T cells and inflammatory macrophages in visceral adipose tissue. Journal of immunology *187*, 6208-6216.
294. Coppe, J.P., Patil, C.K., Rodier, F., Sun, Y., Munoz, D.P., Goldstein, J., Nelson, P.S., Desprez, P.Y., and Campisi, J. (2008). Senescence-associated secretory phenotypes reveal cell-

nonautonomous functions of oncogenic RAS and the p53 tumor suppressor. PLoS biology *6*, 2853-2868.

295. van Deursen, J.M. (2014). The role of senescent cells in ageing. Nature *509*, 439-446.
296. Harman, D. (1956). Aging: a theory based on free radical and radiation chemistry. Journal of gerontology *11*, 298-300.
297. Huang, H., and Manton, K.G. (2004). The role of oxidative damage in mitochondria during aging: a review. Frontiers in bioscience : a journal and virtual library *9*, 1100-1117.
298. Bernet, J.D., Doles, J.D., Hall, J.K., Kelly Tanaka, K., Carter, T.A., and Olwin, B.B. (2014). p38 MAPK signaling underlies a cell-autonomous loss of stem cell self-renewal in skeletal muscle of aged mice. Nat Med *20*, 265-271.
299. Aouadi, M., Laurent, K., Prot, M., Le Marchand-Brustel, Y., Binetruy, B., and Bost, F. (2006). Inhibition of p38MAPK increases adipogenesis from embryonic to adult stages. Diabetes *55*, 281-289.
300. Aubert, G., and Lansdorp, P.M. (2008). Telomeres and aging. Physiological reviews *88*, 557-579.
301. Niehrs, C., and Schafer, A. (2012). Active DNA demethylation by Gadd45 and DNA repair. Trends in cell biology *22*, 220-227.
302. Ziller, M.J., Hansen, K.D., Meissner, A., and Aryee, M.J. (2015). Coverage recommendations for methylation analysis by whole-genome bisulfite sequencing. Nature methods *12*, 230-232, 231 p following 232.
303. Laurent, L., Wong, E., Li, G., Huynh, T., Tsirigos, A., Ong, C.T., Low, H.M., Kin Sung, K.W., Rigoutsos, I., Loring, J., et al. (2010). Dynamic changes in the human methylome during differentiation. Genome research *20*, 320-331.
304. Shen, Y., Yue, F., McCleary, D.F., Ye, Z., Edsall, L., Kuan, S., Wagner, U., Dixon, J., Lee, L., Lobanenkov, V.V., et al. (2012). A map of the cis-regulatory sequences in the mouse genome. Nature *488*, 116-120.
305. Patterson, A.D., Hildesheim, J., Fornace, A.J., Jr., and Hollander, M.C. (2006). Neural tube development requires the cooperation of p53- and Gadd45a-associated pathways. Birth defects research. Part A, Clinical and molecular teratology *76*, 129-132.
306. Copp, A.J., Greene, N.D., and Murdoch, J.N. (2003). The genetic basis of mammalian neurulation. Nature reviews. Genetics *4*, 784-793.
307. Harris, M.J., and Juriloff, D.M. (2007). Mouse mutants with neural tube closure defects and their role in understanding human neural tube defects. Birth defects research. Part A, Clinical and molecular teratology *79*, 187-210.
308. Harris, M.J., and Juriloff, D.M. (2010). An update to the list of mouse mutants with neural tube closure defects and advances toward a complete genetic perspective of neural tube closure. Birth defects research. Part A, Clinical and molecular teratology *88*, 653-669.
309. Gerits, N., Kostenko, S., Shiryaev, A., Johannessen, M., and Moens, U. (2008). Relations between the mitogen-activated protein kinase and the cAMP-dependent protein kinase pathways: comradeship and hostility. Cellular signalling *20*, 1592-1607.
310. Regnier, C.H., Masson, R., Kedinger, V., Textoris, J., Stoll, I., Chenard, M.P., Dierich, A., Tomasetto, C., and Rio, M.C. (2002). Impaired neural tube closure, axial skeleton malformations, and tracheal ring disruption in TRAF4-deficient mice. Proceedings of the National Academy of Sciences of the United States of America *99*, 5585-5590.
311. Kuan, C.Y., Yang, D.D., Samanta Roy, D.R., Davis, R.J., Rakic, P., and Flavell, R.A. (1999). The Jnk1 and Jnk2 protein kinases are required for regional specific apoptosis during early brain development. Neuron *22*, 667-676.
312. del Barco Barrantes, I., Coya, J.M., Maina, F., Arthur, J.S., and Nebreda, A.R. (2011). Genetic analysis of specific and redundant roles for p38alpha and p38beta MAPKs during mouse

development. Proceedings of the National Academy of Sciences of the United States of America *108*, 12764-12769.

313. Abell, A.N., Rivera-Perez, J.A., Cuevas, B.D., Uhlik, M.T., Sather, S., Johnson, N.L., Minton, S.K., Lauder, J.M., Winter-Vann, A.M., Nakamura, K., et al. (2005). Ablation of MEKK4 kinase activity causes neurulation and skeletal patterning defects in the mouse embryo. Molecular and cellular biology *25*, 8948-8959.
314. Chi, H., Sarkisian, M.R., Rakic, P., and Flavell, R.A. (2005). Loss of mitogen-activated protein kinase kinase kinase 4 (MEKK4) results in enhanced apoptosis and defective neural tube development. Proceedings of the National Academy of Sciences of the United States of America *102*, 3846-3851.
315. Dawlaty, M.M., Breiling, A., Le, T., Raddatz, G., Barrasa, M.I., Cheng, A.W., Gao, Q., Powell, B.E., Li, Z., Xu, M., et al. (2013). Combined deficiency of Tet1 and Tet2 causes epigenetic abnormalities but is compatible with postnatal development. Developmental cell *24*, 310-323.
316. Wang, X., Wang, R.H., Li, W., Xu, X., Hollander, M.C., Fornace, A.J., Jr., and Deng, C.X. (2004). Genetic interactions between Brca1 and Gadd45a in centrosome duplication, genetic stability, and neural tube closure. The Journal of biological chemistry *279*, 29606-29614.
317. Wu, C.C., Wu, X., Han, J., and Sun, P. (2010). p38gamma regulates UV-induced checkpoint signaling and repair of UV-induced DNA damage. Protein & cell *1*, 573-583.
318. Zhao, Q., Barakat, B.M., Qin, S., Ray, A., El-Mahdy, M.A., Wani, G., Arafa el, S., Mir, S.N., Wang, Q.E., and Wani, A.A. (2008). The p38 mitogen-activated protein kinase augments nucleotide excision repair by mediating DDB2 degradation and chromatin relaxation. The Journal of biological chemistry *283*, 32553-32561.
319. Barnhoorn, S., Uittenboogaard, L.M., Jaarsma, D., Vermeij, W.P., Tresini, M., Weymaere, M., Menoni, H., Brandt, R.M., de Waard, M.C., Botter, S.M., et al. (2014). Cell-autonomous progeroid changes in conditional mouse models for repair endonuclease XPG deficiency. PLoS genetics *10*, e1004686.
320. Dolle, M.E., Busuttil, R.A., Garcia, A.M., Wijnhoven, S., van Drunen, E., Niedernhofer, L.J., van der Horst, G., Hoeijmakers, J.H., van Steeg, H., and Vijg, J. (2006). Increased genomic instability is not a prerequisite for shortened lifespan in DNA repair deficient mice. Mutation research *596*, 22-35.
321. Harada, Y.N., Shiomi, N., Koike, M., Ikawa, M., Okabe, M., Hirota, S., Kitamura, Y., Kitagawa, M., Matsunaga, T., Nikaido, O., et al. (1999). Postnatal growth failure, short life span, and early onset of cellular senescence and subsequent immortalization in mice lacking the xeroderma pigmentosum group G gene. Molecular and cellular biology *19*, 2366-2372.
322. Tian, M., Jones, D.A., Smith, M., Shinkura, R., and Alt, F.W. (2004). Deficiency in the nuclease activity of xeroderma pigmentosum G in mice leads to hypersensitivity to UV irradiation. Molecular and cellular biology *24*, 2237-2242.
323. Cortazar, D., Kunz, C., Selfridge, J., Lettieri, T., Saito, Y., MacDougall, E., Wirz, A., Schuermann, D., Jacobs, A.L., Siegrist, F., et al. (2011). Embryonic lethal phenotype reveals a function of TDG in maintaining epigenetic stability. Nature *470*, 419-423.
324. Li, Z., Cai, X., Cai, C.L., Wang, J., Zhang, W., Petersen, B.E., Yang, F.C., and Xu, M. (2011). Deletion of Tet2 in mice leads to dysregulated hematopoietic stem cells and subsequent development of myeloid malignancies. Blood *118*, 4509-4518.
325. Quivoron, C., Couronne, L., Della Valle, V., Lopez, C.K., Plo, I., Wagner-Ballon, O., Do Cruzeiro, M., Delhommeau, F., Arnulf, B., Stern, M.H., et al. (2011). TET2 inactivation results in pleiotropic hematopoietic abnormalities in mouse and is a recurrent event during human lymphomagenesis. Cancer cell *20*, 25-38.
326. Velasco, G., Hube, F., Rollin, J., Neuillet, D., Philippe, C., Bouzinba-Segard, H., Galvani, A., Viegas-Pequignot, E., and Francastel, C. (2010). Dnmt3b recruitment through E2F6

transcriptional repressor mediates germ-line gene silencing in murine somatic tissues. Proceedings of the National Academy of Sciences of the United States of America *107*, 9281-9286.

327. Qian, Y., Tu, J., Tang, N.L., Kong, G.W., Chung, J.P., Chan, W.Y., and Lee, T.L. (2015). Dynamic changes of DNA epigenetic marks in mouse oocytes during natural and accelerated aging. The international journal of biochemistry & cell biology.
328. Okano, M., Bell, D.W., Haber, D.A., and Li, E. (1999). DNA methyltransferases Dnmt3a and Dnmt3b are essential for de novo methylation and mammalian development. Cell *99*, 247-257.
329. Zhang, R.R., Cui, Q.Y., Murai, K., Lim, Y.C., Smith, Z.D., Jin, S., Ye, P., Rosa, L., Lee, Y.K., Wu, H.P., et al. (2013). Tet1 regulates adult hippocampal neurogenesis and cognition. Cell stem cell *13*, 237-245.
330. Gonzalo, S., Jaco, I., Fraga, M.F., Chen, T., Li, E., Esteller, M., and Blasco, M.A. (2006). DNA methyltransferases control telomere length and telomere recombination in mammalian cells. Nature cell biology *8*, 416-424.
331. Yang, F., Zhang, W., Li, D., and Zhan, Q. (2013). Gadd45a suppresses tumor angiogenesis via inhibition of the mTOR/STAT3 protein pathway. The Journal of biological chemistry *288*, 6552-6560.
332. Butin-Israeli, V., Adam, S.A., Goldman, A.E., and Goldman, R.D. (2012). Nuclear lamin functions and disease. Trends in genetics : TIG *28*, 464-471.
333. Lombard, D.B., Chua, K.F., Mostoslavsky, R., Franco, S., Gostissa, M., and Alt, F.W. (2005). DNA repair, genome stability, and aging. Cell *120*, 497-512.
334. Chen, J.H., Hales, C.N., and Ozanne, S.E. (2007). DNA damage, cellular senescence and organismal ageing: causal or correlative? Nucleic acids research *35*, 7417-7428.
335. Garinis, G.A., van der Horst, G.T., Vijg, J., and Hoeijmakers, J.H. (2008). DNA damage and ageing: new-age ideas for an age-old problem. Nature cell biology *10*, 1241-1247.
336. Massip, L., Garand, C., Paquet, E.R., Cogger, V.C., O'Reilly, J.N., Tworek, L., Hatherell, A., Taylor, C.G., Thorin, E., Zahradka, P., et al. (2010). Vitamin C restores healthy aging in a mouse model for Werner syndrome. FASEB journal : official publication of the Federation of American Societies for Experimental Biology *24*, 158-172.
337. Hemmeryckx, B., Hoylaerts, M.F., and Lijnen, H.R. (2012). Effect of premature aging on murine adipose tissue. Experimental gerontology *47*, 256-262.
338. Karakasilioti, I., Kamileri, I., Chatzinikolaou, G., Kosteas, T., Vergadi, E., Robinson, A.R., Tsamardinos, I., Rozgaja, T.A., Siakouli, S., Tsatsanis, C., et al. (2013). DNA damage triggers a chronic autoinflammatory response, leading to fat depletion in NER progeria. Cell metabolism *18*, 403-415.
339. Lopez-Mejia, I.C., de Toledo, M., Chavey, C., Lapasset, L., Cavelier, P., Lopez-Herrera, C., Chebli, K., Fort, P., Beranger, G., Fajas, L., et al. (2014). Antagonistic functions of LMNA isoforms in energy expenditure and lifespan. EMBO reports *15*, 529-539.
340. Shimba, S., Ishii, N., Ohta, Y., Ohno, T., Watabe, Y., Hayashi, M., Wada, T., Aoyagi, T., and Tezuka, M. (2005). Brain and muscle Arnt-like protein-1 (BMAL1), a component of the molecular clock, regulates adipogenesis. Proceedings of the National Academy of Sciences of the United States of America *102*, 12071-12076.
341. Nedergaard, J., and Cannon, B. (2014). The browning of white adipose tissue: some burning issues. Cell metabolism *20*, 396-407.
342. Vegiopoulos, A., Muller-Decker, K., Strzoda, D., Schmitt, I., Chichelnitskiy, E., Ostertag, A., Berriel Diaz, M., Rozman, J., Hrabe de Angelis, M., Nusing, R.M., et al. (2010). Cyclooxygenase-2 controls energy homeostasis in mice by de novo recruitment of brown adipocytes. Science *328*, 1158-1161.

343. Kajimura, S., Seale, P., and Spiegelman, B.M. (2010). Transcriptional control of brown fat development. Cell metabolism *11*, 257-262.
344. Schulz, T.J., and Tseng, Y.H. (2013). Brown adipose tissue: development, metabolism and beyond. The Biochemical journal *453*, 167-178.
345. Bordicchia, M., Liu, D., Amri, E.Z., Ailhaud, G., Dessi-Fulgheri, P., Zhang, C., Takahashi, N., Sarzani, R., and Collins, S. (2012). Cardiac natriuretic peptides act via p38 MAPK to induce the brown fat thermogenic program in mouse and human adipocytes. The Journal of clinical investigation *122*, 1022-1036.
346. Gantner, M.L., Hazen, B.C., Conkright, J., and Kralli, A. (2014). GADD45gamma regulates the thermogenic capacity of brown adipose tissue. Proceedings of the National Academy of Sciences of the United States of America *111*, 11870-11875.
347. Villarroya, F., and Vidal-Puig, A. (2013). Beyond the sympathetic tone: the new brown fat activators. Cell metabolism *17*, 638-643.
348. Whittle, A.J., Lopez, M., and Vidal-Puig, A. (2011). Using brown adipose tissue to treat obesity - the central issue. Trends in molecular medicine *17*, 405-411.
349. Champagne, K.S., and Kutateladze, T.G. (2009). Structural insight into histone recognition by the ING PHD fingers. Current drug targets *10*, 432-441.
350. So, K., Tamura, G., Honda, T., Homma, N., Waki, T., Togawa, N., Nishizuka, S., and Motoyama, T. (2006). Multiple tumor suppressor genes are increasingly methylated with age in non-neoplastic gastric epithelia. Cancer science *97*, 1155-1158.
351. Tra, J., Kondo, T., Lu, Q., Kuick, R., Hanash, S., and Richardson, B. (2002). Infrequent occurrence of age-dependent changes in CpG island methylation as detected by restriction landmark genome scanning. Mechanisms of ageing and development *123*, 1487-1503.
352. Siegmund, K.D., Connor, C.M., Campan, M., Long, T.I., Weisenberger, D.J., Biniszkiewicz, D., Jaenisch, R., Laird, P.W., and Akbarian, S. (2007). DNA methylation in the human cerebral cortex is dynamically regulated throughout the life span and involves differentiated neurons. PloS one *2*, e895.
353. Richie, J.P., Jr., Leutzinger, Y., Parthasarathy, S., Malloy, V., Orentreich, N., and Zimmerman, J.A. (1994). Methionine restriction increases blood glutathione and longevity in F344 rats. FASEB journal : official publication of the Federation of American Societies for Experimental Biology *8*, 1302-1307.
354. Orentreich, N., Matias, J.R., DeFelice, A., and Zimmerman, J.A. (1993). Low methionine ingestion by rats extends life span. The Journal of nutrition *123*, 269-274.
355. Chen, R.Z., Pettersson, U., Beard, C., Jackson-Grusby, L., and Jaenisch, R. (1998). DNA hypomethylation leads to elevated mutation rates. Nature *395*, 89-93.
356. Lengauer, C., Kinzler, K.W., and Vogelstein, B. (1997). DNA methylation and genetic instability in colorectal cancer cells. Proceedings of the National Academy of Sciences of the United States of America *94*, 2545-2550.
357. Sambrook, J., Fritsch, E.F., and Maniatis, T. (2001). Molecular Cloning: A Laboratory Manual, (Cold Spring Harbor Laboratory Press).
358. Ray, A., and Dittel, B.N. (2010). Isolation of mouse peritoneal cavity cells. Journal of visualized experiments : JoVE.
359. Dimri, G.P., Lee, X., Basile, G., Acosta, M., Scott, G., Roskelley, C., Medrano, E.E., Linskens, M., Rubelj, I., Pereira-Smith, O., et al. (1995). A biomarker that identifies senescent human cells in culture and in aging skin in vivo. Proceedings of the National Academy of Sciences of the United States of America *92*, 9363-9367.
360. Debacq-Chainiaux, F., Erusalimsky, J.D., Campisi, J., and Toussaint, O. (2009). Protocols to detect senescence-associated beta-galactosidase (SA-betagal) activity, a biomarker of senescent cells in culture and in vivo. Nature protocols *4*, 1798-1806.

361. Kallio, M.A., Tuimala, J.T., Hupponen, T., Klemela, P., Gentile, M., Scheinin, I., Koski, M., Kaki, J., and Korpelainen, E.I. (2011). Chipster: user-friendly analysis software for microarray and other high-throughput data. BMC genomics *12*, 507.
362. Huang, D.W., Sherman, B.T., Tan, Q., Collins, J.R., Alvord, W.G., Roayaei, J., Stephens, R., Baseler, M.W., Lane, H.C., and Lempicki, R.A. (2007). The DAVID Gene Functional Classification Tool: a novel biological module-centric algorithm to functionally analyze large gene lists. Genome biology *8*, R183.
363. Anders, S., and Huber, W. (2010). Differential expression analysis for sequence count data. Genome biology *11*, R106.

8. LIST OF ABBREVIATIONS

5'UTR	5' Untranslated region
5mC	5-methylcytosine
5hmC	5-hydroxymethylcytosine
5fC	5-formylcytosine
5caC	5-carboxylcytosine
5hmU	5-hydroxymethyluracil
AID	Activation-induced deaminase
BAT	Brown adipose tissue
bp	Base pair
BSA	Bovine serum albumin
cDNA	Copy DNA
C.elegans	*Caenorhabditis elegans*
C/EBP	CCAAT-enhancer-binding protein
cAMP	Cyclic adenosine monophosphate
CFU-F	Colony-forming unit-fibroblasts
ChIP	Chromatin immunoprecipitation
ChIP-Seq	Chromatin immunoprecipitation followed by sequencing
CpG	Cytosine-Guanine dinucleotide
DNA	Deoxyribonucleic acid
DKFZ	Deutsches Krebsforschungszentrum
DMEM	Dulbecco's modified Eagle's medium
DMR	Differentially methylated region
DMSO	Dimethylsulfoxide
Dnmt	DNA methyltransferase
dNTP	Nucleoside triphosphate
DTT	Dithiothreitol
ERK	Extracellular signal-regulated kinase
FABP4	Fatty acid binding protein 4
FBS	Fetal bovine serum
FDR	False discovery rate
FOXO3a	Forkhead box O3a
Gadd45a, G45a	Growth arrest and DNA-damage-inducible protein 45 alpha
Gadd45g	Growth arrest and DNA-damage-inducible protein 45 gamma
GO	Gene ontology
gWAT	Gonadal white adipose tissue
H&E	Hematoxylin & Eosin
H3K14ac	Histone 3 acetylated at lysine 14
H3K27ac	Histone 3 acetylated at lysine 27
H3K4me1,2,3	Histone 3 mono-/di-/trimethylated at lysine 4
H3K9me	Histone 3 methylated at lysine 9
HA	Hemaglutinin
HDAC	Histone deacetylase
HEK293T	Human Embryonic Kidney 293T cells
IBMX	Isobutylmethylxanthine
IGF-1	Insulin-like growth factor 1
IgG	Immunoglobulin G
IMB	Institute of Molecular Biology Mainz

Ing1	Inhibitor of growth protein 1
JNK	c-Jun N-terminal kinase
kb	Kilobasepair
lincRNA	Long non-coding RNA
LMR	Low methylated region
M	Mol
MAPK	Mitogen-activated protein kinase
MAP3K4	Mitogen-activated protein kinase kinase kinase 4
MEF	Mouse embryonic fibroblast
min	Minute
mRNA	Messenger RNA
MS-PCR	Methylation sensitive PCR
mTOR	Mammalian target of Rapamycin
NAD^+	Nicotinamide adenine dinucleotide
PBS	Phosphate buffered saline
PCNA	Proliferating cell nuclear antigen
PCR	Polymerase chain reaction
PPARγ	Peroxisome proliferator-activated receptor gamma
qPCR	Quantitative PCR
RIN	RNA integrity number
RNA	Ribonucleic acid
RNA-Seq	RNA sequencing
ROS	Reactive oxygen species
rpm	Rounds per minute
s.d.	Standard deviation
SASP	Senescence-associated secretory phenotype
SDS-PAGE	Sodium dodecyl sulfate polyacrylamide gel electrophoresis
sec	Seconds
TDG	Thymine DNA glycosylase
TET	Ten-eleven translocation methylcytosine dioxigenase
UPL	Universal probe library
UV	Ultraviolet
WAT	White adipose tissue
WGBS-Seq	Whole genome bisulfite sequencing
Wnt	Wingless-type MMTV integration site family member
WT	Wildtype
XP	Xeroderma pigmentosum